Cucurbit[7]uril as a Universal Anchor for Photoswitchable Monolayers on Gold

Doroteja Lončarić,[a,b] Eva Kaletová,[a] Katarina Majerová Varga,[a] Carina Santos Hurtado,[a] Milan Mašát,[a] Ivana Císařová[c] and Jiří Kaleta*[a]

[a] *Institute of Organic Chemistry and Biochemistry of the Czech Academy of Sciences, Flemingovo nám. 2, 160 00 Prague 6, Czech Republic*
[b] *Department of Organic Chemistry, Faculty of Science, Charles University in Prague, Hlavova 2030, 12840 Prague 2, Czech Republic*
[c] *Department of Inorganic Chemistry, Faculty of Science, Charles University in Prague, Hlavova 2030, 128 40 Prague 2, Czech Republic*

Supporting Information

Table of Contents

1. General Information

Materials. We are grateful to Prof. Eric Masson at Ohio University, Athens, OH, USA, for kindly providing us with the cucurbit[7]uril (**CB[7]**) samples. Molar mass of all **CB[7]** samples was calibrated by measurement of ^{1}H NMR spectrum in D_2O with either 1-adamantylamine, *p*-toluidine hydrochloride or DMF as internal standards. Molar mass was determined as an average from at least three independent samples. Calibration experiments were repeated every 3-6 months.

All of the starting materials used for synthesis were purchased from commercial suppliers and used without further purification. Deuterated solvents used for preparation of samples for NMR spectroscopy were purchased from Eurisotop. Deuterated DMSO (DMSO-d_6) was distilled over calcium hydride as needed. TEA and DMF were dried over calcium hydride and distilled over nitrogen prior to use. Toluene was dried over sodium and distilled under argon prior to use. Yields refer to isolated, chromatographically and spectroscopically homogenous materials.

Procedures. Thin-layer chromatography (TLC) was performed using precoated TLC aluminium sheets (Silica gel 60 F254). TLC spots were visualized using UV light (254 nm). Column chromatography was performed using silica gel (high purity grade, pore size 60 Å, 70–230 mesh) as stationary phase.

Nuclear Magnetic Resonance (NMR) Spectroscopy. NMR spectra were acquired on Bruker Avance III^{TM} HD 400 MHz Prodigy, Bruker Avance II^{TM} 500 MHz and JEOL JNM-EZCR 500 MHz spectrometers. Chemical shifts in ^{1}H and ^{13}C spectra are reported in ppm on the δ scale relative to DMSO-d_6 (δ = 2.50 ppm for ^{1}H, and δ = 39.5 ppm for ^{13}C) as an internal reference. Coupling was reported as first-order and coupling constants (*J*) are reported in hertz (Hz). Standard abbreviations were used to indicate multiplicity: s = singlet, br s = broad singlet, d = doublet, m = multiplet, dd = doublet of doublets. Structural assignments were made with additional information from APT, COSY, HSQC, and HMBC experiments.

Melting Points. Melting points were measured on Stuart SMP 3 melting point apparatus and reported data are uncorrected.

Mass Spectrometry. High-resolution mass spectra (HRMS) using ESI or APCI techniques were obtained on ORBITRAP XL (Thermo). MALDI experiments were performed on Bruker Ultraflextreme. EI and CI spectra were recorded using Waters or Agilent 7250 GC/Q-TOF instruments.

Infrared Spectroscopy (IR). FTIR spectra were recorded in KBr pellets on a spectrometer Nicolet 6700 (Thermo Scientific, USA) equipped with standard MIR source, KBr beamsplitter and DTGS detector in transmission mode in the 4000–400 cm^{-1} spectral range with the following setup: 64 scans, 2 cm^{-1} spectral resolution, Happ-Genzel apodization function.

Elementary analysis. Elementary analysis was measured using PE 2400 Series II CHNS/O Analyzer (Perkin Elmer, USA).

Single Crystal X-Ray Diffraction. The diffraction data of single crystals of **2** and **8** were obtained on Bruker D8 VENTURE Kappa Duo PHOTONIII by IμS micro-focus sealed tube MoKα (λ= 0.71073Å) at 120K temperature of the crystal preserved by Cryostream Cooler 800.

The structures were solved by direct methods (XT)[1] and refined by full matrix least squares based on F^2 (SHELXL2019).[2] The hydrogen atoms on carbon were fixed into idealized positions (riding model) and assigned temperature factors either $H_{iso}(H) = 1.2\ U_{eq}$(pivot atom) or $H_{iso}(H) = 1.5\ U_{eq}$ (pivot atom) for methyl moiety.

Calculations. Rods **1-4** and corresponding **CB[7]**-complexes were optimized in the gas phase with the semiempirical tight-binding method provided by the GFN2-xTB program[3,4,5] with a very tight convergence criterion.

1. Sheldrick, G. M. *SHELXT* – Integrated Space-Group and Crystal-Structure Determination. *Acta Crystallogr. Sect. Found. Adv.* **2015**, *71* (1), 3–8. https://doi.org/10.1107/S2053273314026370.
2. Sheldrick, G. M. Crystal Structure Refinement with *SHELXL*. *Acta Crystallogr. Sect. C Struct. Chem.* **2015**, *71* (1), 3–8. https://doi.org/10.1107/S2053229614024218.
3. Bannwarth, C.; Caldeweyher, E.; Ehlert, S.; Hansen, A.; Pracht, P.; Seibert, J.; Spicher, S.; Grimme, S. Extended Tight-Binding Quantum Chemistry Methods. *WIREs Comput. Mol. Sci.* **2021**, *11*, e01493. https://doi.org/10.1002/wcms.1493.
4. Bannwarth, C.; Ehlert, S.; Grimme, S. GFN2-xTB–An Accurate and Broadly Parametrized Self-Consistent Tight-Binding Quantum Chemical Method with Multipole Electrostatics and Density-Dependent Dispersion Contributions. *J. Chem. Theory Comput.* **2019**, *15*, 1652-1671. https://doi.org/10.1021/acs.jctc.8b01176.
5. Grimme, S.; Bannwarth, C.; Shushkov, P. A Robust and Accurate Tight-Binding Quantum Chemical Method for Structures, Vibrational Frequencies, and Noncovalent Interactions of Large Molecular Systems Parametrized for All spd-Block Elements (Z = 1–86). *J. Chem. Theory Comput.* **2017**, *13*, 1989-2009. https://doi.org/10.1021/acs.jctc.7b00118.

2. Synthesis of Guests

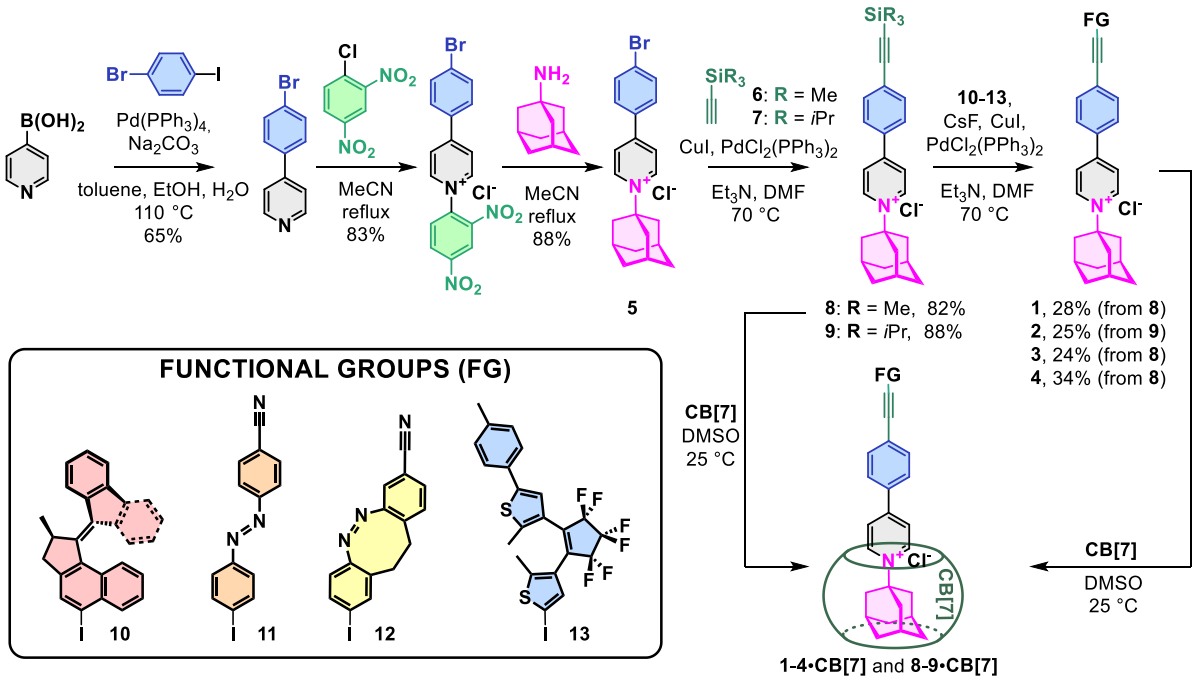

Scheme S1. Synthesis of guests **1-4** and supramolecular complexes **1-4·CB[7]**, **8·CB[7]**, and **9·CB[7]**.

Compounds **5**,[6] **10**,[7] **11**,[8] **12**,[9] and **13**[10] were prepared following already published procedures.

General procedure for Sonogashira cross-coupling of photoactive units 10-13 and silyl-protected CB[7] binding site precursors 8 and 9 (GP1).

Flame dried Schlenk flask equipped with magnetic stir bar and filled with nitrogen atmosphere was loaded with iodides **10-13** (1 equiv.), silyl derivative **8** or **9** (1.2 equiv.), $Pd(PPh_3)_4$ (4 mol%) or $Pd(PPh_3)_2Cl_2$ (4 mol%), CuI (4 mol%) and CsF (1.4 equiv.). After ten vacuum/nitrogen cycles, anhydrous DMF (25 mL per 1 mmol of iodide) and TEA (4.5 mL) were added. The reaction mixture was stirred at 70 °C in an oil bath for 2.5-3 hours. The progress was followed by TLC in $CHCl_3$, checking for depletion of iodide. After reaction completion, DMF and TEA were distilled by connecting the reaction vessel to the vacuum pump (1 mbar) and heating the mixture up to 70 °C. The dark brown solid residue was washed with water (2 × 30 mL per 1 mmol of starting iodide), triturated with diethyl ether (2 × 15 mL per 1 mmol of starting iodide) and ethyl acetate (2 × 15 mL per 1 mmol of starting iodide),

6. Santos, C.; Bastien, G.; Lončarić, D.; Dračínský, M.; Císařová, I.; Masson, E.; Kaleta, J. Surface Inclusion and Dynamics of Cucurbit[7]Uril-Based Supramolecular Complexes. *Chem. Sci.* **2025**, *16*, 14081-14087. https://doi.org/10.1039/D5SC03152D.
7. Kaleta, J.; Chen, J.; Bastien, G.; Dračínský, M.; Mašát, M.; Rogers, C. T.; Feringa, B. L.; Michl, J. Surface Inclusion of Unidirectional Molecular Motors in Hexagonal Tris(*o*-Phenylene)Cyclotriphosphazene. *J. Am. Chem. Soc.* **2017**, *139* (30), 10486–10498. https://doi.org/10.1021/jacs.7b05404.
8. Zarwell, S.; Rück-Braun, K. Synthesis of an Azobenzene-Linker-Conjugate with Tetrahedrical Shape. *Tetrahedron Lett.* **2008**, *49* (25), 4020–4025. https://doi.org/10.1016/j.tetlet.2008.04.086.
9. Bastien, G.; Severa, L.; Škuta, M.; Santos Hurtado, C.; Rybáček, J.; Šolínová, V.; Císařová, I.; Kašička, V.; Kaleta, J. Triptycene-Based Tripodal Molecular Platforms. *Chem. – Eur. J.* **2024**, e202401889. https://doi.org/10.1002/chem.202401889.
10. Severa, L.; Santos Hurtado, C.; Rončević, I.; Mašát, M.; Bastien, G.; Štoček, J. R.; Dračínský, M.; Houska, V.; Kaletová, E.; Garza, D. J.; Císařová, I.; Cimatu, K. L. A.; Bastl, Z.; Kaleta, J. Regular Arrays of Rod-Shaped Molecular Photoswitches: Synthesis, Preparation, Characterization, and Selective Photoswitching within Mono- and Bilayer Systems. *Chem. – Eur. J.* **2024**, *30* (4), e202302828. https://doi.org/10.1002/chem.202302828.

sonicating thoroughly. The residue was dissolved in methanol and passed through a celite plug or a PTFE microfilter. The solvent was evaporated and the residue was purified by column chromatography on silica gel ((a) HCOOH/MeOH = 5:95 or (b) HCOOH/acetone/MeOH = 2:20:78). Solvent was removed from fractions containing product on rotavapor, and the residue was triturated with water, which afforded products **1-4**.

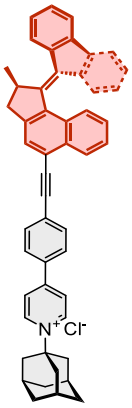

Compound 1 was prepared from iodide **10** (97 mg, 0.21 mmol), silyl derivative **8** (88 mg, 0.21 mmol), $Pd(PPh_3)_2Cl_2$ (8 mg, 11 μmol), CuI (2 mg, 11 μmol) and CsF (49 mg, 0.32 mmol) according to **GP1**. Solvent system (b) was used for column chromatography. Compound **1** (40 mg, 58 μmol, 28%) was isolated as a dark red powder.

Mp >219 °C (dec.). **^{1}H NMR** (500 MHz, DMSO-d_6): δ 1.33 (d, J = 6.7 Hz, 3H), 1.73-1.81 (m, 6H), 2.35 (br s, 9H), 2.85 (d, J = 15.5 Hz, 1H), 3.60 (dd, J_1 = 5.6 Hz, J_2 = 15.5 Hz, 1H), 4.26-4.34 (m, 1H), 6.56 (d, J = 8.0 Hz, 1H), 6.78-6.84 (m, 1H), 7.25 (dd, J_1 = J_2 = 7.4 Hz, 1H), 7.43-7.51 (m, 3H), 7.67-7.75 (m, 2H), 7.90 (d, J = 7.6 Hz, 1H), 7.94-8.05 (m, 4H), 8.09 (s, 1H), 8.29 (d, J = 8.6 Hz, 2H), 8.56-8.62 (m, 3H), 9.35 (d, J = 7.2 Hz, 2H). **^{13}C {^{1}H} NMR** (125 MHz, DMSO-d_6): δ 19.1, 29.5, 34.5, 41.0, 41.1, 44.9, 68.7, 91.0, 95.3, 119.6, 120.1, 121.6, 124.1, 124.4, 125.1, 125.9, 126.0, 126.7, 127.0, 127.3, 127.5, 128.8, 129.0, 130.9, 131.8, 132.6, 133.5, 136.1, 137.3, 138.8, 139.3, 139.5, 141.9, 146.8, 150.1, 153.3. **IR** (KBr): 3419, 3094, 3037, 2910, 2853, 2195, 1630, 1600, 1567, 1494, 1447, 1404, 1377, 1361, 1224, 1124, 1101, 1050, 1028, 1009, 829, 815, 779, 759, 735, 711, 532 cm^{-1}. **MS**, *m/z* (%): 656.3 (100, M^+). **HRMS** (ESI+) *m/z*: $[M]^+$ Calcd for $C_{50}H_{42}N^+$ 656.3312; Found 656.3305.

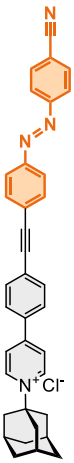

Compound 2 was prepared from iodide **11** (434 mg, 1.3 mmol), silyl derivative **9** (717 mg, 1.4 mmol), $Pd(PPh_3)_4$ (62 mg, 54 μmol), CuI (8 mg, 40 μmol) and TBAF in THF (1.8 mL, 1 M, 1.8 mmol), using **GP1**. Solvent system (a) was used for column chromatography. Compound **2** (181 mg, 0.33 mmol, 25%) was isolated as a red-orange powder.

Mp >239 °C (dec.). **^{1}H NMR** (400 MHz, DMSO-d_6): δ 1.71-1.82 (m, 6H), 2.34 (bs, 9H), 7.86 (d, J = 5.6 Hz, 2H), 7.89 (d, J = 5.3 Hz, 2H), 8.03 (d, J = 7.0 Hz, 2H), 8.05 (d, J = 7.1 Hz, 2H), 8.11 (d, J = 8.7 Hz, 2H), 8.23 (d, J = 8.6 Hz, 2H), 8.54 (d, J = 7.0 Hz, 2H), 9.34 (d, J = 6.8 Hz, 2H). **^{13}C {^{1}H} NMR** (100 MHz, DMSO-d_6): δ 29.5, 34.5, 41.0, 68.7, 91.7, 91.9, 113.6, 118.4, 123.3, 123.5, 124.4, 125.5, 125.7, 128.7, 132.6, 133.0, 133.6, 133.9, 141.9, 151.3, 153.2, 153.9. **IR** (KBr): 3432, 3092, 3025, 2913, 2854, 2224, 1629, 1601, 1500, 1449, 1406, 1384, 1306, 1226, 1188, 1124, 1101, 1030, 1011, 854, 842, 820, 815, 568 cm^{-1}. **MS**, *m/z* (%): 519.3 (100, M^+). **HRMS** (ESI+) *m/z*: $[M]^+$ Calcd for $C_{36}H_{31}N_4^+$ 519.2543; Found 519.2543.

Compound **2** was analyzed by Inductively Coupled Plasma Optical Emission Spectroscopy (ICP–OES). The measured chlorine content (5–10%) was consistent with the theoretical value for the chloride salt $C_{36}H_{31}N_4Cl$ (6.39%). In contrast, the iodine content was found to be only 0.01–0.1%, far below the theoretical value for the corresponding iodide $C_{36}H_{31}N_4I$ (19.63%). These results clearly indicate that the isolated material is the chloride salt. Since compounds **1**, **3**, and **4** were synthesized using analogous procedures, they were also assigned as chloride salts.

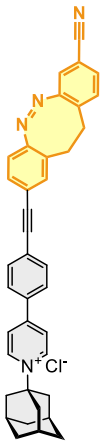

Compound 3 was prepared from iodide **12** (59 mg, 0.16 mmol), silyl derivative **8** (76 mg, 0.18 mmol), $Pd(PPh_3)_2Cl_2$ (7 mg, 9 µmol), CuI (2 mg, 12 µmol) and CsF (36 mg, 0.24 mmol) according to **GP1**. Solvent system (a) was used for column chromatography. Compound **3** (23 mg, 40 µmol, 24%) was isolated as a yellow powder.

Mp >200 °C (dec.). **^{1}H NMR** (500 MHz, DMSO-d_6): δ 1.71-1.81 (m, 6H), 2.33 (bs, 9H), 2.83-3.03 (m, 4H), 6.99 (d, *J* = 8.1 Hz, 1H), 7.35 (d, *J* = 7.9 Hz, 1H), 7.39 (s, 1H), 7.43-7.50 (m, 2H), 7.54-7.64 (m, 1H), 7.77 (d, *J* = 8.3 Hz, 2H), 8.19 (d, *J* = 8.3 Hz, 2H), 8.51 (d, *J* = 6.6 Hz, 2H), 9.33 (d, *J* = 6.7 Hz, 2H). **^{13}C {^{1}H} NMR** (125 MHz, DMSO-d_6): δ 29.5, 30.0, 30.8, 34.5, 41.0, 68.6, 89.0, 91.6, 109.8, 118.0, 119.0, 120.8, 122.1, 124.3, 125.7, 128.6, 128.7, 130.4, 131.1, 131.3, 132.4, 133.0, 133.3, 134.3, 141.8, 153.3, 155.2, 155.3. **IR** (KBr): 3429, 3097, 3022, 2910, 2854, 2229, 2204, 1630, 1602, 1567, 1541, 1524, 1495, 1449, 1404, 1360, 1346, 1306, 1226, 1125, 1101, 1030, 1011, 900, 869, 829, 814, 774, 745, 621, 534, 466 cm^{-1}. **MS**, *m/z* (%): 545.3 (100, M^+). **HRMS** (ESI+) *m/z*: $[M]^+$ Calcd for $C_{38}H_{33}N_4^+$ 545.2700; Found 545.2699.

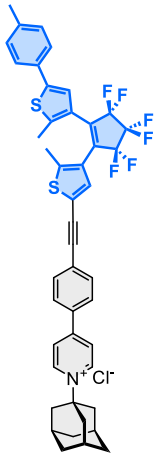

Compound 4 was prepared from iodide **13** (149 mg, 0.25 mmol), silyl derivative **8** (111 mg, 0.26 mmol), $Pd(PPh_3)_2Cl_2$ (8 mg, 11 µmol), CuI (1 mg, 6 µmol) and CsF (60 mg, 0.39 mmol) according to **GP1**. Compound **4** (68 mg, 84 µmol, 34%) was isolated as a dark blue powder.

Mp >139 °C (dec.). **^{1}H NMR** (400 MHz, DMSO-d_6): δ 1.71-1.82 (m, 6H), 1.98 (s, 3H), 2.00 (s, 3H), 2.28-2.37 (m, 12H), 7.24 (d, *J* = 7.9 Hz, 2H), 7.43 (s, 1H), 7.49-7.56 (m, 3H), 7.83 (d, *J* = 8.2 Hz, 2H), 8.21 (d, *J* = 8.3 Hz, 2H), 8.53 (d, *J* = 6.7 Hz, 2H), 9.34 (d, *J* = 6.8 Hz, 2H). **^{13}C {^{1}H} NMR** (100 MHz, DMSO-d_6): δ 14.10, 14.13, 20.7, 29.5, 34.5, 41.0, 68.7, 84.5, 93.2, 120.1, 121.8, 124.3, 124.5, 124.7, 125.1, 125.2, 128.7, 128.8, 129.7, 129.8, 132.3, 132.6, 133.5, 137.8, 140.8, 141.9, 142.0, 144.9, 153.2. **IR** (KBr): 3436, 3103, 3024, 2917, 2856, 2202, 1630, 1602, 1496, 1449, 1406, 1336, 1307, 1275, 1230, 1189, 1117, 1099, 1045, 1012, 986, 899, 816, 744, 529, 484 cm^{-1}. **MS**, *m/z* (%): 770.2 (100, M^+). **HRMS** (ESI+) *m/z*: $[M]^+$ Calcd for $C_{45}H_{38}F_6NS_2^+$ 770.2344; Found 770.2343.

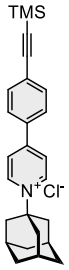

1-(Adamantan-1-yl)-4-((trimethylsilyl)ethynyl)phenyl)pyridin-1-ium chloride (**8**). Flame dried Schlenk flask equipped with magnetic stir bar and filled with nitrogen was loaded with bromide **5** (506 mg, 1.3 mmol, 1 equiv.), $PdCl_2(PPh_3)_2$ (41 mg, 0.06 mmol, 5 mol%) and CuI (9 mg, 0.05 mmol, 4 mol%). After five vacuum-nitrogen cycles, anhydrous DMF (9.5 mL) and TEA (4 mL) were added. Lastly, TMSA (**6**) (0.26 mL, 1.8 mmol, 1.4 equiv.) was added. The dark brown reaction mixture was stirred at 70 °C in an oil bath. After 45 minutes, DMF and TEA were distilled by connecting the reaction vessel to the vacuum pump (1 mbar) and heating the mixture up to 110 °C. The solid brown residue was washed with water (45 mL) and triturated with ether (3 × 35 mL), sonicating thoroughly. The residue was dissolved in methanol (50 mL) and passed through celite plug. The solvent was evaporated and the product was subsequently dried on Kugelrohr apparatus (0.1 mbar, 50 °C) to afford **8** (420 mg, 1.0 mmol, 82%) as a light brown powder.

Mp >279 °C (dec.) **^{1}H NMR** (400 MHz, DMSO-d_6): δ 0.26 (s, 9H), 1.76 (m, 6H), 2.30-2.35 (m, 9H), 7.72 (d, *J* = 8.5 Hz, 2H), 8.16 (d, *J* = 8.8 Hz, 2H), 8.51 (d, *J* = 7.3 Hz, 2H), 9.36 (d, *J* = 7.2 Hz, 2H) **^{13}C {^{1}H} NMR** (100 MHz, DMSO-d_6): δ -0.2, 29.5, 34.5, 41.0, 68.7, 98.0, 104.1, 124.4, 125.7, 128.6, 132.7, 133.4, 141.9, 153.2. **IR** (KBr): 3446, 3388, 3254, 3122, 3080, 3032, 2913, 2855, 2157, 1632, 1602, 1569, 1543, 1493, 1451, 1404, 1379, 1363, 1347, 1309, 1260, 1249, 1221, 1128, 1102, 1029, 1012, 867, 843, 817, 759, 689, 669, 538, 527, 451 cm^{-1}. **MS**, *m/z* (%): 386.2 (100, M^+). **HRMS** (ESI+) *m/z*: $[M]^+$ Calcd for $C_{26}H_{32}NSi^+$ 386.2299; Found

386.2301. **Anal.** Calcd. for $C_{26}H_{32}NSiCl \cdot H_2O$: C, 70.96; H, 7.79; N, 3.18. Found: C, 70.01; H, 7.68; N, 2.80.

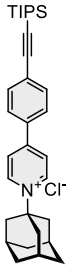

1-(Adamantan-1-yl)-4-((triisopropylsilyl)ethynyl)phenyl)pyridin-1-ium chloride (**9**). Bromide **5** (1.5 g, 3.8 mmol, 1 equiv.) was dissolved in anhydrous DMF (30 mL) and TEA (16 mL) in a flame dried Schlenk flask equipped with magnetic stir bar and septum. The reaction mixture was degassed by performing three freeze-pump-thaw cycles in acetone/dry ice bath. The reaction vessel was then opened under nitrogen overpressure and $Pd(PPh_3)_4$ (177 mg, 0.15 mmol, 4 mol%) and CuI (29 mg, 0.15 mmol, 4 mol%) were added. Lastly, the vessel was sealed with septum and TIPSA (**7**) (2.0 mL, 8.9 mmol, 2.3 equiv.) was added by syringe. The reaction mixture was heated in an oil bath for 20 hours at 70 °C, while checking the progress by TLC. DMF and TEA were distilled under reduced pressure (1 mbar) and heating the mixture up to 70 °C. The black residue was purified by column chromatography on silica gel (MeOH/DCM = 5:95). Product was subsequently dried on Kugelrohr apparatus (0.1 mbar, 50 °C) to afford **9** as light brown powder (1.1 g, 3.3 mmol, 88%).
Mp >277 °C (dec.). **^{1}H NMR** (400 MHz, DMSO-d_6): δ 1.10-1.14 (m, 21H), 1.76 (bs, 6H), 2.32 (bs, 9H), 7.71 (d, J = 8.7 Hz, 2H), 8.15 (d, J = 8.6 Hz, 2H), 8.49 (d, J = 7.3 Hz, 2H), 9.33 (d, J = 7.4 Hz, 2H). **^{13}C {^{1}H} NMR** (100 MHz, DMSO-d_6): δ 10.7, 18.5, 29.6, 34.5, 41.1, 68.7, 94.1, 106.2, 124.4, 125.9, 128.6, 132.8, 133.5, 141.9, 153.3. **IR** (KBr): 3436, 3108, 3084, 3019, 2941, 2919, 2864, 2156, 1632, 1602, 1568, 1542, 1491, 1450, 1402, 1382, 1366, 1347, 1320, 1309, 1218, 1200, 1190, 1181, 1128, 1110, 1102, 1071, 1029, 1011, 996, 920, 883, 847, 831, 817, 753, 692, 676, 659, 638, 567, 547, 528, 465 cm^{-1}. **MS**, *m/z* (%): 470.3 (100, M^+). **HRMS** (ESI+) *m/z*: $[M]^+$ Calcd for $C_{32}H_{44}NSi^+$ 470.3238; Found 470.3234. **Anal.** Calcd. for $C_{26}H_{32}NSiCl \cdot H_2O$: C, 70.96; H, 7.79; N, 3.18. Found: C, 70.01; H, 7.68; N, 2.80.

General procedure for preparation of CB[7] complexes of *N*-(1-adamantyl)pyridinium guests from DMSO (GP2).

Appropriate quantity of **1-4**, **8** or **9** (5-50 μmol) was dissolved in DMSO (c = 10 mmol L^{-1}). Equimolar quantity of solid **CB[7]** was added, and the mixture was diluted to $c \approx 1$ mmol L^{-1} by addition of DMSO, at which point all material was dissolved. Alternatively, **CB[7]** was added as a solution in DMSO (c = 0.7 mmol L^{-1}) by 0.5 equiv. additions. The stoichiometric ratio of **CB[7]** to guest was checked by ^{1}H NMR. The analyzed samples were prepared by distillation of DMSO on Kugelrohr apparatus (60 °C, 0.1 mbar) from an aliquot (2 mL) and redissolution in DMSO-d_6 (0.5 mL).

After addition of equimolar quantity of **CB[7]**, DMSO was evaporated at 60 °C under reduced pressure (0.1 mbar) to yield the solid complexes quantitatively. ^{1}H NMR signals of the 1:1 **CB[7]** complexes overlap with the signals of trimeric assembly.

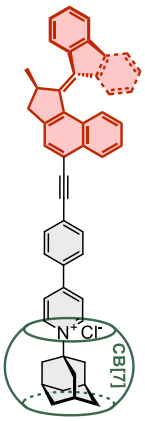

Complex **1·CB[7]** was prepared from compound **1** (4 mg, 12 μmol) and **CB[7]** (9 mg, 12 μmol) in DMSO (15 mL) following **GP2**. Complex **1·CB[7]** was obtained quantitatively as a red-brown solid.
^{1}H NMR (500 MHz, DMSO-d_6): δ 0.90-1.09 (m, 6H), 1.35 (d, J = 6.6 Hz, 3H), 1.41-1.62 (m, 9H), 2.81-2.89 (m, 1H), 4.09-4.49 (m, 14H), 5.33-5.50 (s, 14H), 5.59-5.77 (m, 14H), 6.54-6.61 (m, 1H), 6.78-6.89 (m, 1H), 7.22-7.31 (1H), 7.45-7.54 (m, 2H), 7.60-7.65 (m, 1H), 7.70-7.75 (m, 1H), 7.89-7.94 (m, 1H), 7.95-8.05 (m, 3H), 8.09-8.14 (m, 1H), 8.30-8.44 (m, 3H), 8.55-8.65 (m, 2H), 9.03-9.20 (m, 2H). **IR** (KBr): 3430, 2920, 2854, 1739, 1635, 1603, 1569, 1468, 1420, 1376, 1320, 1295, 1229, 1188, 1153, 1136, 1081, 1027, 988, 967, 824, 803, 756, 672, 628 cm^{-1}. **MS**, *m/z* (%): 1818.6 (100, M$^+$); 1185.3 (9, [CB[7] + Na$^+$]). **HRMS** (MALDI) *m/z*: [M]$^+$ Calcd for $C_{92}H_{84}N_{29}O_{14}^+$ 1818.6747; Found 1818.6663.

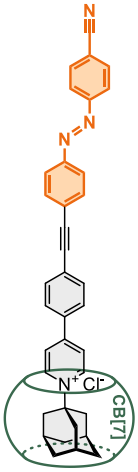

Complex **2·CB[7]** was prepared from compound **2** (3 mg, 5 μmol) and **CB[7]** (8 mg, 5 μmol) in DMSO (10 mL) following **GP2**. Complex **2·CB[7]** was obtained quantitatively as an orange solid.
^{1}H NMR (500 MHz, DMSO-d_6): δ 0.97 (m, 6H), 1.37-1.70 (m, 9H), 4.07-4.64 (m, 14H), 5.42 (s, 14H), 5.64 (d, J = 14.5 Hz, 7H), 5.69 (d, J = 14.2 Hz, 7H), 7.83-7.93 (m, 4H), 8.00-8.09 (m, 4H), 8.11 (d, J = 8.5 Hz, 2H), 8.24-8.39 (m, 4H), 9.01-9.14 (m, 2H). **IR** (KBr): 3460, 3001, 2922, 2227, 1739, 1635, 1603, 1467, 1420, 1376, 1321, 1283, 1229, 1188, 1030, 968, 824, 803, 756, 672, 638, 570, 517, 497, 464 cm^{-1}. **MS**, *m/z* (%): 1681.6 (100, M$^+$); 1201.3 (9). **HRMS** (MALDI) *m/z*: [M]$^+$ Calcd for $C_{78}H_{73}N_{32}O_{14}^+$ 1681.5979; Found 1681.6141.

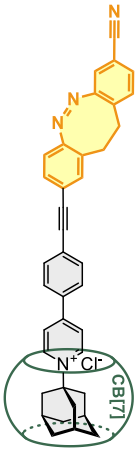

Complex **3·CB[7]** was prepared from compound **3** (8 mg, 14 μmol) and **CB[7]** (18 mg, 14 μmol) in DMSO (15 mL) following **GP2**. Complex **3·CB[7]** was obtained quantitatively as a yellow solid.
^{1}H NMR (400 MHz, DMSO-d_6): δ 0.88-1.05 (m, 6H), 1.37-1.60 (m, 9H), 2.86-3.02 (m, 4H), 4.07-4.50 (m, 14H), 5.39 (s, 14H), 5.55-5.79 (m, 14H), 6.99 (d, J = 8.2 Hz, 1H), 7.35 (d, J = 8.1 Hz, 1H), 7.41 (m, 1H), 7.44-7.51 (m, 2H), 7.58 (dd, J_1 = 8.0 Hz, d, J_2 = 1.6 Hz, 1H), 7.75 (d, J = 8.4 Hz, 2H), 8.18-8.30 (m, 3H), 8.99-9.13 (d, 2H). **IR** (KBr): 3426, 2989, 2917, 2230, 1740, 1635, 1604, 1466, 1420, 1376, 1320, 1228, 1187, 1028, 968, 823, 802, 756, 671, 628, 497 cm^{-1}. **MS**, *m/z* (%): 1710.6 (100, M$^+$); 1185.3 (4, [CB[7] + Na$^+$]), 960.5 (13). **HRMS** (MALDI) *m/z*: [M]$^+$ Calcd for $C_{80}H_{75}N_{32}O_{14}^+$ 1707.6135; Found 1707.6188.

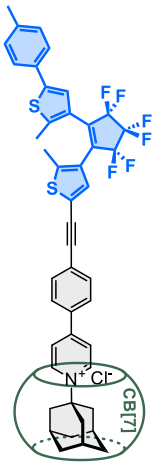

Complex **4·CB[7]** was prepared from compound **4** (20 mg, 25 µmol) and **CB[7]** (36 mg, 25 µmol) in DMSO (40 mL) following **GP2**. Complex **4·CB[7]** was obtained quantitatively as a green-blue solid.
^{1}H NMR (400 MHz, DMSO-d_6): δ 0.87-1.09 (m, 6H), 1.38-1.60 (m, 9H), 1.95-2.04 (m, 6H), 2.32 (3H, s), 4.05-4.51 (m, 14H), 5.39 (s, 14H), 5.55-5.80 (m, 14H), 7.24 (d, *J* = 7.9 Hz, 2H), 7.40-7.46 (m, 1H), 7.50-7.58 (m, 3H), 7.78-7.86 (m, 2H), 8.22-8.37 (m, 4H) , 8.99-9.16 (m, 2H). **IR** (KBr): 3436, 3135, 2992, 2919, 2859, 2202, 1740, 1636, 1604, 1468, 1421, 1376, 1321, 1283, 1230, 1189, 1139, 1047, 1029, 987, 968, 900, 824, 803, 756, 690, 673, 629 cm^{-1}. **MS**, *m/z* (%): 2067.6 (5), 1933.6 (100, M$^+$); 1510.5 (9), 1185.3 (38, [CB[7] + Na$^+$]), 939.4 (11). **HRMS** (ESI+) *m/z*: [M]$^+$ Calcd for $C_{87}H_{80}F_6N_{29}O_{14}S_2^+$ 1932.5780; Found 1932.5705.

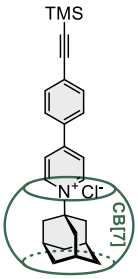

Complex **8·CB[7]** was prepared from compound **8** (2 mg, 5 µmol) and **CB[7]** (6 mg, 5 µmol) in DMSO (6 mL) following **GP2**. Complex **8·CB[7]** was obtained quantitatively as a yellow-brown solid.
^{1}H NMR (500 MHz, DMSO-d_6): δ 0.27 (s, 9H), 0.95 (bs, 6H), 1.37-1.67 (m, 9H), 4.05-4.62 (m, 14H), 5.40 (s, 14H), 5.62 (d, *J* = 14.7 Hz, 7H), 5.68 (d, *J* = 14.4 Hz, 7H), 7.66-7.74 (m, 2H), 8.11-8.33 (m, 4H), 9.02-9.11 (m, 2H). **IR** (KBr): 3432, 3136, 2992, 2921, 2860, 2155, 1738, 1636, 1468 ,1421, 1376, 1321, 1295, 1230, 1189, 1151, 1100, 1043, 1027, 988, 968, 863, 824, 803, 756, 689, 672, 629, 510, 464 cm^{-1}. **MS** *m/z* (%): 1702.6 (13); 1548.6 (100, M$^+$), 1185.3 ([CB[7] + Na]$^+$, 9). **HRMS** (MALDI) *m/z*: [M]$^+$ Calcd for $C_{68}H_{74}N_{29}O_{14}Si^+$ 1548.5734; Found 1548.5774.

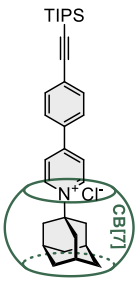

Complex **9·CB[7]** was prepared from compound **9** (26 mg, 51 µmol) and **CB[7]** (78 mg, 51 µmol) in DMSO (45 mL) following **GP2**. Complex **9·CB[7]** was obtained quantitatively as a yellow-brown solid.
^{1}H NMR (400 MHz, DMSO-d_6) δ 0.96 (bs, 6H), 1.14 (s, 21 H), 1.38-1.67 (m, 9H), 4.01-4.71 (m, 14H), 5.43 (s, 14H), 5.55-5.88 (m, 14H), 7.70 (d, *J* = 8.3 Hz, 2H), 8.11-8.35 (m, 4H), 8.97-9.22 (m, 2H). **IR** (KBr): 3432, 3136, 2991, 2922, 2863, 2153, 1738, 1635, 1469, 1420, 1376, 1321, 1294, 1230, 1188, 1151, 1027, 987, 968, 883, 824, 803, 756, 691, 672, 629, 510, 464 cm^{-1}.

3. ^{1}H NMR Study of CB[7] Binding to Guests 1-4 and 8

^{1}H NMR spectra of guests **1-4** with added **CB[7]** (**Figures S1-S8**) were obtained from solutions prepared as following. Stock solutions of guests (c = 10-15 mmol L^{-1}) and **CB[7]** (c = 0.7 mmol L^{-1}) were prepared in DMSO-d_6. Followingly, these stock solutions were used to prepare separate solutions with 0.5 equiv. and 1 equiv. of added **CB[7]**. Total concentration of guests was between 0.2-2 mmol L^{-1}, while the total concentration of **CB[7]** was close to 0.6 mmol L^{-1} for all solutions.

^{1}H NMR spectra of **8** with added **CB[7]** (**Figures S9** and **S10**) in DMSO-d_6 were obtained from titration experiments, where **CB[7]** ($c \approx 9$ mmol L^{-1}) was added step-wise to the solution of guest (c = 5.0 mmol L^{-1}).

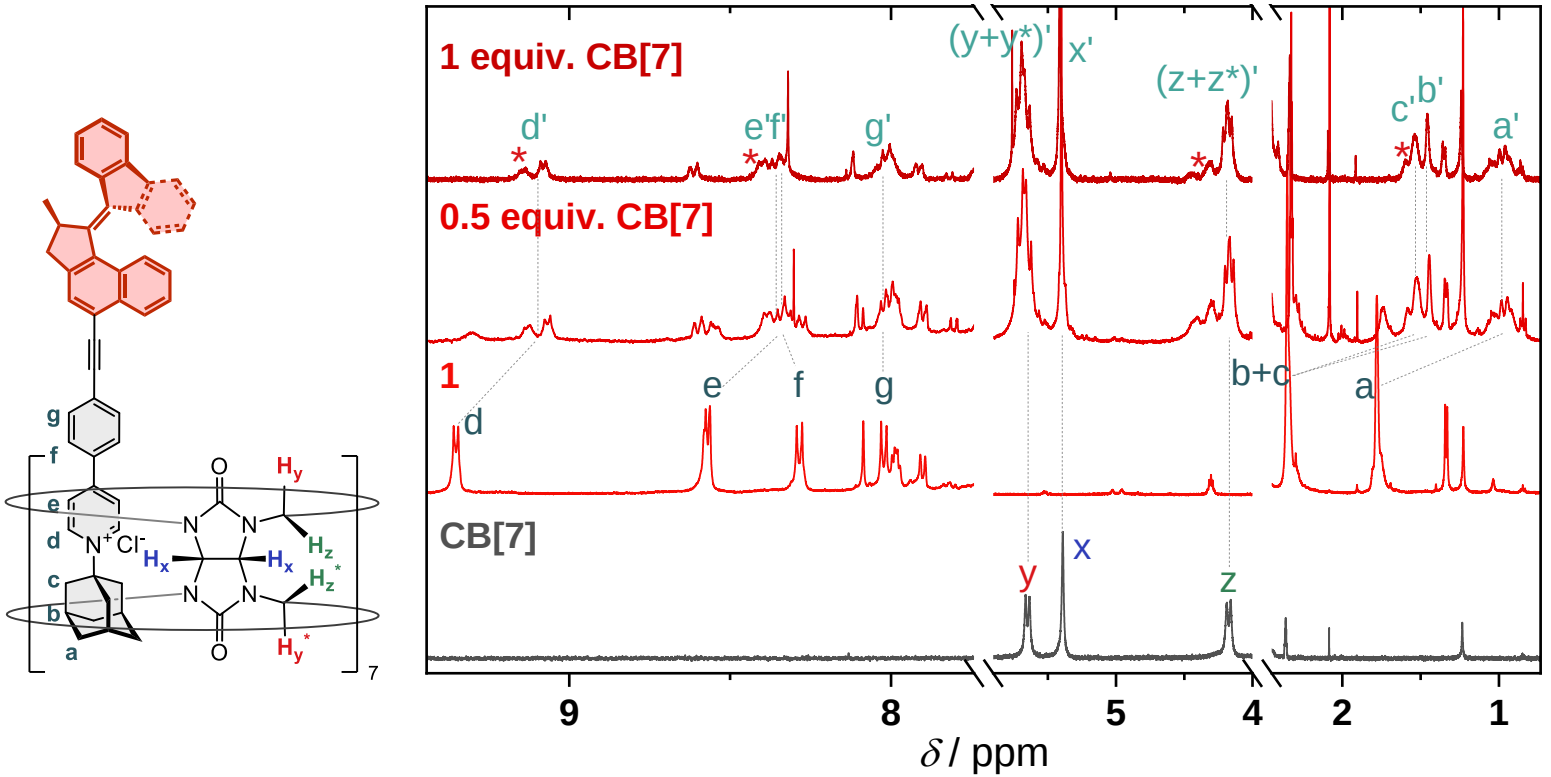

Figure S1. Left: Host-guest complex **1**·**CB[7]**. Right: Selected regions of ^{1}H NMR spectra of neat **CB[7]**, neat **1**, and after addition of 0.5 and 1 equiv. of **CB[7]** in DMSO-d_6 at 25 °C. Signals of the alkali or alkaline-earth metal-promoted trimers are marked with red asterisks (*).

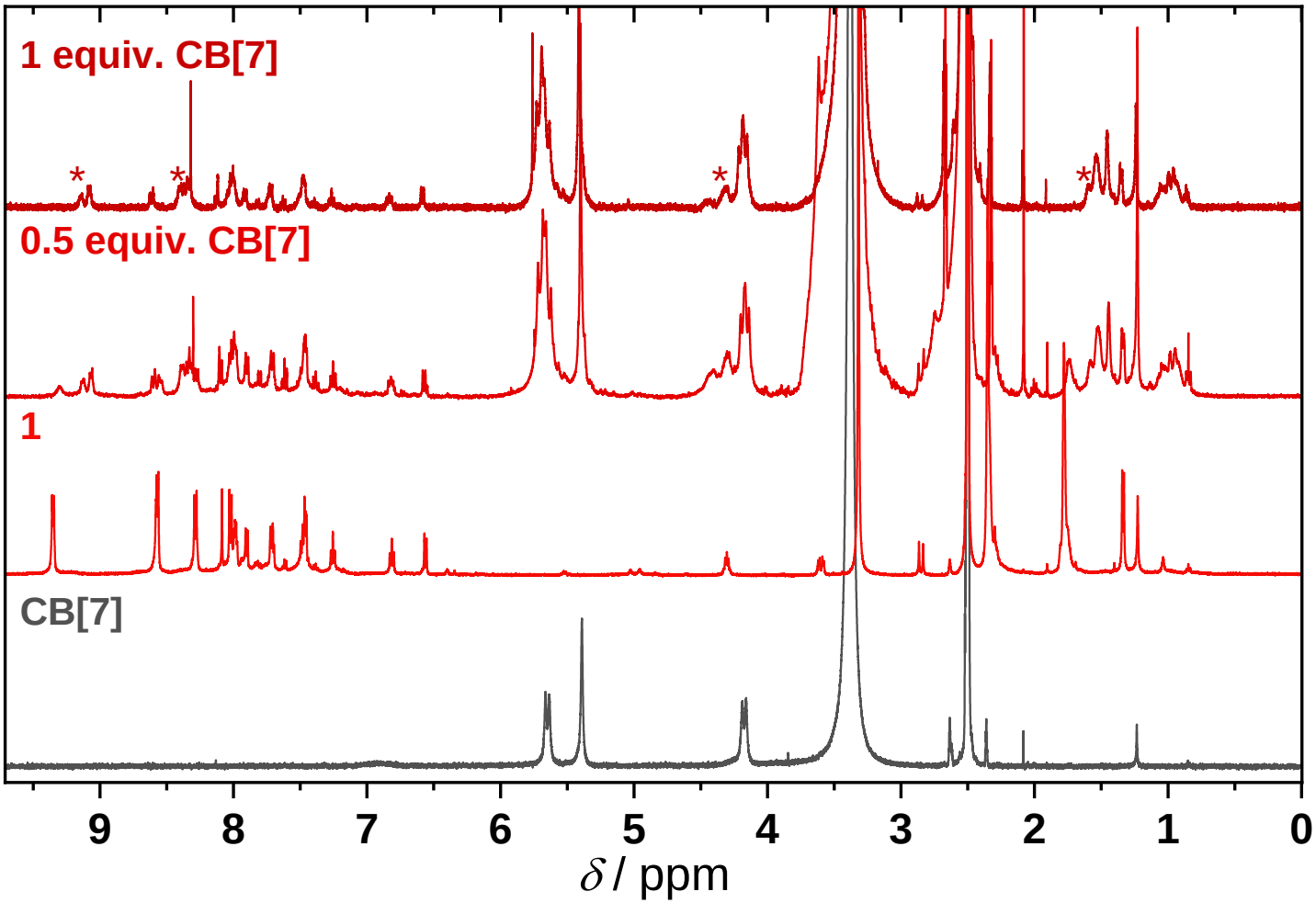

Figure S2. ^{1}H NMR spectra of neat **CB[7]**, neat **1**, and with addition of 0.5 and 1 equiv. of **CB[7]** in DMSO-d_6 at 25 °C. Signals of the alkali or alkaline-earth metal-promoted trimers are marked with red asterisks (*).

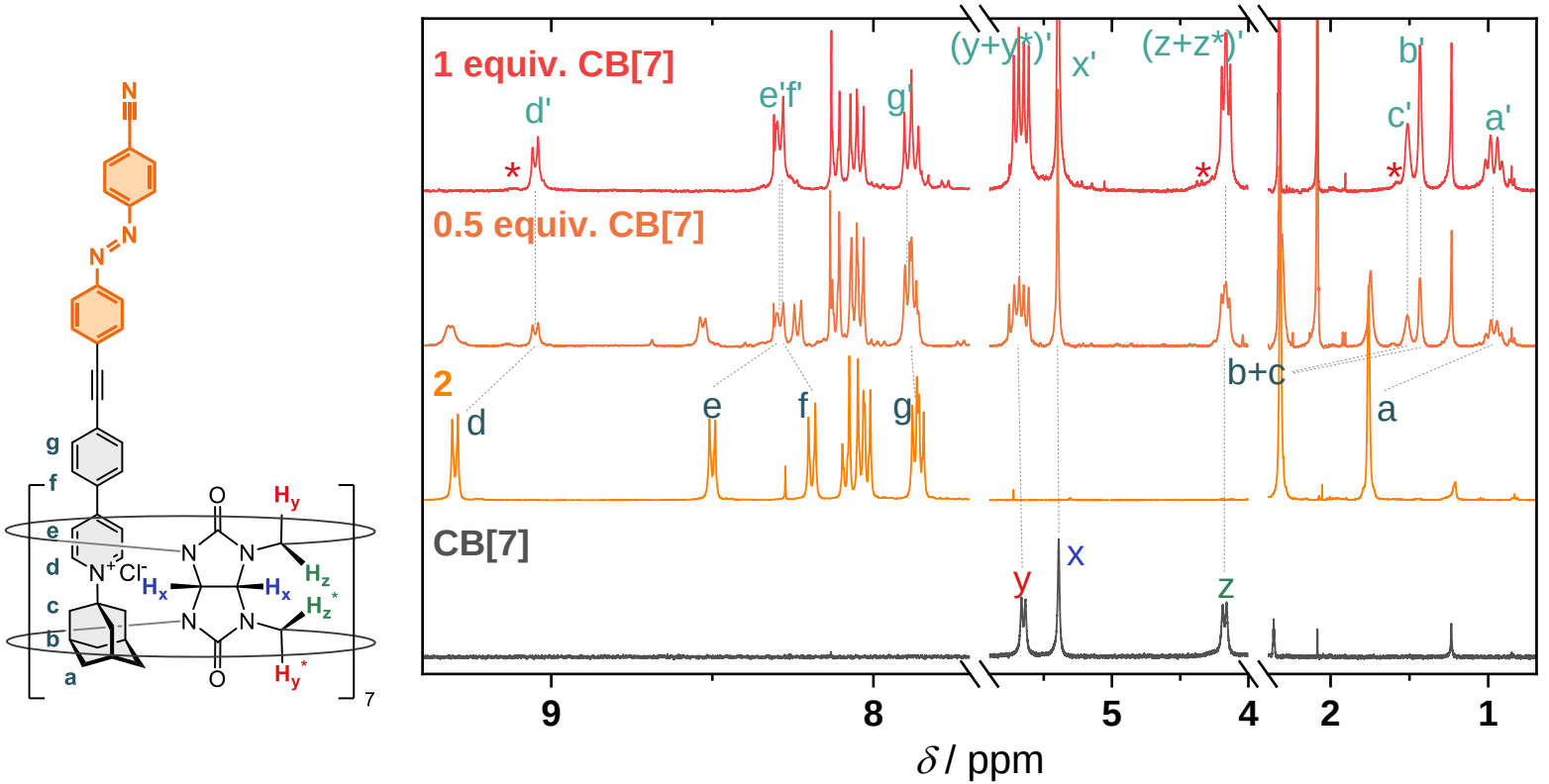

Figure S3. Left: Host-guest complex **2·CB[7]**; Right: Selected regions of ^{1}H NMR spectra of neat **CB[7]**, neat **2**, and after addition of 0.5 and 1 equiv. of **CB[7]** in DMSO-d_6 at 25 °C. Signals of the alkali or alkaline-earth metal-promoted trimers are marked with red asterisks (*).

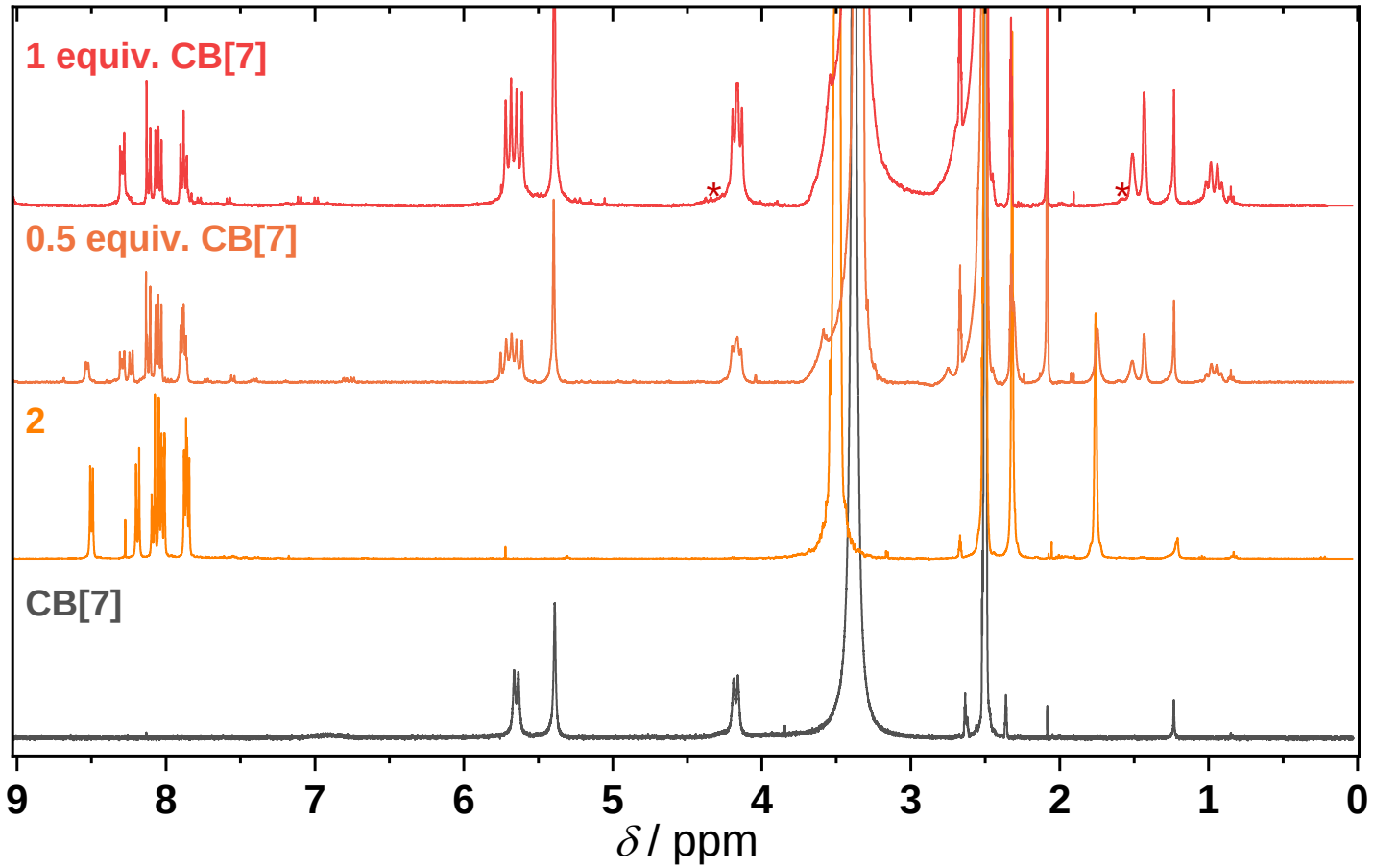

Figure S4. ^{1}H NMR spectra of neat **CB[7]**, neat **2**, and with addition of 0.5 and 1 equiv. of **CB[7]** in DMSO-d_6 at 25 °C. Signals of the alkali or alkaline-earth metal-promoted trimers are marked with red asterisks (*).

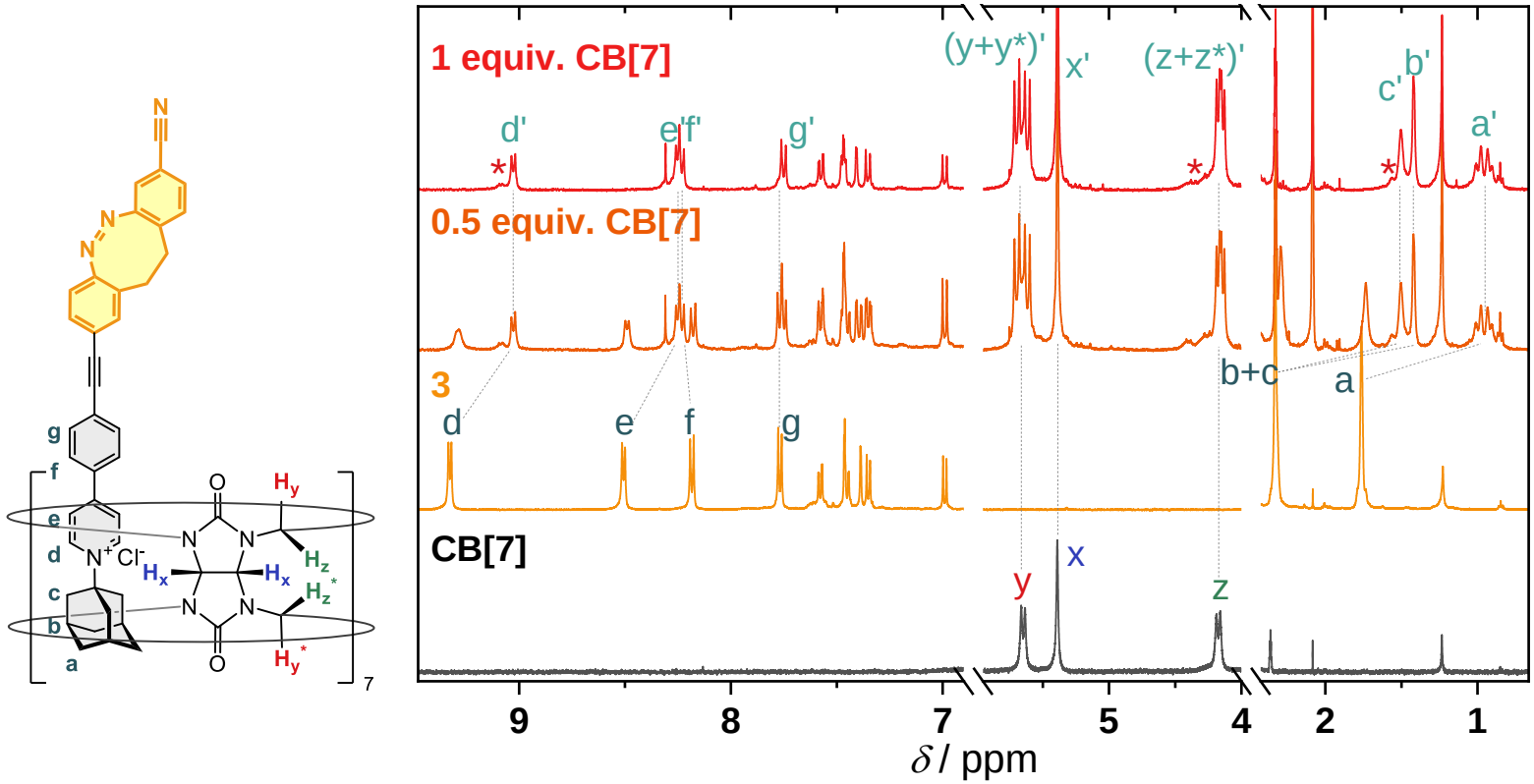

Figure S5. Left: Host-guest complex **3**·**CB[7]**; Right: Selected regions of ^{1}H NMR spectra of neat **CB[7]**, neat **3**, and after addition of 0.5 and 1 equiv. of **CB[7]** in DMSO-d_6 at 25 °C. Signals of the alkali or alkaline-earth metal-promoted trimers are marked with red asterisks (*).

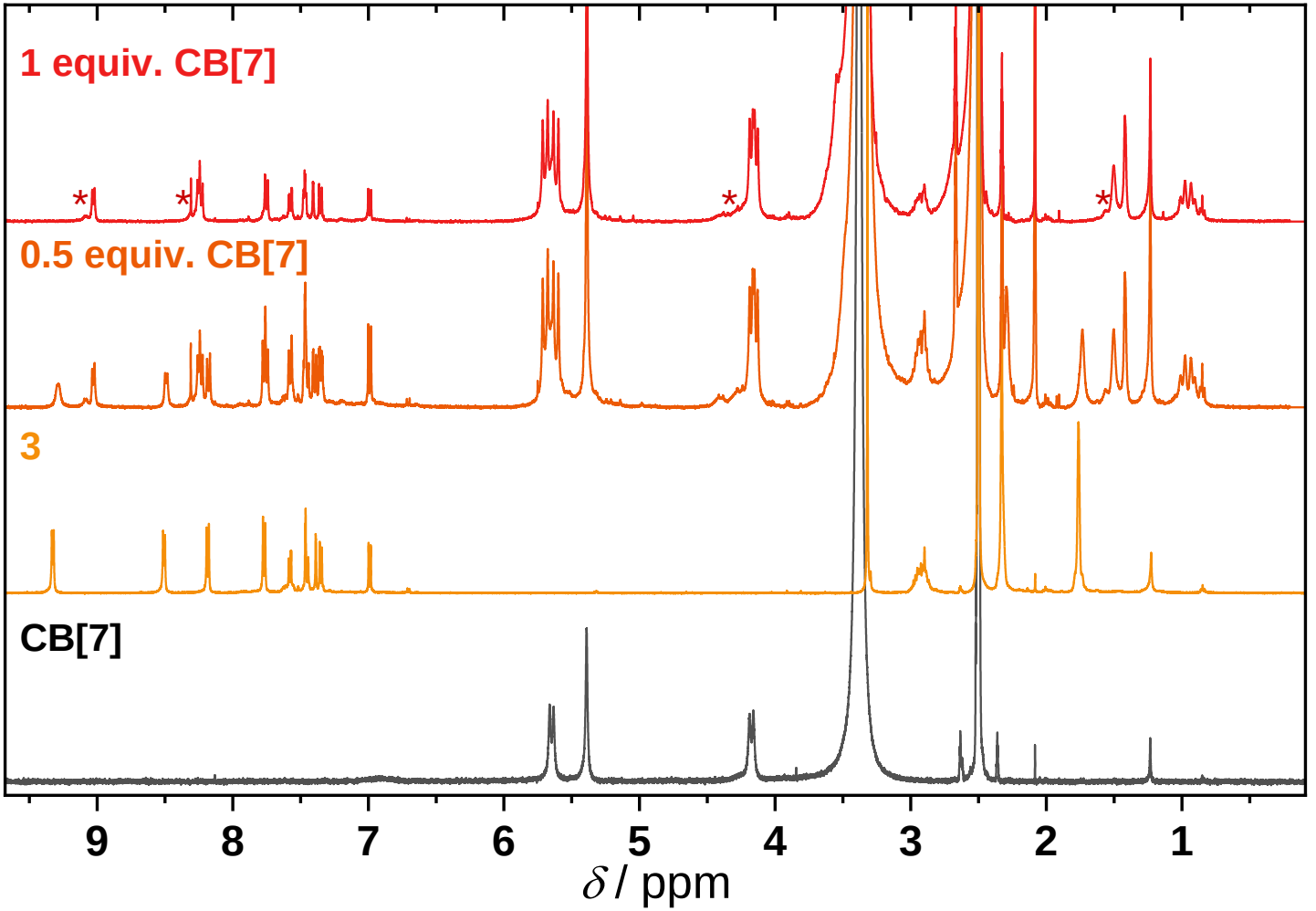

Figure S6. ^{1}H NMR spectra of neat **CB[7]**, neat **3**, and with addition of 0.5 and 1 equiv. of **CB[7]** in DMSO-d_6 at 25 °C. Signals of the alkali or alkaline-earth metal-promoted trimers are marked with red asterisks (*).

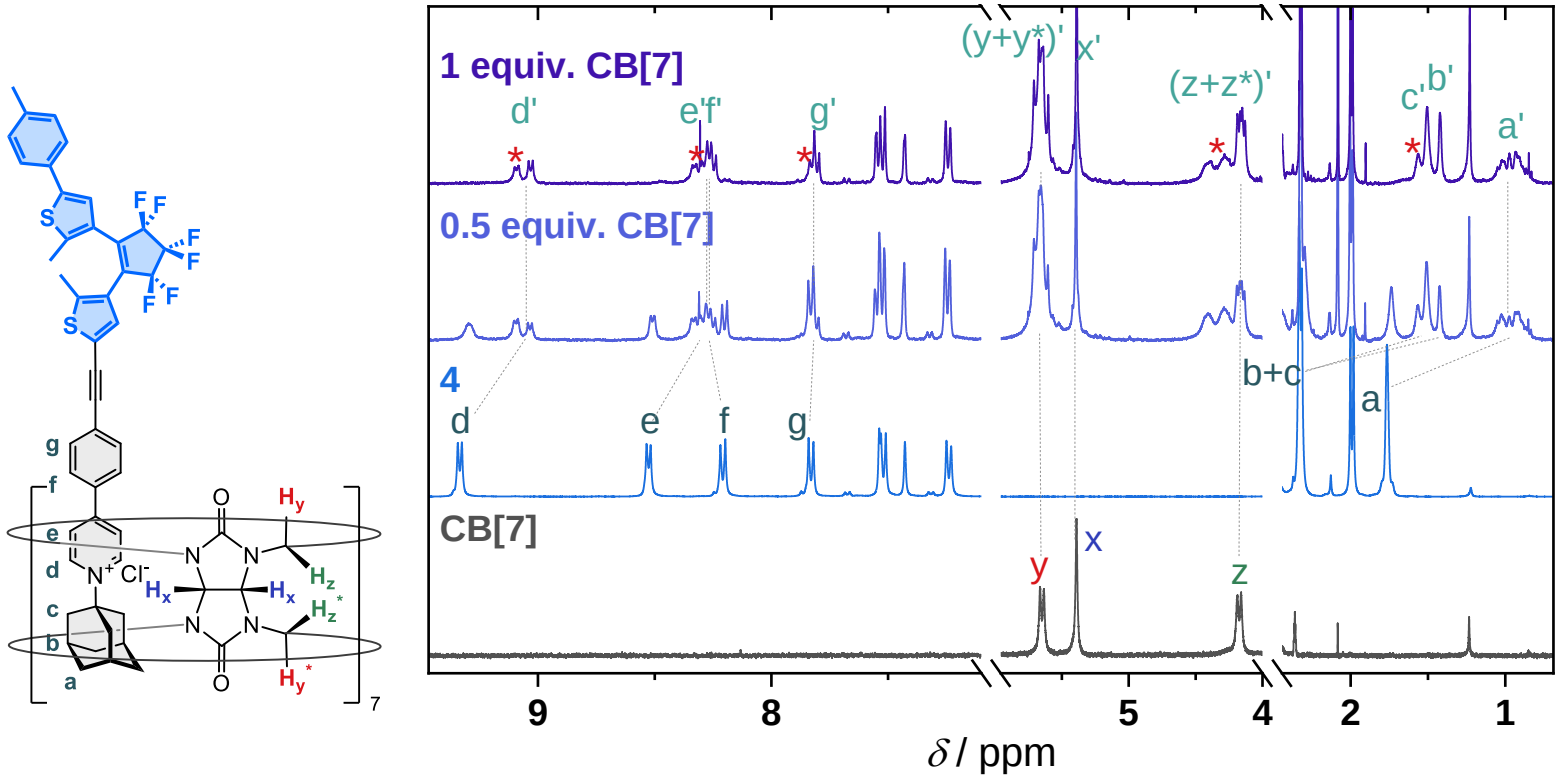

Figure S7. Left: Host-guest complex **4**·**CB[7]**; Right: Selected regions of ^{1}H NMR spectra of neat **CB[7]**, neat **4**, and after addition of 0.5 and 1 equiv. of **CB[7]** in DMSO-d_6 at 25 °C. Signals of the alkali or alkaline-earth metal-promoted trimers are marked with red asterisks (*).

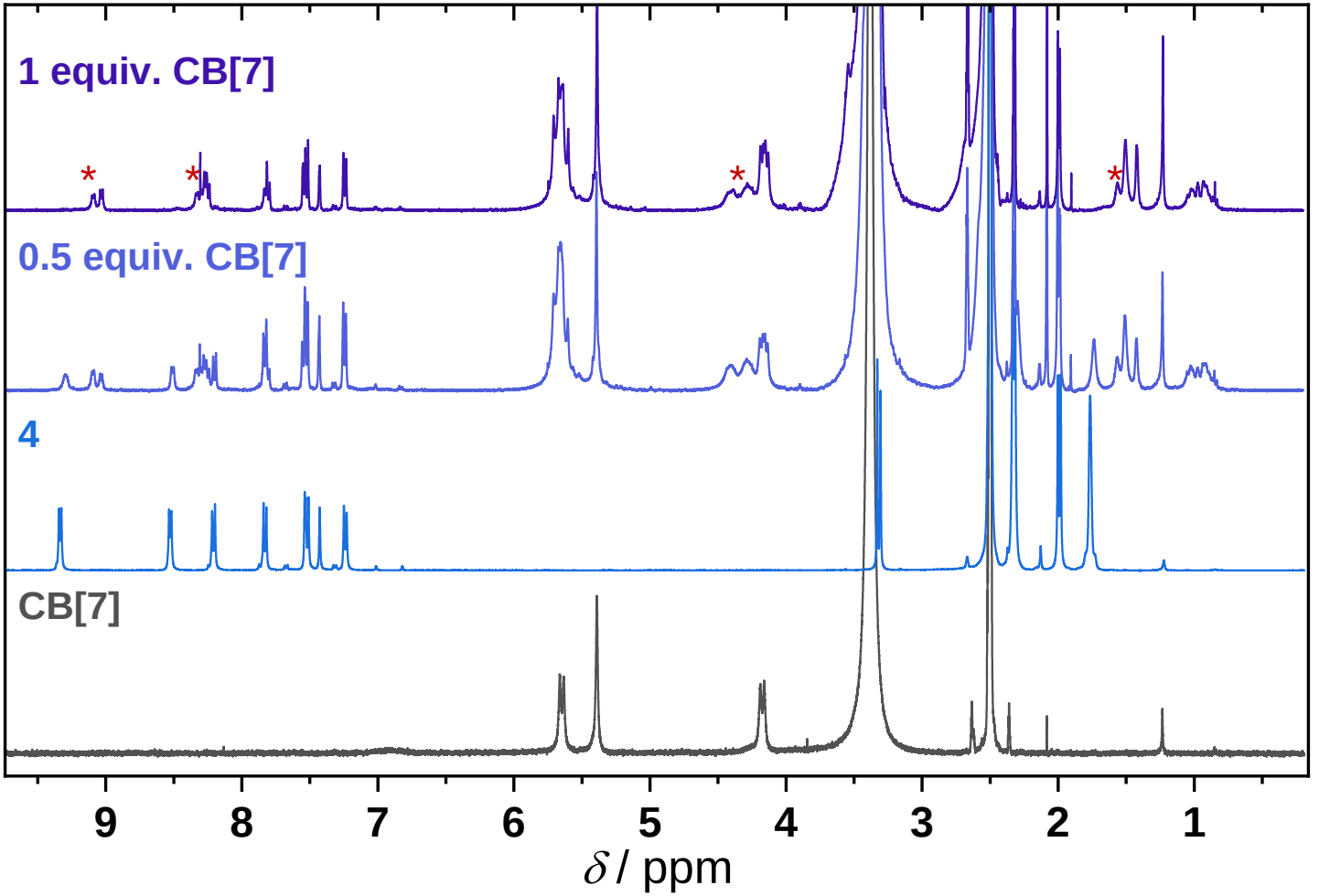

Figure S8. ^{1}H NMR spectra of neat **CB[7]**, neat **4**, and with addition of 0.5 and 1 equiv. of **CB[7]** in DMSO-d_6 at 25 °C. Signals of the alkali or alkaline-earth metal-promoted trimers are marked with red asterisks (*).

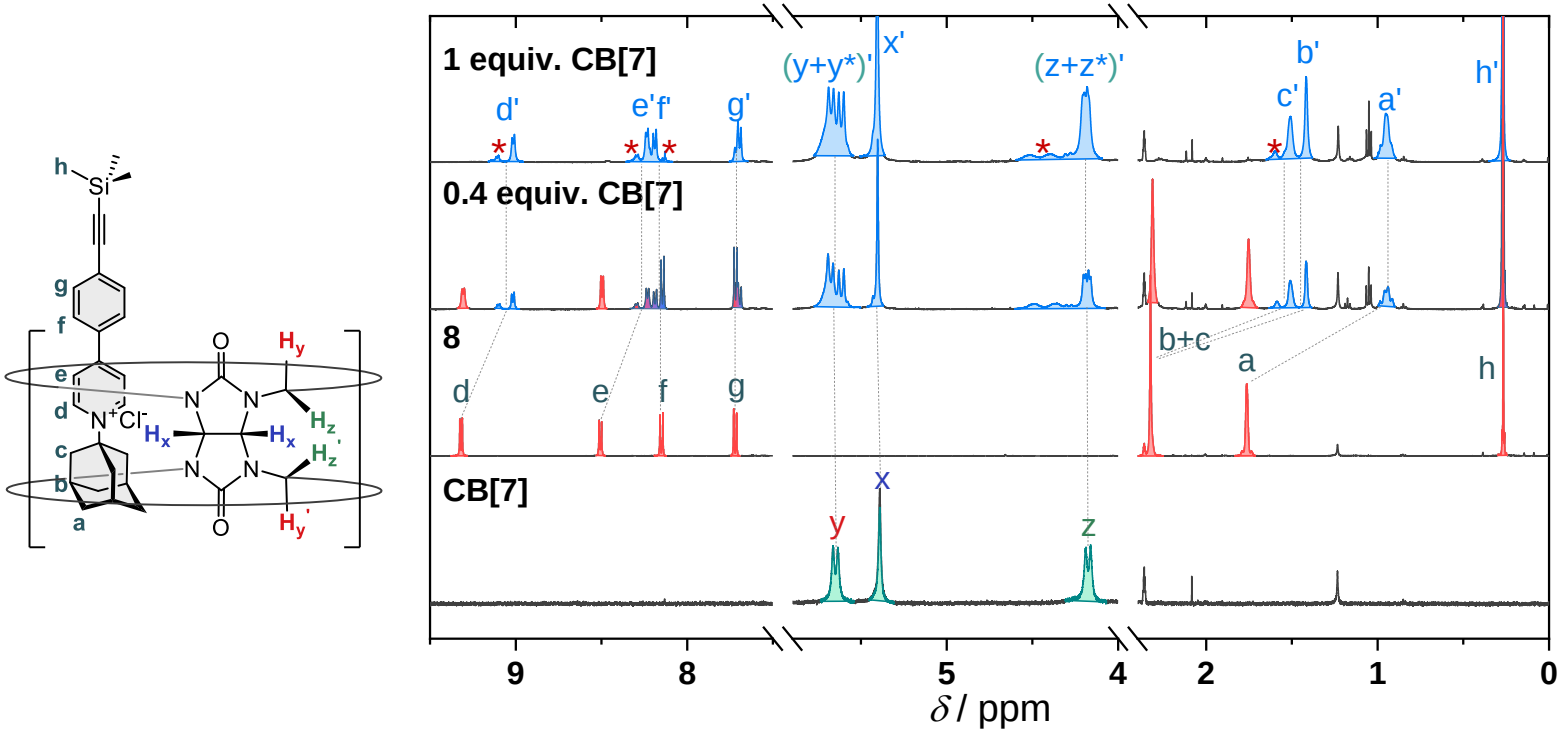

Figure S9. Left: Host-guest complex **8·CB[7]**. Right: Selected regions of ^{1}H NMR spectra of neat **CB[7]**, neat **8**, and after addition of 0.4 and 1 equiv. of **CB[7]** in DMSO-d_6 at 25 °C. Signals of the alkali or alkaline-earth metal-promoted trimers are marked with red asterisks (*).

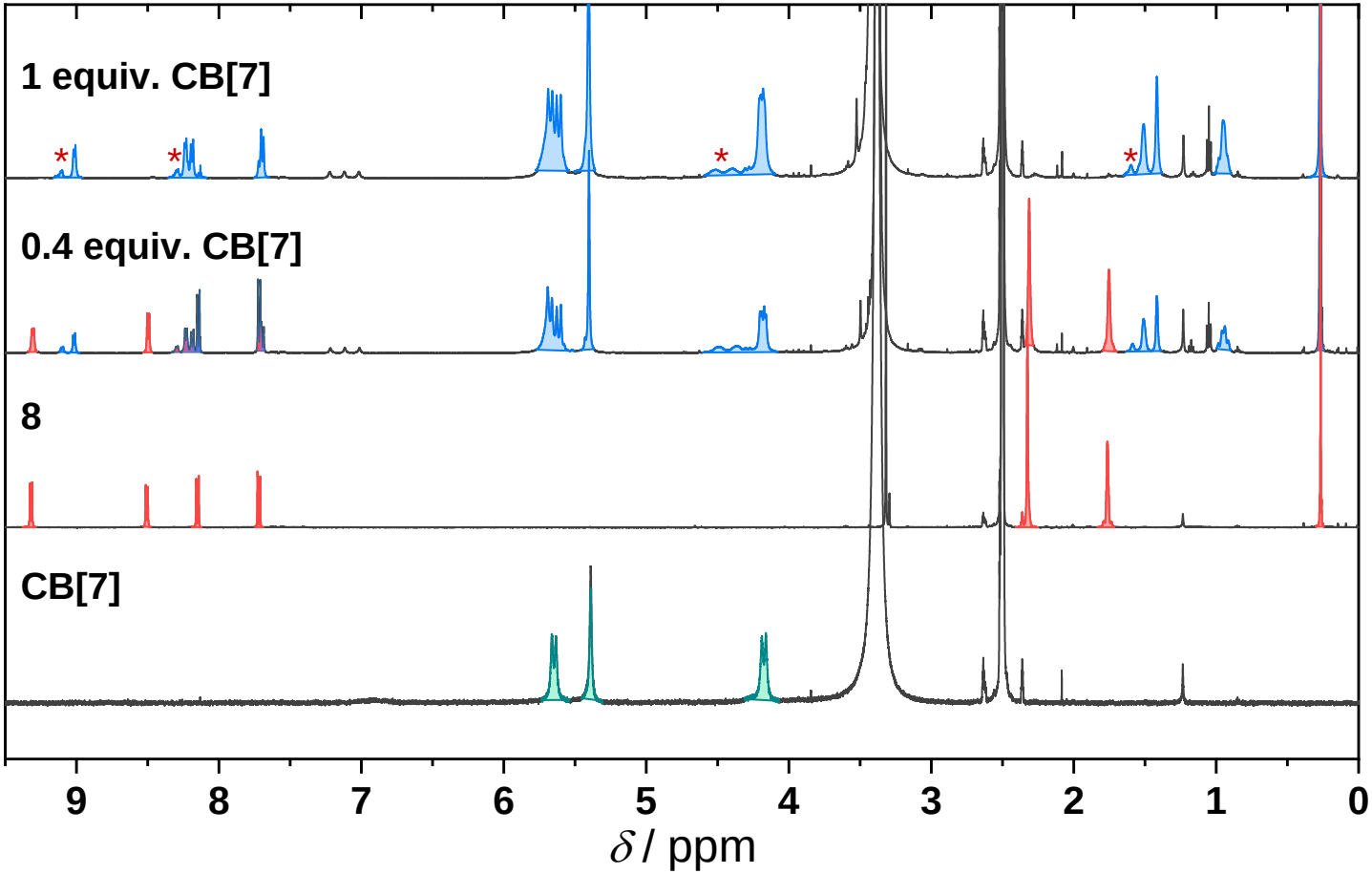

Figure S10. ^{1}H NMR spectra of neat **CB[7]**, neat **8**, and with addition of 0.5 and 1 equiv. of **CB[7]** in DMSO-d_6 at 25 °C. Signals of the alkali or alkaline-earth metal-promoted trimers are marked with red asterisks (*).

4. UV-Vis Characterization of Photoswitching and Thermal Isomerization Kinetics

UV–vis spectra were recorded on a Varian Cary 5000 spectrophotometer equipped with Cary WinUV software. Spectroscopic grade acetonitrile, chloroform, and DMSO were used for solution preparation. Measurements were performed in quartz cuvettes with a 1 cm optical path length.

Temperature control, cooling, and irradiation were achieved using a custom-built cell holder (**Figure S11**), designed and manufactured at the Institute of Organic Chemistry and Biochemistry. The setup incorporates a water-cooled Peltier element and integrated LED modules, enabling precise thermal regulation and sample illumination. The system interfaces with a PC via USB connection and is operated by custom-written software for temperature control, maintaining a stability of ±0.06 °C over the entire experimental range.

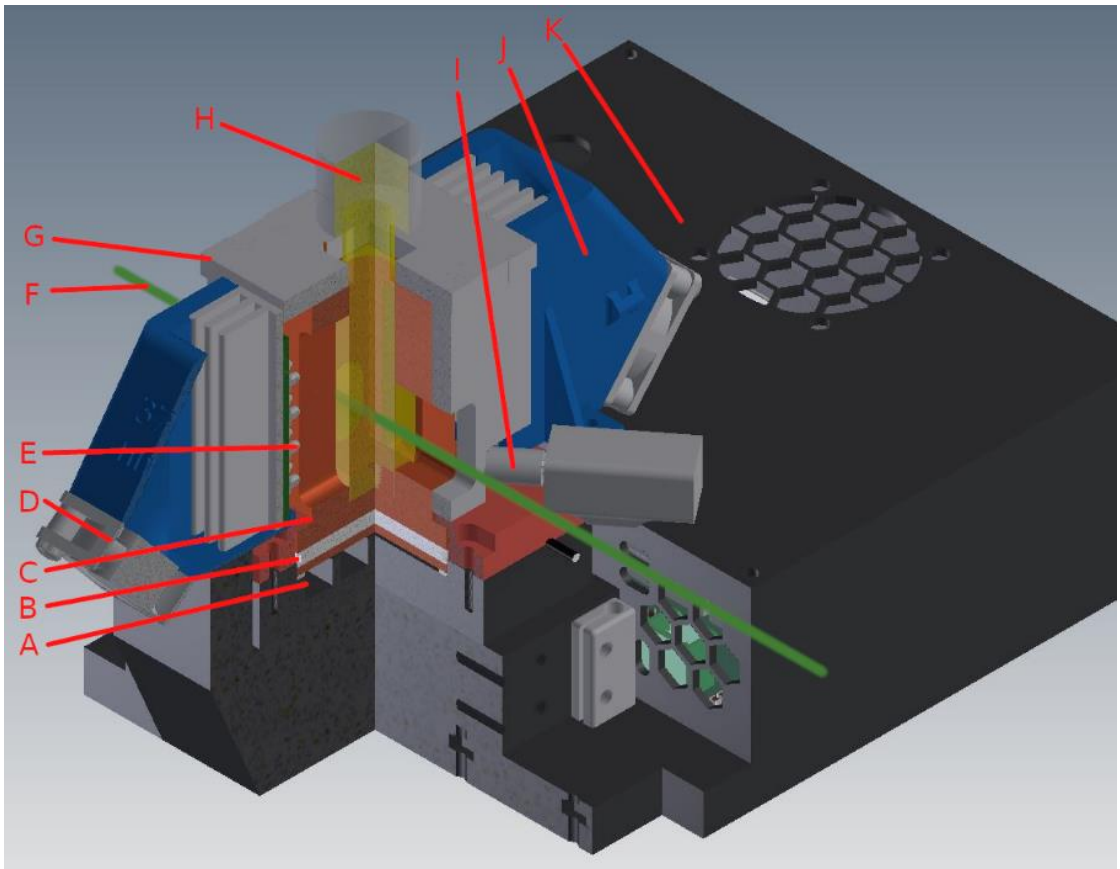

Figure S11. Schematic representation of the Thermophotoreactor setup: (a) Core thermal management assembly showing the copper holder (**C**) mounted on the Peltier element (**B**), equipped with water cooling (**A**), and encased in insulating foam (**G**) for optimal thermal control; (b) Illumination system comprising two diode modules: the first module shown in cross-section reveals its internal components, cooling fan (**D**) and diodes (**E**), while the second module is depicted as a complete sealed unit (**J**); (c) Measurement configuration displaying the measuring beam (**F**) path through the cuvette with sample (**H**); (d) Additional components including the stirrer (**I**) and electronic controller case (**K**) for system operation and control.

The cell holder design includes dual LED module slots, allowing simultaneous irradiation of UV–vis cuvette samples with two distinct LED diodes. The LED modules are easily interchangeable and positioned at a working distance of 1 cm from the sample through direct mounting on the temperature-controlled holder. Both the temperature and LED modules

are operated via the same control software, which enables adjustment of irradiation time and intensity. Integration of the LED modules within the UV–vis spectrometer eliminates the need for sample manipulation between irradiation and spectroscopic measurement, thereby preventing exposure to ambient light and minimizing delay between irradiation and data acquisition. The light fluxes and spectral bandwidths of the irradiation LEDs are summarized in **Table S1**; unless otherwise stated, all LEDs were operated at 100% output intensity.

Table S1. Light fluxes and spectral widths of diodes used to irradiate the samples.

λ_{max}[a] / nm	275	308 (312)	309 (306)[b]	370 (365)	400 (396)	400 (398)[b]
light flux / W cm^{-2}	0.016	0.0043	0.014	0.13	0.98	0.019
full width at half maximum / nm	269-281	305-319	300-312	359-376	390-401	393-403
full width at 5% of maximum / nm	262-293	298-345	264-331	354-392	382-416	385-416

λ_{max}[a] / nm	450 (452)	505 (504)	530 (528)	590 (589)[b]	600 (595)
light flux / W cm^{-2}	0.79	0.13	0.95	0.011	0.086
full width at half maximum / nm	447-457	489-520	517-542	582-594	587-601
full width at 5% of maximum / nm	430-487	472-555	498-575	565-604	565-615

[a] LEDs were referred throughout the text by the nominal wavelengths of irradiation maxima that are provided by the manufacturer. Wavelengths of irradiation maxima determined by measurement of LED spectral profiles are given in parentheses. [b] LEDs that were used solely for quantum yield determination.

Rates of thermal isomerization were determined by recording up to 220 sequential UV–vis spectra immediately after establishing the metastable photostationary state, while maintaining constant sample temperature using the custom-built cell holder. The time intervals between individual measurements were adjusted such that the total acquisition time corresponded approximately to three half-lives of the metastable species. For systems exhibiting very fast relaxation, where the optimal acquisition interval was shorter than one minute, only the spectral region containing relevant absorption bands (for example, 350–600 nm) was monitored. The experimental data were fitted to a single-exponential decay model (Eq. 1) using the least-squares method:

$$A = A_0 \times 0.5^{\frac{t}{t_{1/2}}} \qquad \text{(Eq. 1)}$$

UV–vis spectra of compounds **10–13** were recorded in chloroform, displaying the typical spectral features characteristic of these previously reported molecular switches (**Figure S12-S18**).[5,6] Conjugation to the phenyl-pyridinium moiety results in distinct spectral differences between compounds **1–4** and their corresponding iodide precursors **10–13**; however, the spectral changes observed upon photoisomerization of **1–4** are analogous to those of the parent iodides.

For the overcrowded alkene **1**, a characteristic absorption band with a maximum at λ_{max} = 437 nm was observed in DMSO (**Figure S19**). Upon irradiation at 400 nm, the compound is converted to the metastable form, accompanied by a slight bathochromic shift and a decrease in absorbance intensity. The stable form is regenerated either by irradiation at 525 nm or via thermal helix inversion (**Figure S20**). Compound **1** exhibited excellent photochemical stability, retaining over 99% of its initial absorbance intensity at 430 nm after ten consecutive switching cycles in acetonitrile.

The UV–vis spectrum of azobenzene derivative **2** in DMSO exhibits an absorption band corresponding to the π-π* transition with a maximum at λ_{max} = 374 nm (**Figure S21**). Irradiation at 400 nm induces *trans*-to-*cis* photoisomerization, establishing a photostationary state (PSS) between the two isomers. This process is accompanied by a decrease in the π–π* band intensity, while the n–π* transition characteristic of the *cis* isomer appears only as a weak band. The *trans* form can be regenerated either by irradiation at 450 nm or by thermal relaxation in the dark (**Figure S22**). After ten consecutive photoisomerization cycles in acetonitrile, the absorbance of the *trans* form at 370 nm decreased by approximately 1%, indicating negligible photodegradation.

The UV–vis spectrum of diazocine *cis*-**3** in DMSO displays an absorption band with a maximum at λ_{max} = 349 nm. Irradiation at 400 nm generates a PSS between the *cis* and *trans* isomers, accompanied by a slight decrease in the 349 nm band intensity and the appearance of a new absorption band between 435 and 615 nm (**Figure S23**). Subsequent irradiation at 505 nm induces the reverse *cis*-to-*trans* photoisomerization, while the *cis* form can also be regenerated thermally in the dark (**Figure S24**). Compound **3** exhibited excellent fatigue resistance, maintaining its spectral characteristics after ten consecutive switching cycles in acetonitrile.

Irradiation of the open form of dithienylethene **4o** in DMSO at 308 nm induces electrocyclization to the closed form **4c**, as evidenced by the appearance of a new absorption band with a maximum at λ_{max} = 623 nm (**Figure S25**). The closed form is thermally stable and remains indefinitely persistent under dark conditions. The open form can be regenerated by photochemical ring-opening upon irradiation at 600 nm. Similar to the iodide precursor **13**, compound **4** exhibited noticeable photodegradation after ten photoisomerization cycles in acetonitrile. The formation of photochemical byproducts during electrocyclization has previously been reported for dithienylperfluorocyclopentenes lacking substitution at the **4-** and **4′-**positions of the thienyl rings.[11]

UV–vis spectra of the complexes **1–4·CB[7]** were recorded in DMSO solution. A decrease in the molar attenuation coefficients of the guest absorption bands was observed compared to the spectra of the free guests. This effect is most likely attributed to the hygroscopic nature of **CB[7]** and the presence of minor impurities remaining after the separation process,[12] which increase the apparent molar mass of the complexes. The photostability and kinetic parameters of the thermal isomerization processes were comparable to those of the corresponding uncomplexed guests. (**Figures S26-S32**).

11. Irie, M.; Lifka, T.; Uchida, K.; Kobatake, S.; Shindo, Y. Fatigue Resistant Properties of Photochromic Dithienylethenes: By-Product Formation. *Chem. Commun.* **1999**, No. 8, 747–750. https://doi.org/10.1039/a809410a.
12. Yi, S.; Kaifer, A. E. Determination of the Purity of Cucurbit[*n*]Uril (*n* = 7, 8) Host Samples. *J. Org. Chem.* **2011**, *76* (24), 10275–10278. https://doi.org/10.1021/jo2018312.

5.1 Compounds 10-13

Compound **10**

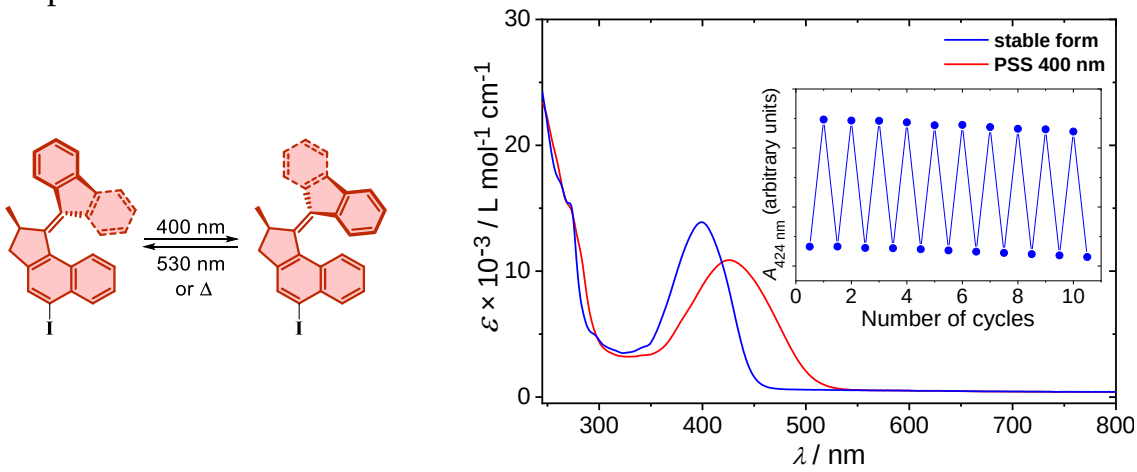

Figure S12. Left: Switching of **10**. Right: UV-Vis spectra of **10** (c = 2.8 × 10^{-5} mol L^{-1}) in chloroform: — in stable form and — in PSS reached after 4 min of irradiation with 400 nm light (used at 1% intensity); Insert: absorbance of **10** (c = 2.8 × 10^{-5} mol L^{-1}) in chloroform at 424 nm after subsequent cycles of irradiation with 400 nm light (4 min, used at 1% intensity) and 530 nm light (6 min).

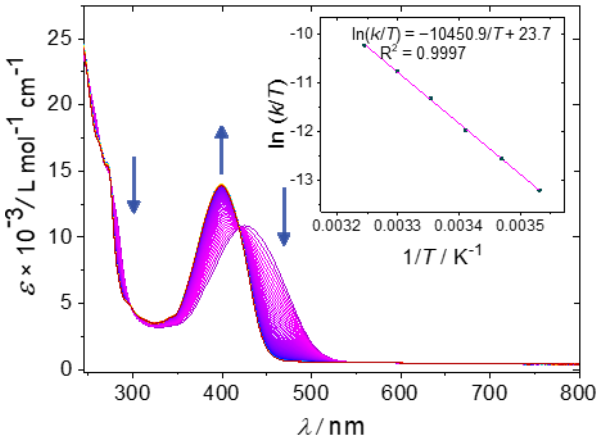

Figure S13. Thermal helix inversion of overcrowded alkene **10** (c = 2.8 × 10^{-5} mol L^{-1}) in chloroform after 4 min of irradiation with 400 nm light at 10 °C; Insert: Eyring plot of thermal helix inversion of **10** in chloroform.

Compound **11**

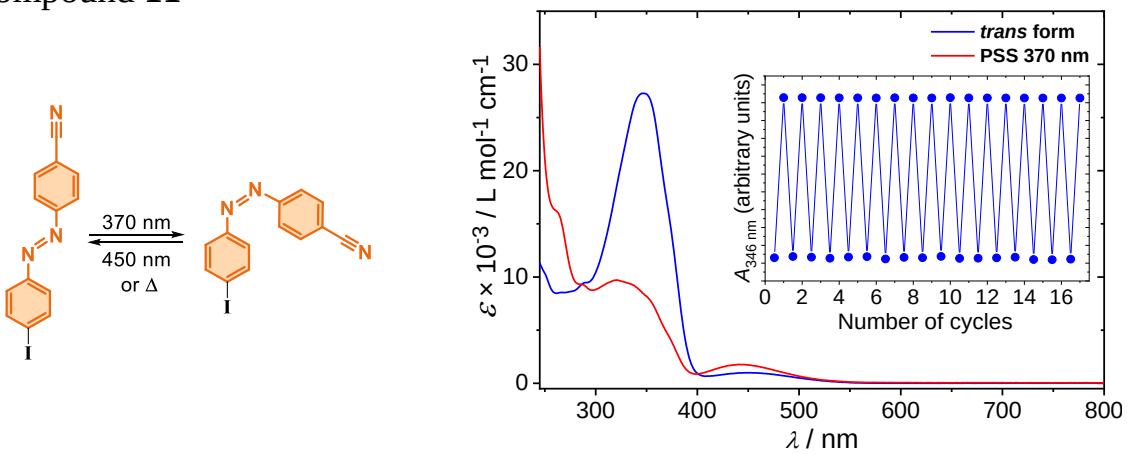

Figure S14. Left: Switching of **11**. Right: UV-Vis spectra of **11** (c = 9.0 × 10^{-6} mol L^{-1}) in chloroform: — before irradiation and — in PSS reached after 5 seconds of irradiation with 370 nm light; Insert: absorbance of **11** in chloroform at 346 nm after subsequent cycles of irradiation with 370 nm light (10 s) and 450 nm light (15 s).

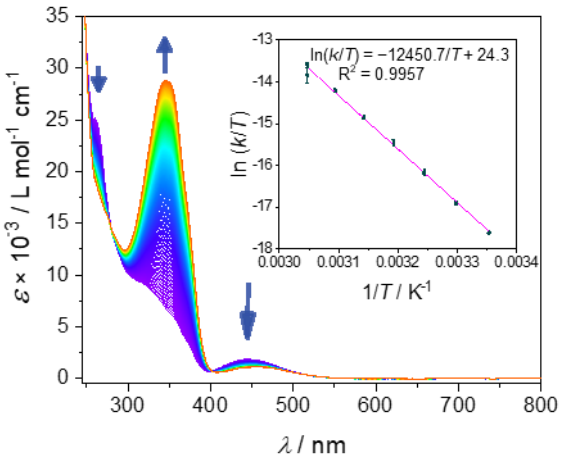

Figure S15. Thermal *cis*-to-*trans* interconversion of azobenzene **11** (c = 9.0 × 10^{-6} mol L^{-1}) in chloroform after 10 s of irradiation with 370 nm light at 25 °C; Insert: Eyring plot of thermal *cis*-to-*trans* interconversion of **11** in chloroform.

Compound **12**

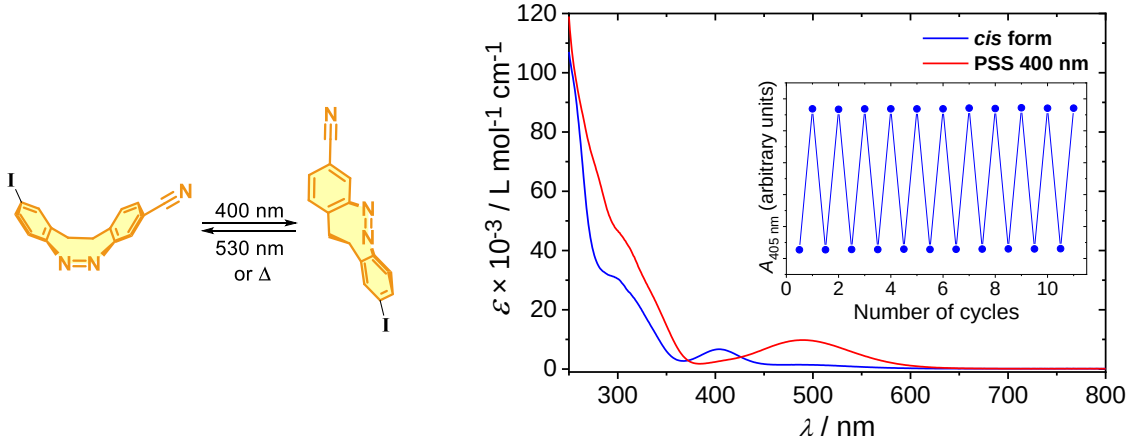

Figure S16. Left: Switching of **12**. Right: UV-Vis spectra of **12** (c = 1.9 × 10^{-5} mol L^{-1}) in chloroform: — before irradiation and — in PSS reached after 15 s of irradiation with 400 nm light; Insert: absorbance of **12** (c = 1.9 × 10^{-5} mol L^{-1}) in chloroform at 405 nm after subsequent cycles of irradiation with 400 nm light (15 s) and 530 nm light (15 s).

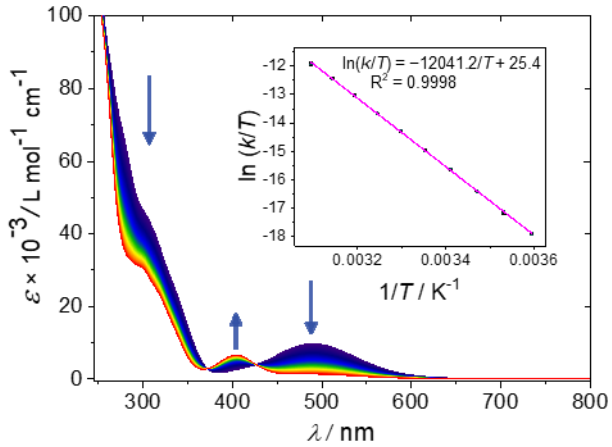

Figure S17. Thermal *trans*-to-*cis* interconversion of diazocine **12** (c = 1.9 × 10^{-5} mol L^{-1}) in chloroform after 15 s of irradiation with 400 nm light at 20 °C; Insert: Eyring plot of thermal *trans*-to-*cis* interconversion of **12** in chloroform.

Compound **13**

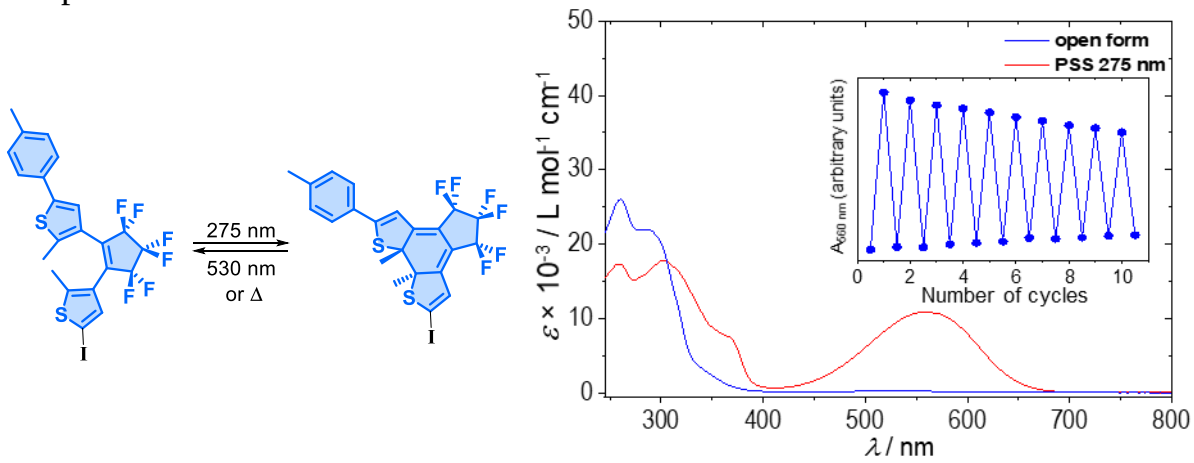

Figure S18. Left: switching of **13**. Right: UV-Vis spectra of **13** (c = 2.3 × 10^{-5} mol L^{-1}) in chloroform:— open form and — in PSS reached after 1 min of irradiation with 275 nm light; Insert: Absorbance of **13** in acetonitrile at 560 nm after subsequent cycles of irradiation with 275 nm light (70 s, used at 70% intensity) and 530 nm light (120 s, used at 70% intensity).

5.2 Compounds 1-4

Compound **1**

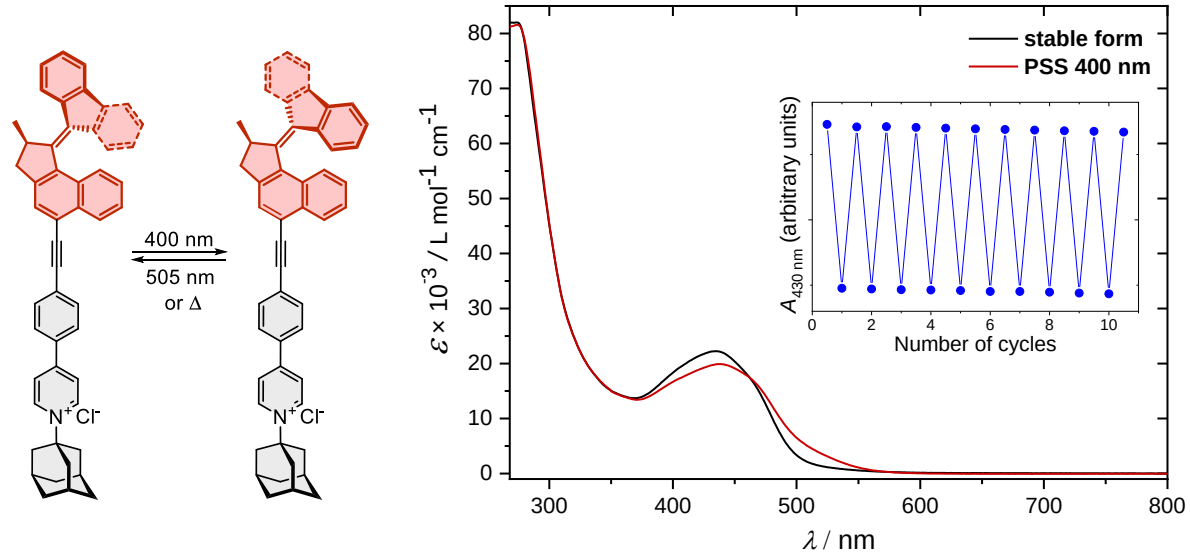

Figure S19. Left: Switching of **1**. Right: UV-Vis spectra of **1** (c = 1.3 × 10^{-5} mol L^{-1}) in DMSO: — before irradiation and — in PSS reached after 55 seconds of irradiation with 400 nm light; Insert: absorbance of **1** (c = 1.4 × 10^{-5} mol L^{-1}) in acetonitrile at 430 nm after subsequent cycles of irradiation with 400 nm light (4 min, used at 1% intensity) and 525 nm light (1 min) at 10 °C.

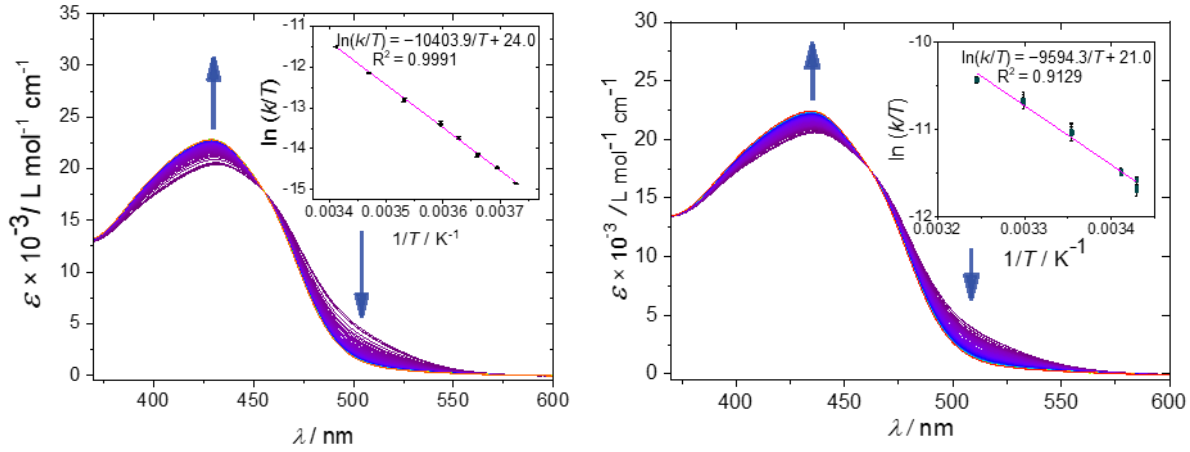

Figure S20. Left: Thermal helix interconversion of guest **1** (c = 1.6 × 10^{-5} mol L^{-1}) in acetonitrile after 55 seconds of irradiation with 400 nm light at 20 °C; Insert: Eyring plot of thermal helix inversion of **1** in acetonitrile. Left: Thermal helix inversion of guest **1** (c = 1.5 × 10^{-5} mol L^{-1}) in DMSO after 55 seconds of irradiation with 400 nm light at 20 °C; Insert: Eyring plot of thermal helix inversion of **1** in DMSO.

Compound **2**

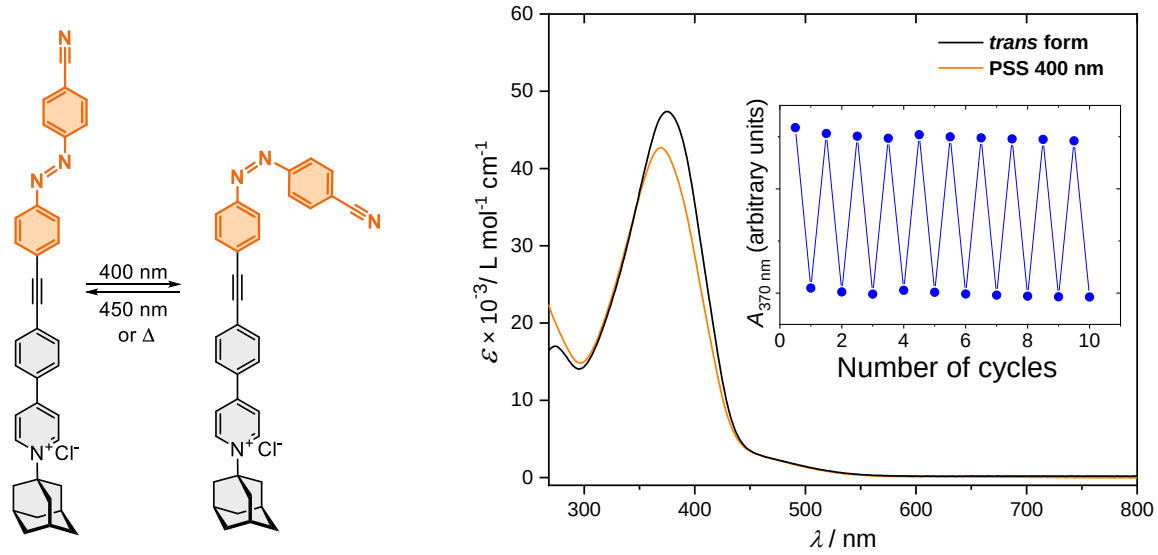

Figure S21. Left: Switching of **2**. Right: UV-Vis spectra of **2** (c = 1.0 × 10^{-5} mol L^{-1}) in DMSO: — before irradiation and — in PSS reached after 20 minutes of irradiation with 400 nm light; Insert: Absorbance of **2** (c = 1.5 × 10^{-5} mol L^{-1}) in acetonitrile at 370 nm after subsequent cycles of irradiation with 400 nm light (20 min) and 450 nm light (1 min).

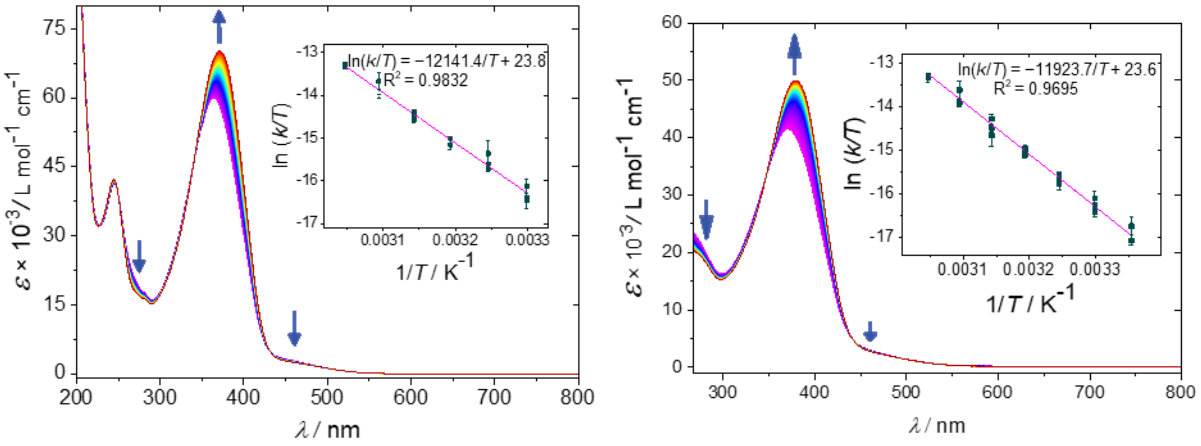

Figure S22. Left: Thermal *cis*-to-*trans* interconversion of guest **2** (c = 1.5 × 10^{-5} mol L^{-1}) in acetonitrile after 20 min of irradiation with 400 nm light at 30 °C; Insert: Eyring plot of *cis*-to-*trans* interconversion of guest **2** in acetonitrile. Right: Thermal *cis*-to-*trans* interconversion of guest **2** (c = 1.0 × 10^{-5} mol L^{-1}) in DMSO after 20 min of irradiation with 400 nm light at 25 °C; Insert: Eyring plot of *cis*-to-*trans* interconversion of guest **2** in DMSO.

Compound **3**

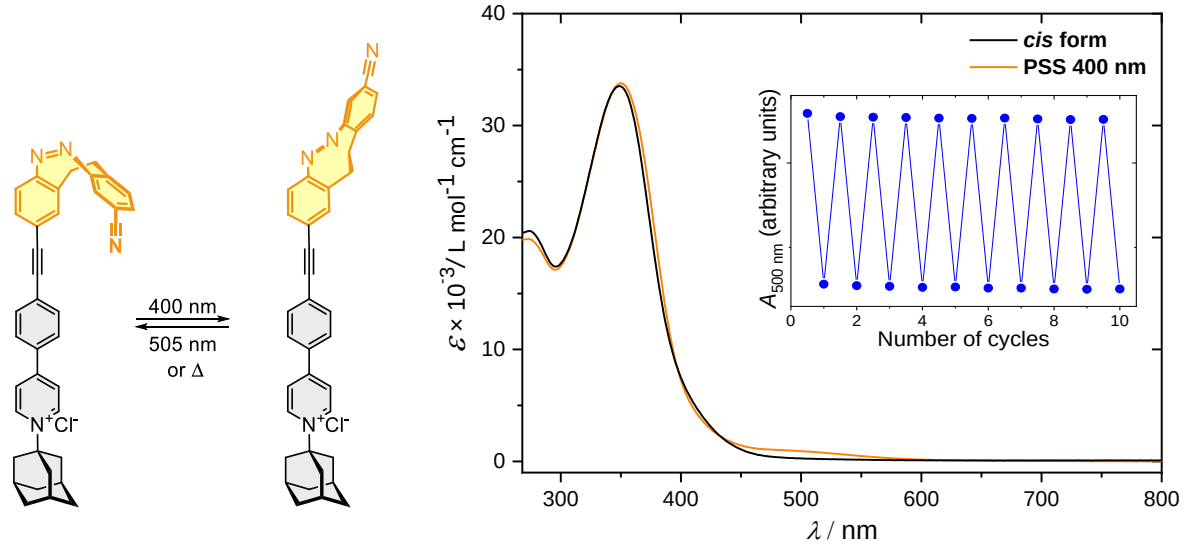

Figure S23. Left: Switching of **3**. Right: UV-Vis spectra of **3** (c = 2.0 × 10^{-5} mol L^{-1}) in DMSO: — before irradiation and — in PSS reached after 8 minutes of irradiation with 400 nm light; Insert: absorbance of **3** (c = 3.0 × 10^{-5} mol L^{-1}) in acetonitrile at 500 nm after subsequent cycles of irradiation with 400 nm light (8 min) and 505 nm light (3 min).

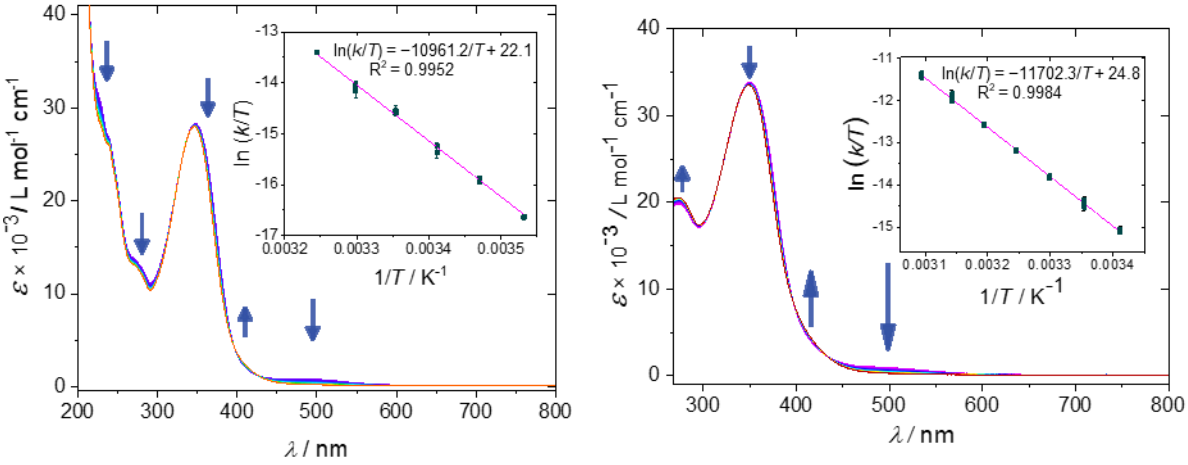

Figure S24. Left: Thermal *trans*-to-*cis* interconversion of guest **3** (c = 3.0 × 10^{-5} mol L^{-1}) in acetonitrile after 8 min of irradiation with 400 nm light at 25 °C; Insert: Eyring plot of thermal *trans*-to-*cis* interconversion of **3** in acetonitrile. Right: Thermal *trans*-to-*cis* interconversion of guest **3** (c = 2.0 × 10^{-5} mol L^{-1}) in DMSO after 8 minutes of irradiation with 400 nm light at 25 °C; Insert: Eyring plot of *trans*-to-*cis* interconversion of **3** in DMSO.

Compound **4**

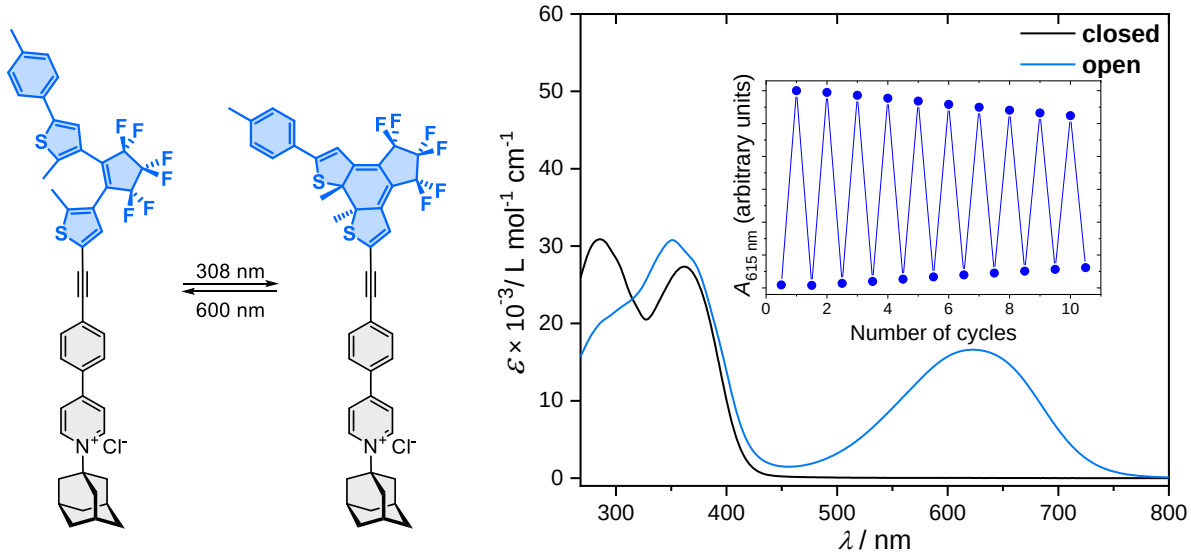

Figure S25. Left: Switching of **4**. Right: UV-Vis spectra of **4** (c = 2.6 × 10^{-5} mol L^{-1}) in DMSO: — before irradiation and — in PSS reached after 4 minutes of irradiation with 308 nm light; Insert: absorbance of **4** (c = 2.6 × 10^{-5} mol L^{-1}) in acetonitrile at 615 nm after subsequent cycles of irradiation with 275 nm light (6 min) and 600 nm light (6 min).

5.3 CB[7] Complexes of 1-4

Complex **1·CB[7]**

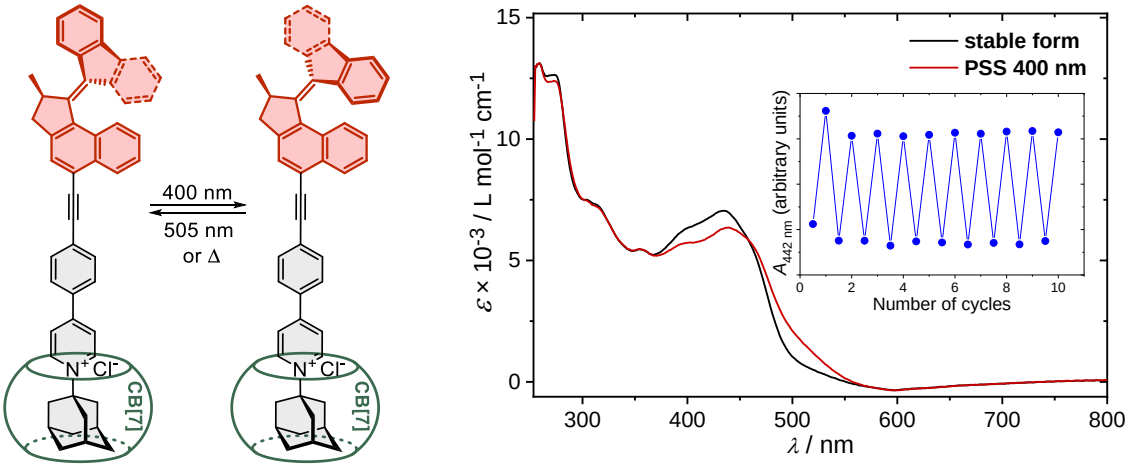

Figure S26. Left: Switching of **1·CB[7]**. Right: UV-Vis spectra of **1·CB[7]** (c = 1.6 × 10^{-5} mol L^{-1}) in DMSO: — before irradiation and — in PSS reached after 8 minutes of irradiation with 400 nm light; Insert: absorbance of **1·CB[7]** in DMSO at 442 nm after subsequent cycles of irradiation with 400 nm light (8 min) and 505 nm light (7 min).

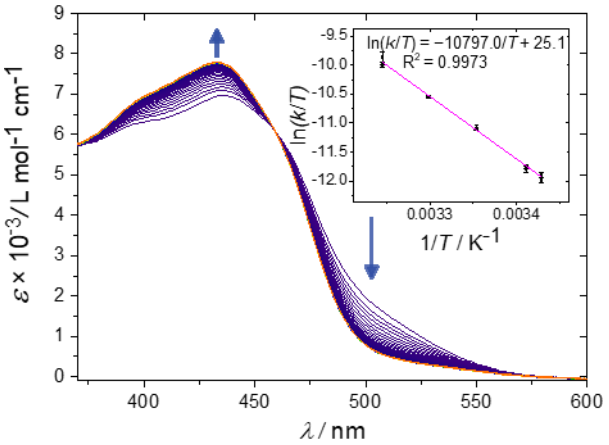

Figure S27. Thermal helix inversion of **1·CB[7]** (c = 1.6 × 10^{-5} mol L^{-1}) in DMSO after 8 minutes of irradiation with 400 nm light at 25 °C; Right: Eyring plot of thermal helix inversion of **1·CB[7]** in DMSO.

Complex **2·CB[7]**

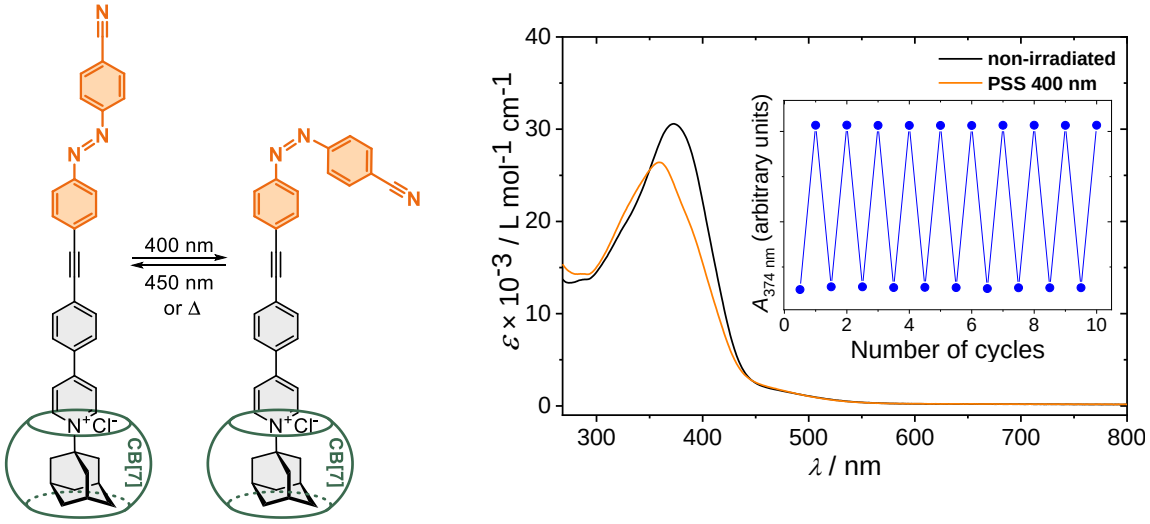

Figure S28. Left: Switching of **2·CB[7]**. Right: UV-Vis spectra of **2·CB[7]** (c = 1.3 × 10^{-5} mol L^{-1}) in DMSO: **—** before irradiation and **—** in PSS reached after 6 minutes of irradiation with 400 nm light; Insert: absorbance of **2·CB[7]** in DMSO at 374 nm after subsequent cycles of irradiation with 400 nm light (6 min) and 450 nm light (1 min).

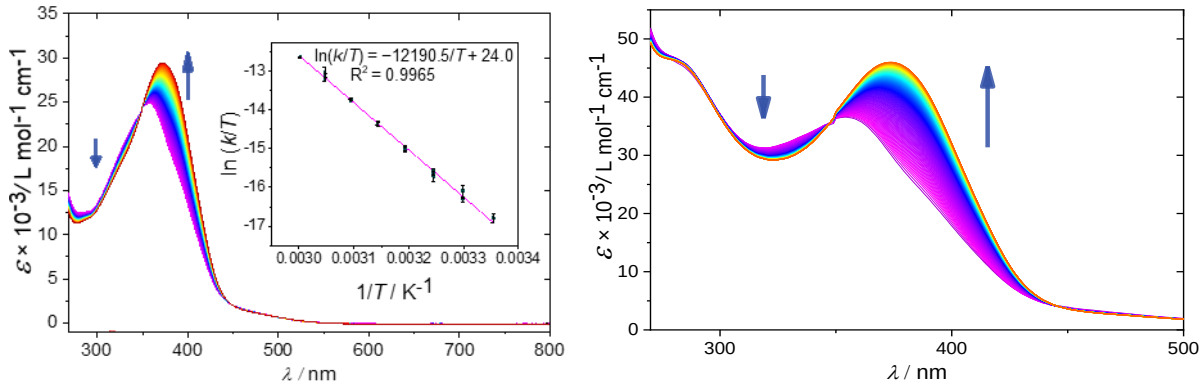

Figure S29. Left: Thermal *cis*-to-*trans* interconversion of **2·CB[7]** (c = 1.3 × 10^{-5} mol L^{-1}) in DMSO after 6 minutes of irradiation with 400 nm light at 30 °C; Insert: Eyring plot of thermal *cis*-to-*trans* interconversion of **2·CB[7]** in DMSO. Right: Thermal *cis*-to-*trans* interconversion of **2** (c = 9.7 × 10^{-6} mol L^{-1}) with the excess of **CB[7]** (c = 0.4 × 10^{-3} mol L^{-1}) in DMSO after 6 minutes of irradiation with 400 nm light at 55 °C. The obtained half-life was 1718 s, while the half-life obtained for 1:1 mixtures at the same temperature was (1855±103) s.

Complex **3·CB[7]**

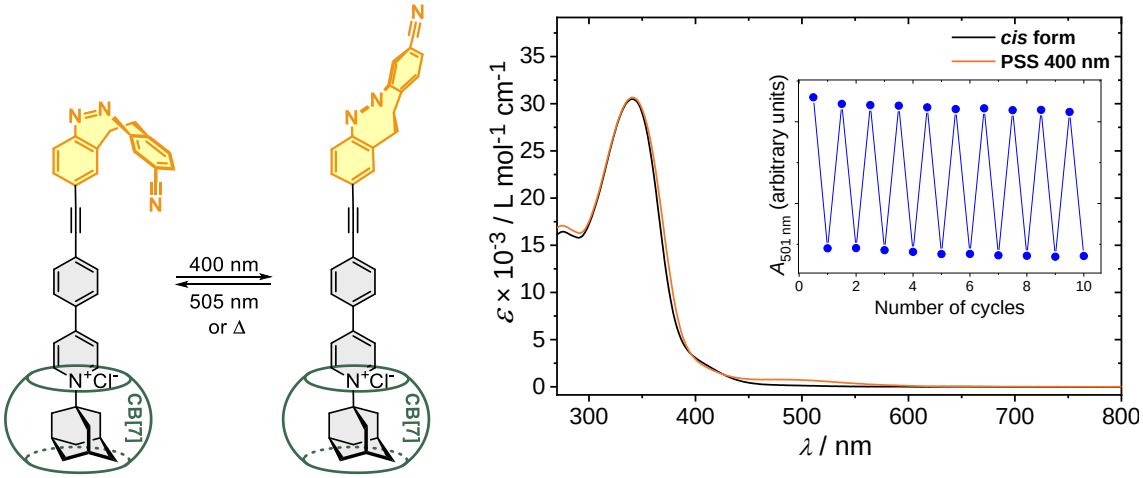

Figure S30. Left: Switching of **3·CB[7]**. Right: UV-Vis spectra of **3·CB[7]** (c = 2.8 × 10^{-5} mol L^{-1}) in DMSO: **—** before irradiation and **—** in PSS reached after 8 minutes of irradiation with 400 nm light; Insert: absorbance of **3·CB[7]** in DMSO at 501 nm after subsequent cycles of irradiation with 400 nm light (8 min) and 505 nm light (15 min).

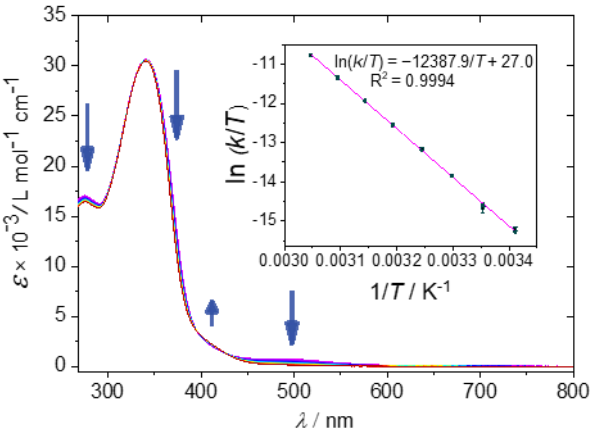

Figure S31. Thermal *trans*-to-*cis* interconversion of **3·CB[7]** (c = 2.8 × 10^{-5} mol L^{-1}) in DMSO after 8 minutes of irradiation with 400 nm light at 20 °C; Insert: Eyring plot of thermal *trans*-to-*cis* interconversion of **3·CB[7]** in DMSO.

Complex **4·CB[7]**

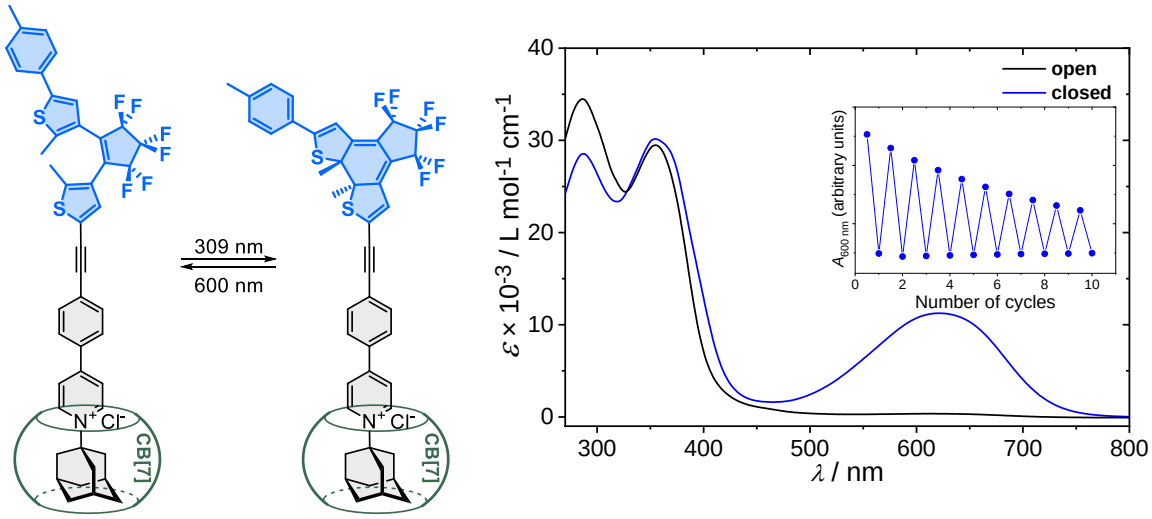

Figure S32. Left: Switching of **4·CB[7]**; Right: UV-Vis spectra of **4·CB[7]** (c = 2.0 × 10^{-5} mol L^{-1}) in DMSO: — before irradiation and — in PSS reached after 13 min irradiation with 308 nm light (diode used at 20% intensity); Insert: Absorbance of **4·CB[7]** in DMSO at 600 nm after subsequent cycles of irradiation with 308 nm light (13 min, diode used at 20% intensity) and 600 nm light (6 min).

5.4 Summary of Kinetic Parameters for Thermal Isomerization of Compounds 10-12, 1-3 and 1-3·CB[7]

Table S2. Summary of determined activation Gibbs energies ($\Delta G^{\ddagger}$), activation enthalpies ($\Delta H^{\ddagger}$), rate constants ($k_{20\ °C}$) and half-lives ($t_{1/2,\ 20\ °C}$) at 20 °C for precursors **10-12**, guests **1-3** and complexes **1-3·CB[7]**.

	Compound	$\Delta G^{\ddagger}$ (kJ mol^{-1})	$\Delta H^{\ddagger}$ (kJ mol^{-1})	$k_{20\ °C}$ (s^{-1})	$t_{1/2,\ 20\ °C}$
Overcrowded Alkenes	**10** ($CHCl_3$)	87 ± 1	87 ± 1	(1.9 ± 0.4) × 10^{-3}	(6 ± 1) min
	1 (MeCN)	86 ± 1	87 ± 1	(2.9 ± 0.6) × 10^{-3}	(4.0 ± 0.8) min
	1 (DMSO)	86 ± 1	79 ± 1	(2.8 ± 0.4) × 10^{-3}	(4.3 ± 0.6) min
	1·CB[7] (DMSO)	87 ± 1	89 ± 1	(2.3 ± 0.1) × 10^{-3}	(5.1 ± 0.2) min
	1·CB[7] (SAM)	86 ± 38	109 ± 19	(2.8 ± 0.8) × 10^{-3}	(4.1 ± 1.2) min
Azobenzenes	**11** ($CHCl_3$)	102 ± 2	104 ± 2	(3.7 ± 0.7) × 10^{-6}	(52 ± 10) h
	2 (MeCN)	102 ± 1	101 ± 1	(6.6 ± 2.4) × 10^{-6}	(26 ± 9) h
	2 (DMSO)	101 ± 1	99 ± 3	(6.9 ± 1.4) × 10^{-6}	(28 ± 6) h
	2·CB[7] (DMSO)	101 ± 1	101 ± 1	(6.6 ± 0.6) × 10^{-6}	(29 ± 3) h
	2·CB[7] (SAM)	101 ± 30	127 ± 14	(5.9 ± 1.7) × 10^{-6}	(33 ± 9) h
Diazocines	**12** ($CHCl_3$)	96 ± 1	101 ± 1	(4.6 ± 0.2) × 10^{-5}	(257 ± 13) min
	3 (MeCN)	91 ± 2	95 ± 1	(6.8 ± 0.6) × 10^{-5}	(170 ± 16) min
	3 (DMSO)	95 ± 2	97 ± 2	(8.2 ± 0.4) × 10^{-5}	(140 ± 5) min
	3·CB[7] (DMSO)	95 ± 1	103 ± 1	(7.0 ± 0.3) × 10^{-5}	(164 ± 7) min
	3·CB[7] (SAM)[a]	93 ± 52	80 ± 26	(1.5 ± 0.8) × 10^{-4}	(76 ± 41) h

[a] Kinetic parameters carry a relatively large uncertainty due to the minimal difference between the UV spectra recorded before and after irradiation (see **Figure S30**).

5. Quantum Yield Determination

Quantum yields were obtained using a set-up devised by the group of Prof. Eberhard Riedle.[13]

Cis-to-*trans* isomerization of **3**

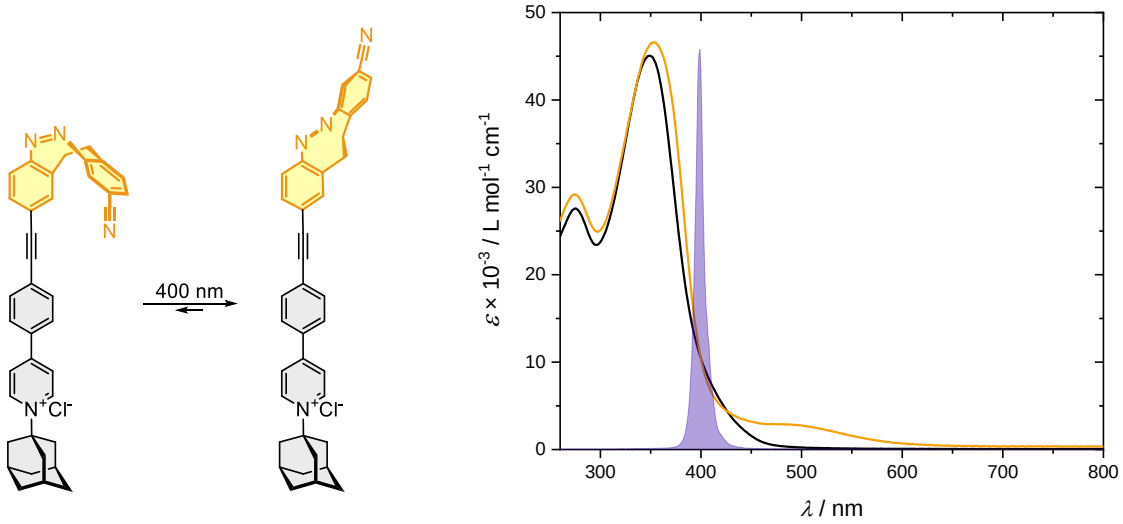

Figure S33. Switching of compound **3** (c = 1.5 × 10^{-5} mol L^{-1}) and UV-Vis spectra of — *cis* and — *trans*-**3** in DMSO with normalized profile of LED (400 nm) used for quantum yield determination. UV-Vis spectra of pure isomers shown in the figure were calculated during data evaluation.

$\Phi_{cis \rightarrow trans,\ 400\ nm}$	21%
$\Phi_{trans \rightarrow cis,\ 400\ nm}$	19%

Ring closure of **4**

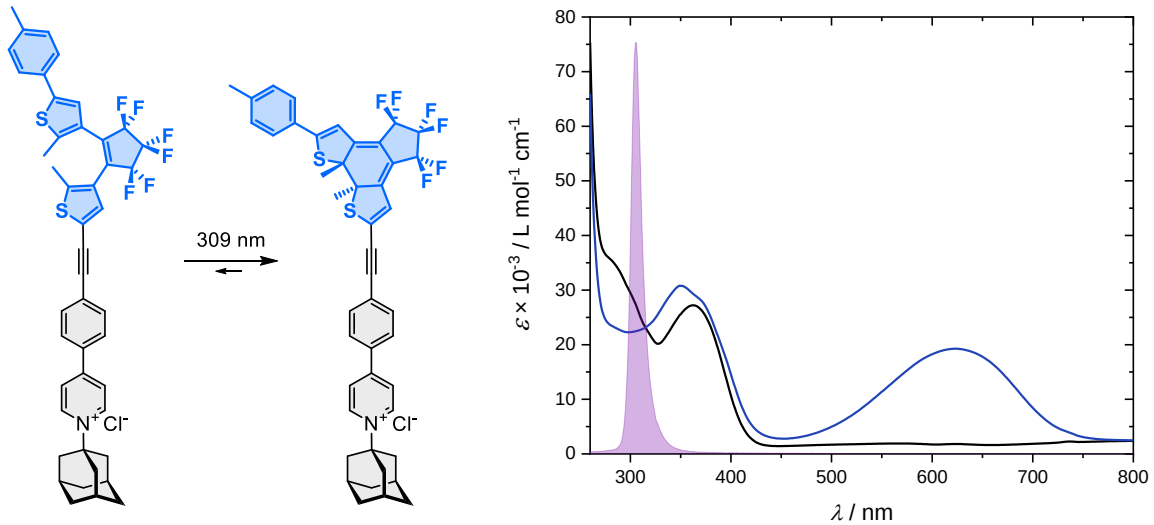

Figure S34. Ring closure of **4** (c = 2.6 × 10^{-5} mol L^{-1}) and UV-Vis spectra of — open and —closed forms in DMSO with normalized profile of LED (309 nm) used for quantum yield determination. UV-Vis spectra of pure isomers shown in the figure were calculated during data evaluation.

$\Phi_{open \rightarrow closed,\ 309\ nm}$	34%
$\Phi_{closed \rightarrow open,\ 309\ nm}$	2%

13. Megerle, U.; Lechner, R.; König, B.; Riedle, E. Laboratory Apparatus for the Accurate, Facile and Rapid Determination of Visible Light Photoreaction Quantum Yields. *Photochem. Photobiol. Sci.* **2010**, *9* (10), 1400–1406. https://doi.org/10.1039/c0pp00195c.

Ring opening of **4**

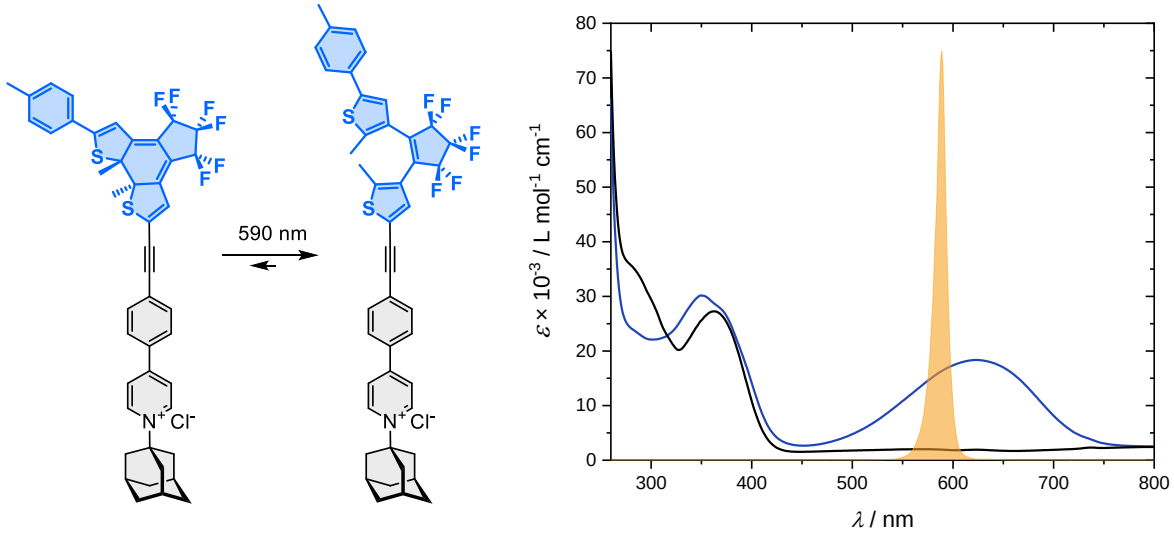

Figure S35. Ring opening of **4** (c = 2.6 × 10^{-5} mol L^{-1}) UV-Vis spectra of — open and —closed forms in DMSO with normalized profile of LED (590 nm) used for quantum yield determination. UV-Vis spectra of pure isomers shown in the figure were calculated during data evaluation.

$\Phi_{\text{closed}\rightarrow\text{open, 590 nm}}$	1%
$\Phi_{\text{open}\rightarrow\text{closed, 590 nm}}$	0%

6. ^{1}H NMR Spectra of Switching in Solution

Compound **10**

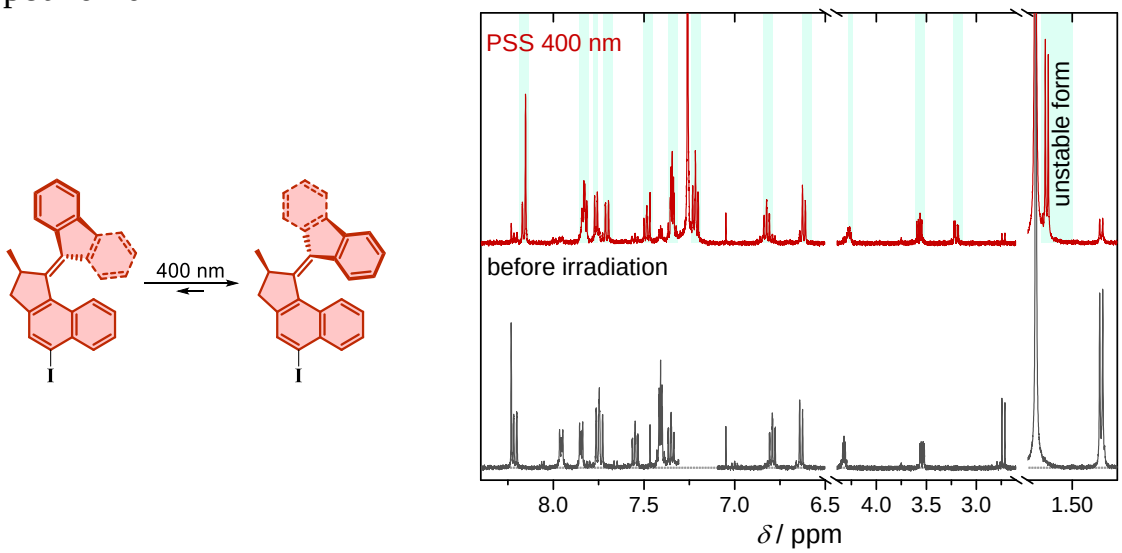

Figure S36. Left: Switching of **10**. Right: Selected regions of ^{1}H NMR spectra of **10** in $CDCl_3$ at -20 °C — before irradiation and — in PSS reached after 3 hours of irradiation at 400 nm.

Compound **11**

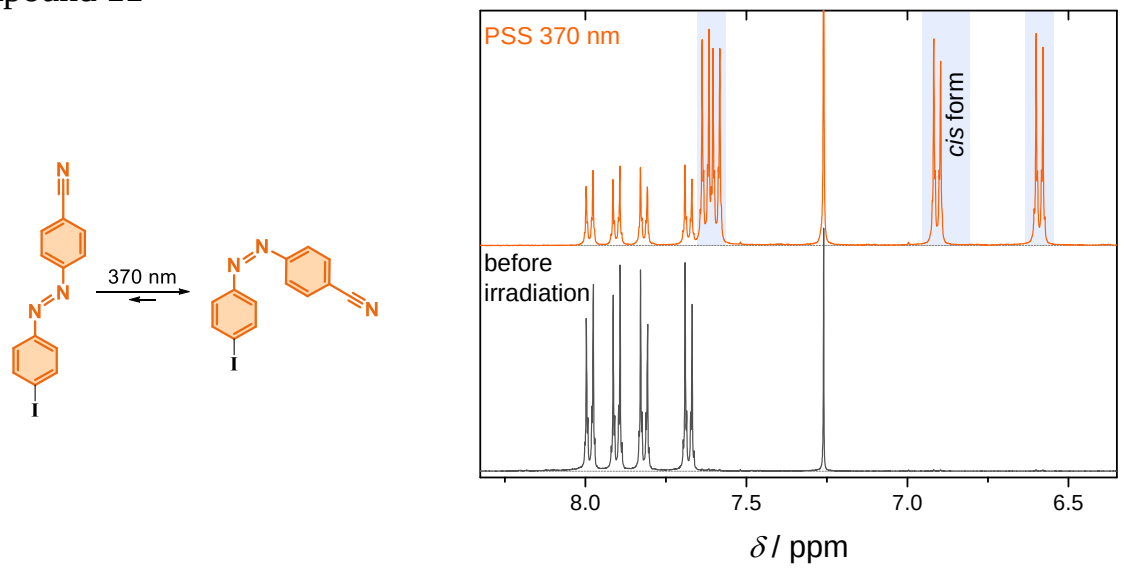

Figure S37. Left: Switching of **11**. Right: Aromatic region of ^{1}H NMR spectra of **11** in $CDCl_3$ at 25 °C — before irradiation and — in PSS reached after 2.8 hours of irradiation at 370 nm.

Compound **12**

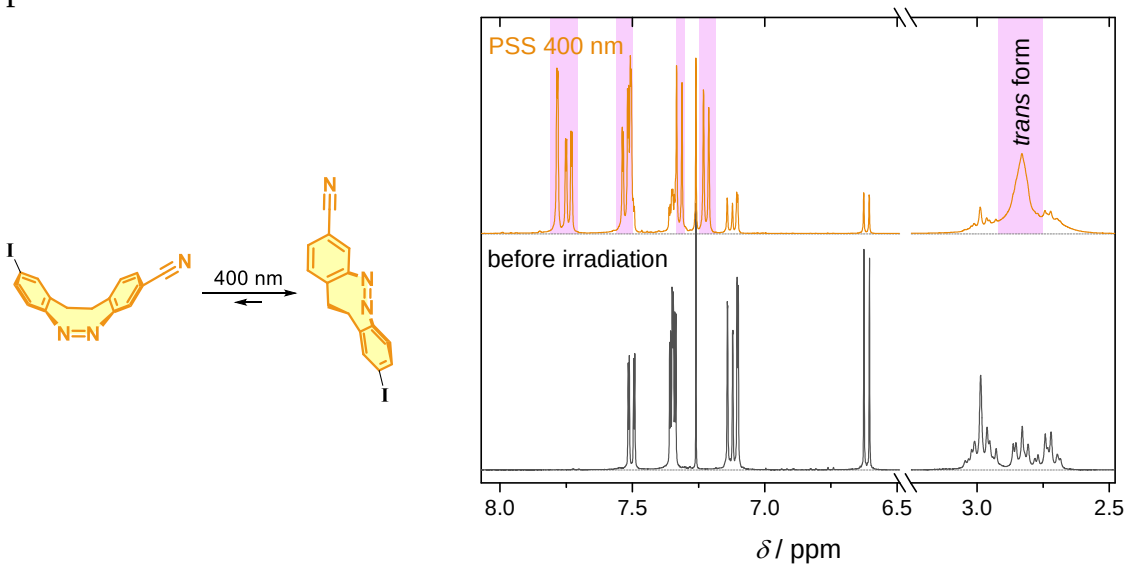

Figure S38. Left: Switching of **12**. Right: Aromatic region of ^{1}H NMR spectra of **12** in $CDCl_3$ at 25 °C — before irradiation and — in PSS reached after 1.6 hours of irradiation at 400 nm.

Compound **13**

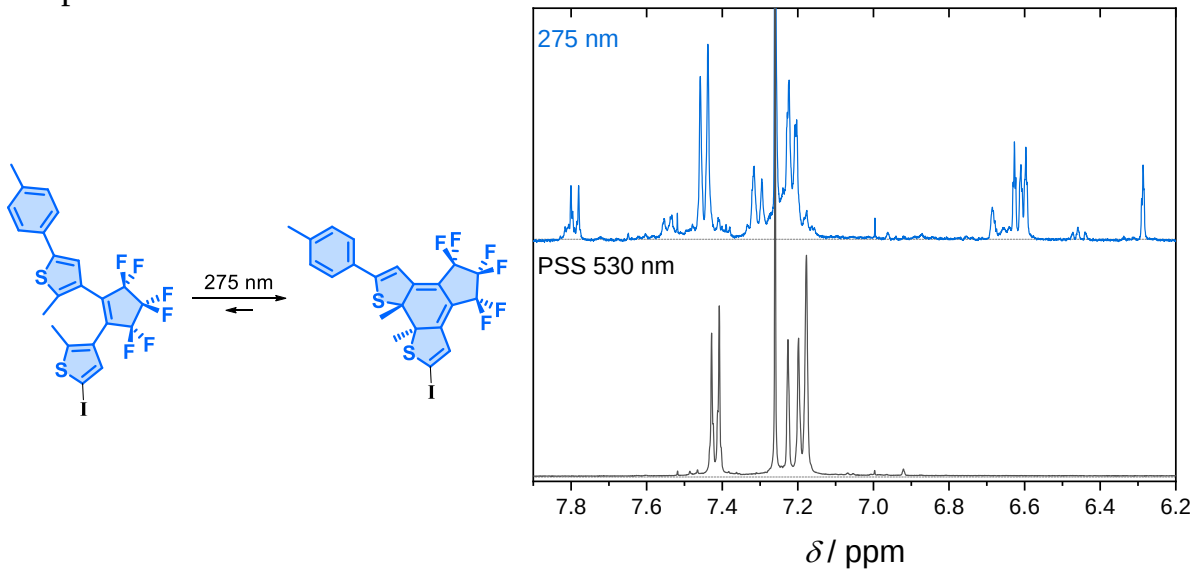

Figure S39. Left: Switching of **13**. Aromatic region of ^{1}H NMR spectra of **13** in $CDCl_3$ at 25 °C — in PSS reached after 15 min of irradiation with 530 nm, — after 3 hours of irradiation at 275 nm.

Compound **2**

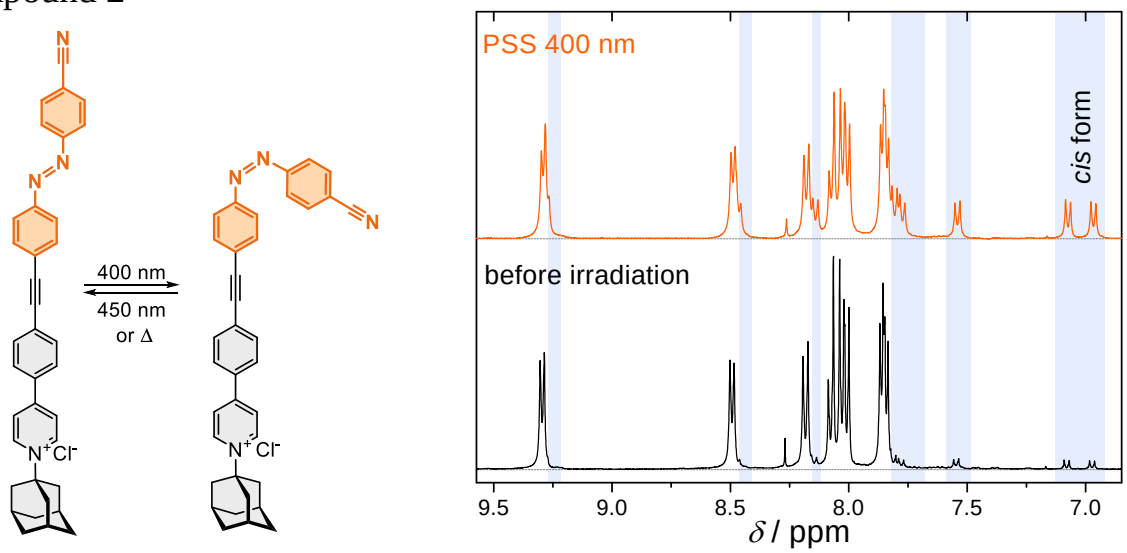

Figure S40. Left: Switching of **2**. Right: Aromatic region of ^{1}H NMR spectra of **2** in DMSO-d_6 at 25 °C — before irradiation and — in PSS reached after 7.1 hours of irradiation at 400 nm.

Compound **3**

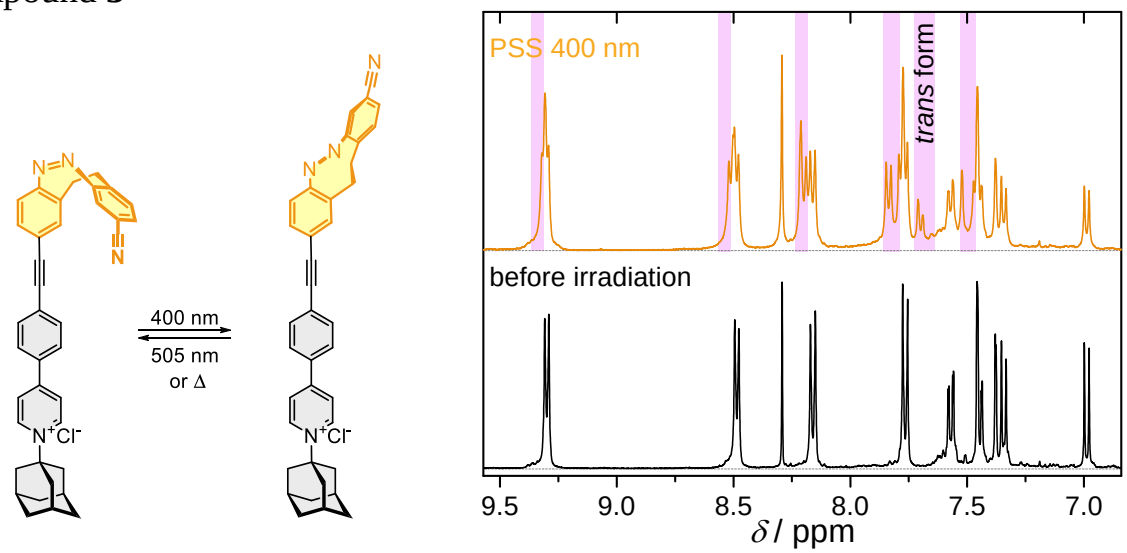

Figure S41. Left: Switching of **3**. Right: Aromatic region of ^{1}H NMR spectra of **3** in DMSO-d_6 at 25 °C — before irradiation and — in PSS reached after 5.8 hours of irradiation at 400 nm.

Compound **4**

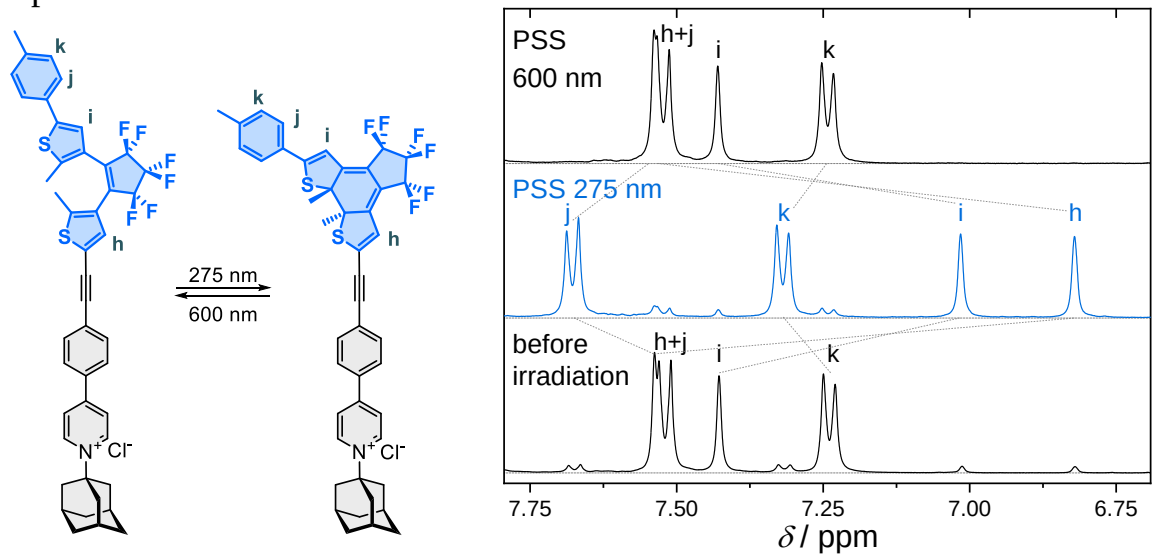

Figure S42. Left: Switching of **4**. Aromatic region of ^{1}H NMR spectra of **4** in DMSO-d_6 at 25 °C — before irradiation, — in PSS reached after 10.7 hours of irradiation at 275 nm, and — in PSS reached after subsequent 12 minutes of irradiation at 600 nm.

The obtained ^{1}H NMR spectra enabled determination of the isomer ratios in the photostationary state.

7. Fluorescence Emission

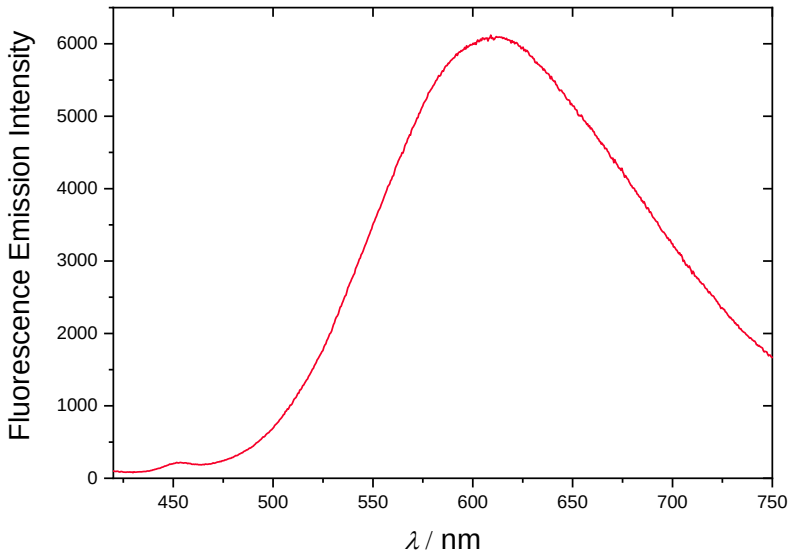

Figure S43. Fluorescence emission spectrum of compound **9** (c = 4.3 × 10^{-5} mol L^{-1}) in DMSO.

8. Characterization of Surface Assemblies

8.1 Preparation of Gold Substrates

Gold substrates were prepared using physical vapor deposition of gold (Safina) in clean room environment. Several different methods were employed to prepare substrates compatible with each individual analytic technique.

Method 1: A 200 nm thick layer of gold was applied by vapor deposition on glass slides at the speed of 2 Å/s. Interlayer of chromium, 5 nm thick, was applied at the speed of 1 Å/s. After gold deposition, the substrates were washed with Hellmanex® and hot water in ultrasonic bath for 5 min, then two times in distilled water in ultrasonic bath for 5 minutes. Finally, substrates were rinsed twice with propyl alcohol. Prior to sample deposition, Au(111) plates were washed three times with MiliQ water and acetone, dried under the flow of nitrogen, annealed with butane flame to obtain gold(111) and immediately immersed into the solution of sample. The samples prepared by this method were analyzed by contact angle goniometry and ellipsometry.

Method 2: A 100 nm thick layer of gold was applied by resistive evaporation in vacuum (base pressure 10^{-7} mbar) onto a freshly cleaved muscovite V4 substrate. To obtain the Au(111) surface, the substrates were thermally annealed in a butane flame immediately after removal from the vacuum chamber. The samples prepared by this method were analyzed by AFM.

Method 3: A 185 nm thick layer of gold was applied by vapor deposition on glass slides at the speed of 0.1 Å/s. Interlayer of titanium, 5 nm thick, was applied at the speed of 1 Å/s. After gold deposition, the substrates were washed with Hellmanex® and hot water in ultrasonic bath for 5 min, then two times in distilled water in ultrasonic bath for 5 minutes. Finally, substrates were rinsed twice with propyl alcohol. Prior to sample deposition, Au(111) plates were washed three times with MiliQ water and acetone, dried under the flow of nitrogen, annealed with butane flame to obtain gold(111) and immediately immersed into the solution of sample. The samples prepared by this method were analyzed by PM-IRRAS.

Method 4: A 10 nm thick layer of gold was applied on quartz slides (UV Fused Silica Plate PFS-2521, UQG Optics) by vapor deposition at the speed of 0.2 Å/s, followed by deposition of a 3 nm thick layer of gold nanoparticles at the speed of 4 Å/s. Before use, substrates were cleaned by sonication in propyl alcohol for 5 min, followed by rinsing with propyl alcohol. The samples prepared by this method were analyzed by Raman spectroscopy.

Method 5: Prior to surface modification, quartz slides (UV Fused Silica Plate PFS-2521, UQG optics), cut into 1.0 cm × 2.0 cm pieces, were cleaned by immersion in a piranha solution at 90 ºC for 1 h, rinsed with MiliQ water, sonicated in water (2 times for 5 min), rinsed with acetone, and finally dried under the flow of nitrogen. Silanization of quartz before gold deposition was performed by adapting a previously published procedure.[14] Substrates were immersed in solution of APTES in toluene (1 mM) for 5 days, then thoroughly rinsed with toluene, sonicated in toluene, then rinsed with methanol and dried under the flow of nitrogen. Gold films were then prepared by vapor deposition of a 5 nm thick layer of gold at the speed of 0.5 Å/s. The samples prepared by this method were analyzed by UV-Vis spectroscopy.

14. Chen, K.-Y.; Ivashenko, O.; Carroll, G. T.; Robertus, J.; Kistemaker, J. C. M.; London, G.; Browne, W. R.; Rudolf, P.; Feringa, B. L. Control of Surface Wettability Using Tripodal Light-Activated Molecular Motors. *J. Am. Chem. Soc.* **2014**, *136* (8), 3219–3224. https://doi.org/10.1021/ja412110t.

8.2 Preparation of Monolayers of Cucurbit[7]uril and the Host-Guest Complexes on the Gold Surface

The layer of **CB[7]** physisorbed from water was prepared by 18 hour immersion of gold substrate into 0.5 mmol L^{-1} aqueous solution of **CB[7]**, followed by rinsing with MiliQ water and drying under the stream of nitrogen.

The layers of **CB[7]** and **CB[7]** complexes of **1-4**, **8** and **9** on gold plates were prepared by immersion in DMSO solution of sample for 18-72 hours at room temperature. In the case of **CB[7]** sample, the concentration of the solution was 0.5 mmol L^{-1}, while in the case of complexes it was 0.1 mmol L^{-1}. The plates were then carefully removed from the solution, rinsed with DMSO using a syringe and thoroughly dried under the flow of nitrogen. Freshly prepared samples were immediately subjected to the measurements described in the following paragraphs, the results of which are summarized in **Table S3**.

Table S3. Preparation and characterization of surface monolayers of **CB[7]** and complexes of guests **1-4** and silyl-protected precursors **8** and **9**.

Sample	Immersion time / h	Average Contact Angle / °	Average Ellipsometric Thickness / Å	Thickness determined from AFM/ Å	Approximate length of the Guest h_g / Å	Theoretical Layer Height h_d [d] / Å
CB[7]	18	52 ± 4	11 ± 1	10 ± 1	9[a]	9
1·CB[7]	72	50 ± 4	15 ± 2	23 ± 2	26[c]	25
2·CB[7]	48	45 ± 2	16 ± 1	24 ± 3	27[b]	26
3·CB[7]	48	40 ± 4	13 ± 2	15 ± 2	21[c]	20
4·CB[7]	48	47 ± 2	18 ± 1	18 ± 1	21[c]	20
8·CB[7]	18	29 ± 2	16 ± 1	17 ± 2	18[b]	17
9·CB[7]	48	40 ± 4	17 ± 2	20 ± 2	19[c]	18

[a] Taken from reference 15. [b] Values obtained from X-Ray crystal structures of free guests. [c] Values obtained from structures of guests optimized using the GFN2-xTB semi-empirical method.[16,17,18] [d] Calculated as $h_d = h_g \times cos(17.8°)$.

8.3 Contact Angle Goniometry

Gold substrates prepared by Method 1 were used. The contact angle between water and the prepared layers on gold(111) surface was determined using the CAM 101 Contact Angle Goniometer (KSV Instruments Ltd., Finland) (**Figure S44**). At least ten measurements per sample were carried out and the contact angle for each compound was calculated as an average of all recorded values, where the values completely out of range were discarded.

15. Assaf, K. I.; Nau, W. M. Cucurbiturils: From Synthesis to High-Affinity Binding and Catalysis. *Chem. Soc. Rev.* **2015**, *44* (2), 394–418. https://doi.org/10.1039/C4CS00273C.
16. Grimme, S.; Bannwarth, C.; Shushkov, P. *J. Chem. Theory Comput.* **2017**, *13*, 1989–2009.
17. Bannwarth, C.; Ehlert, S.; Grimme, S. *J. Chem. Theory Comput.* **2019**, *15*, 1652–1671.
18. Grimme, S. *J. Chem. Theory Comput.* **2019**, *15*, 2847–2862.

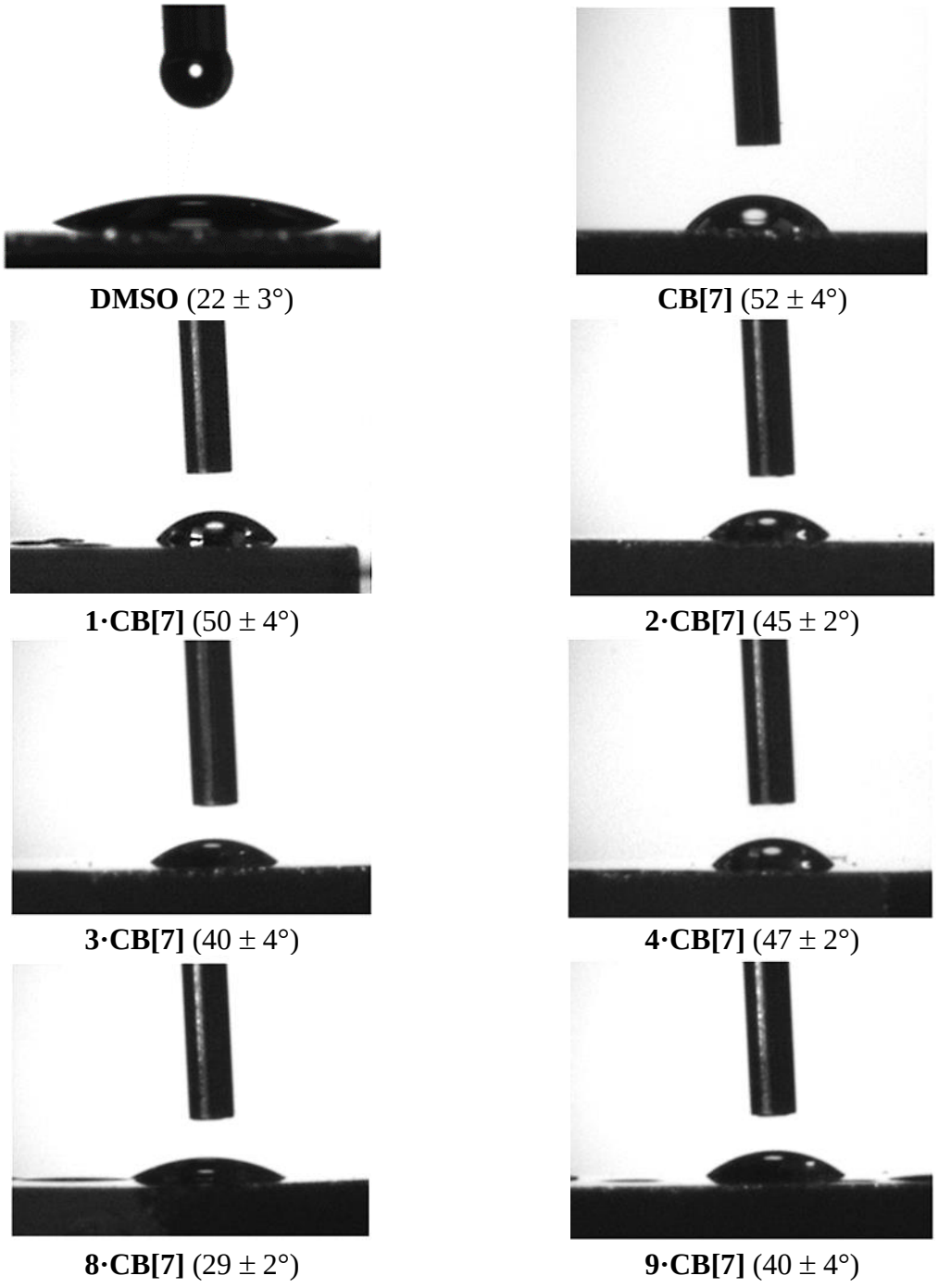

Figure S44. Water contact angle goniometry of DMSO, **CB[7]**, and complexes **1-4·CB[7]**, **8·CB[7]**, and **9·CB[7]** physisorbed on Au(111) surface.

8.4 Atomic Force Microscopy

Gold substrates prepared according to Method 2 were used. AFM measurements were performed on a Veeco–Bruker Multimode instrument. Standard topographical imaging was carried out in PeakForce mode using Bruker SNL-A cantilevers with a nominal tip radius of 2 nm and a positive setpoint of 300–650 pN. AFM data were processed in Gwyddion using standard flattening procedures, including "Align Rows," to remove periodic noise and minor imaging artefacts.

Nanoscale spots were observed on the substrate bearing physisorbed **CB[7]** (**Figure S45**). The apparent lateral diameter of these features (1.7 nm) is consistent with the outer dimension of the **CB[7]** macrocycle (1.6 nm),[19] supporting the assignment to individual **CB[7]** molecules adsorbed on the gold surface.

Nanoshaving experiments were performed separately in contact mode, where a defined area was scanned under the maximum setpoint to remove the monolayer down to the gold surface, followed by topographical profiling of the shaved region. **Figure S46** shows vertical profile measurements of bare **CB[7]** and its complexes **1–4·CB[7]** and **8–9·CB[7]**.

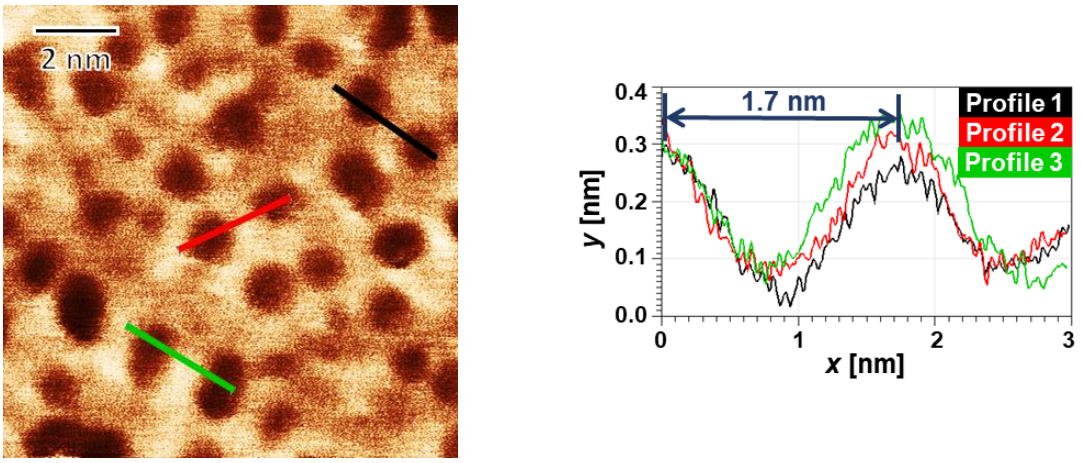

CB[7]

Figure S45. Left: AFM image of gold(111) surface with deposited **CB[7]**; Right: Vertical profile of **CB[7]** layer on gold, deposited by physisorption from DMSO.

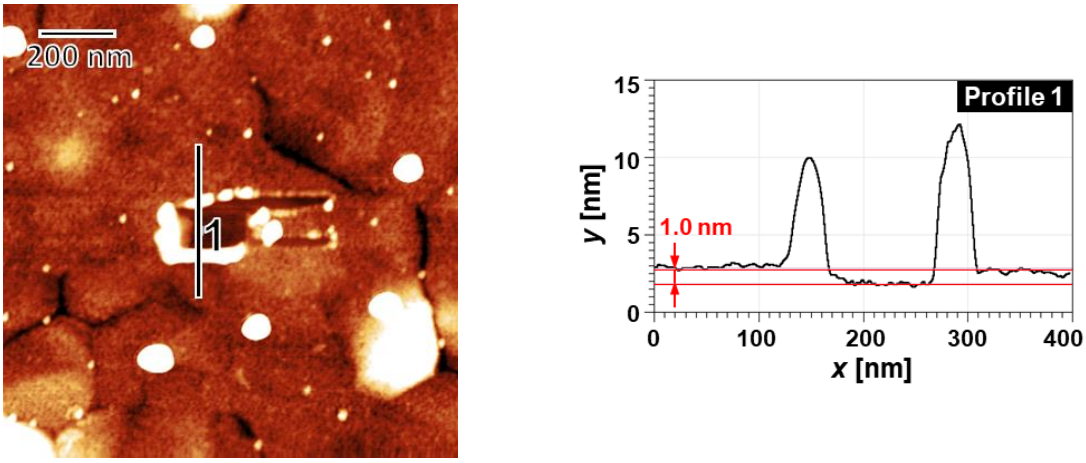

CB[7]

19. Assaf, K. I.; Nau, W. M. Cucurbiturils: From Synthesis to High-Affinity Binding and Catalysis. *Chem. Soc. Rev.* **2015**, *44* (2), 394–418. https://doi.org/10.1039/C4CS00273C.

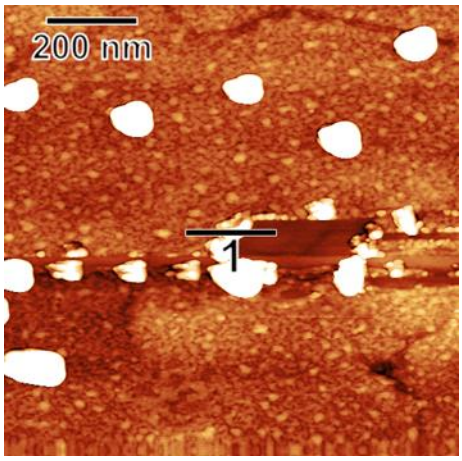

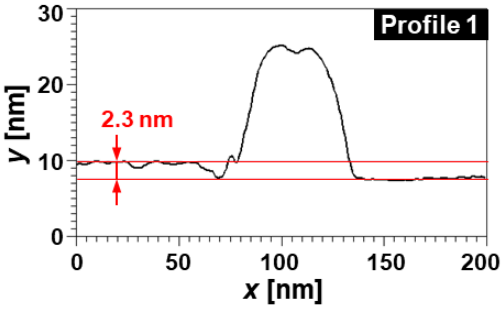

1·CB[7]

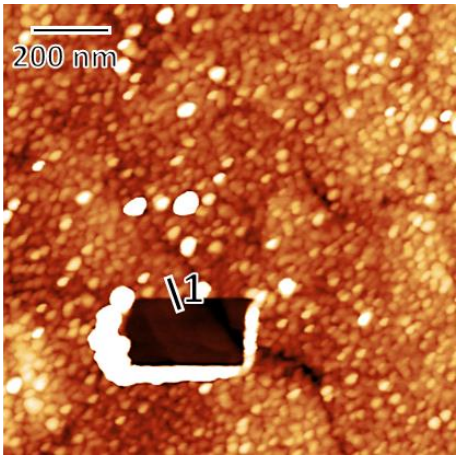

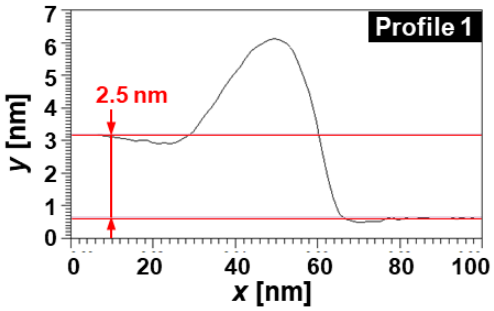

2·CB[7]

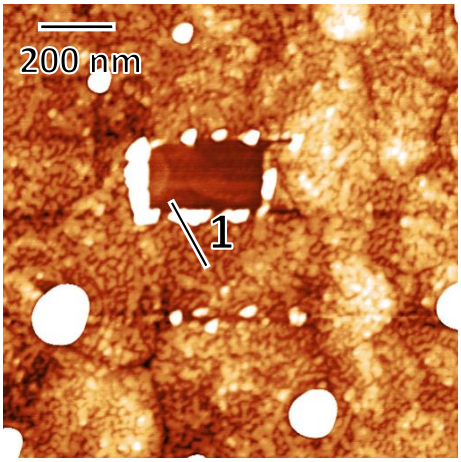

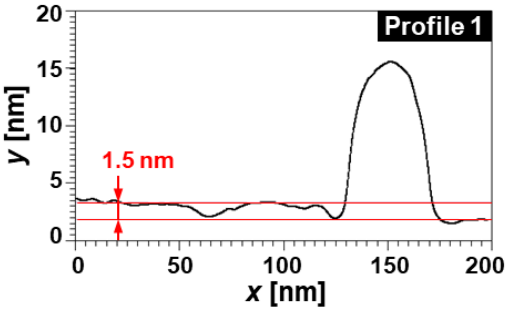

3·CB[7]

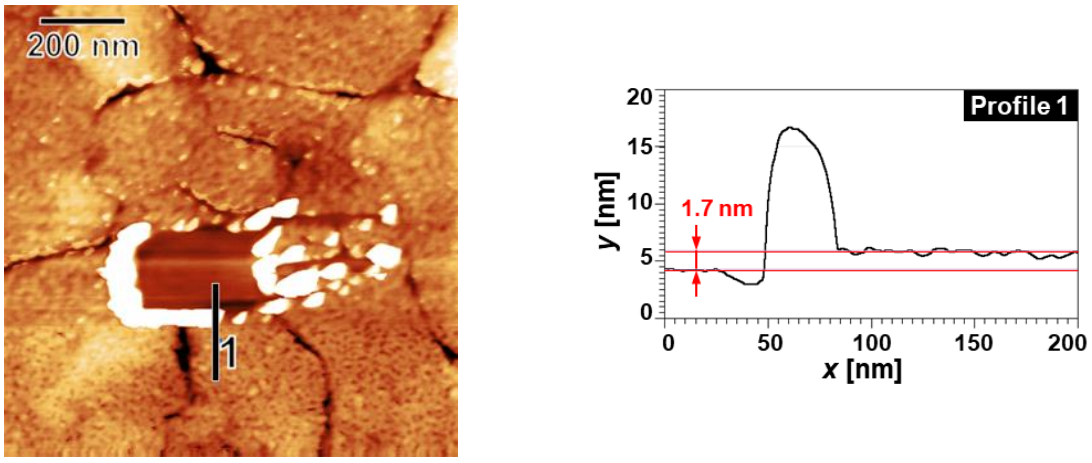

4·CB[7]

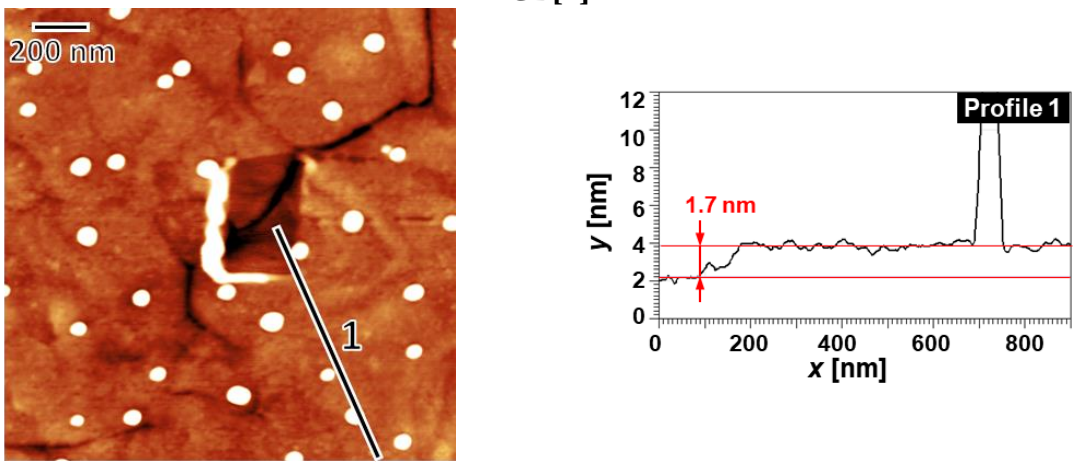

8·CB[7]

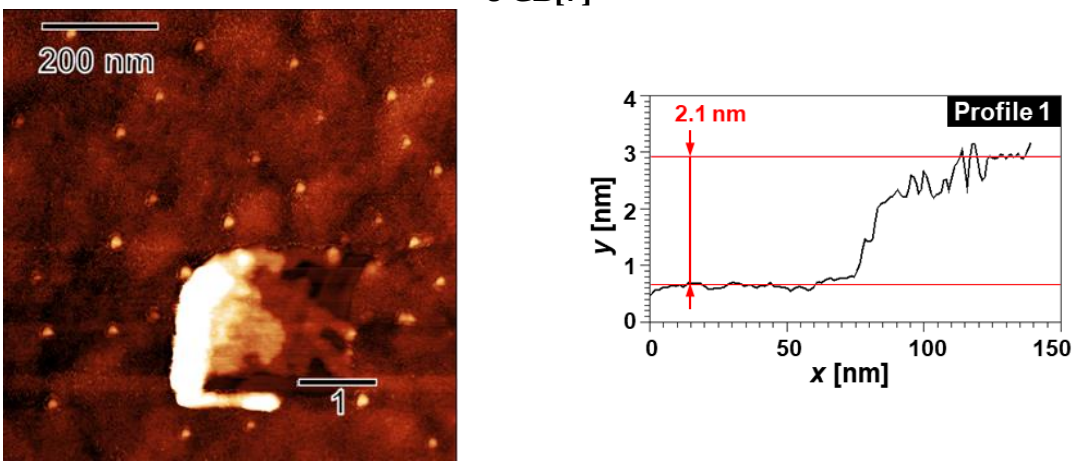

9·CB[7]

Figure S46. Left: AFM images of layers of bare **CB[7]** and **CB[7]** complexes of **1**-**4**, **8** and **9** on Au(111) surface scratched by AFM tip. Right: Vertical profile of the layers on Au(111) surface after scratching with AFM tip.

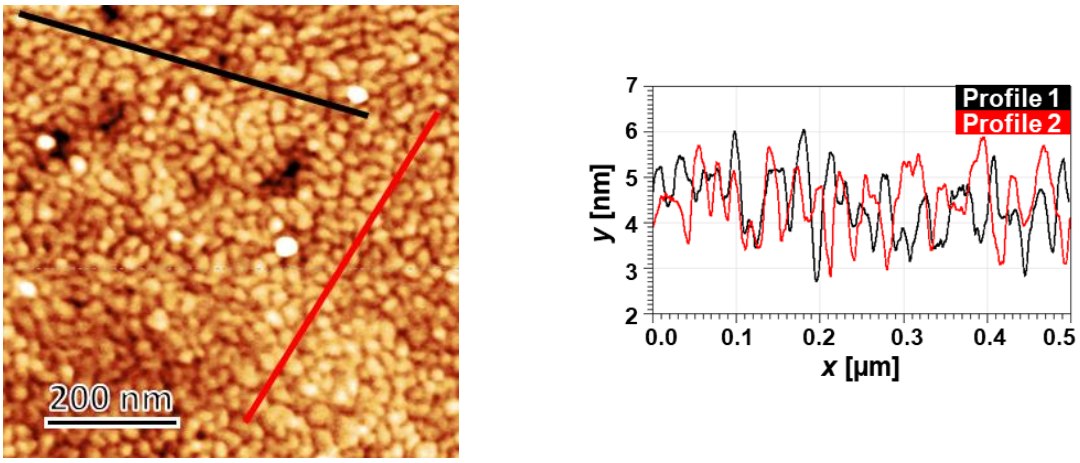

Figure S47. AFM visualization of a 5 nm gold film deposited on a quartz substrate used for UV analysis. Right: Height profiles of the Au layer on the quartz surface.

8.5 Ellipsometry

Gold substrates prepared by Method 1 were used. The ellipsometric thickness of layers was determined using the Variable Angle Stokes Ellipsometer (Geartner Scientific, USA). For each compound, three samples were analyzed by carrying out at least ten measurements per sample. The thickness is then calculated as an average of measured values, where values completely out of the range were discarded. Exceptionally for samples **1·CB[7]**, **4·CB[7]**, **8·CB[7]** and **9·CB[7]**, average value from measuring ten points on one sample is reported. The value of refraction index was set to 1.47, which was determined in previous works.[20]

8.6 Polarization Modulation Infrared Reflection-Absorbtion Spectrocopy (PM-IRRAS)

Gold substrates prepared by Method 3 were used. The PM-IRRAS spectra (**Figure S48**) were measured using polarization modulation infrared reflection-absorption spectrometer (Thermo Fisher Scientific, USA) immediately after sample deposition. The acquisition time was 2 hours (6000 scans), during which the detector was cooled with liquid nitrogen. The background was subtracted from the raw data and the baseline was corrected.

20. Kaletová, E.; Kohutová, A.; Hajduch, J.; Kaleta, J.; Bastl, Z.; Pospíšil, L.; Stibor, I.; Magnera, T. F.; Michl, J. The Scope of Direct Alkylation of Gold Surface with Solutions of C_1–C_4 *n*-Alkylstannanes. *J. Am. Chem. Soc.* **2015**, *137* (37), 12086–12099. https://doi.org/10.1021/jacs.5b07672.

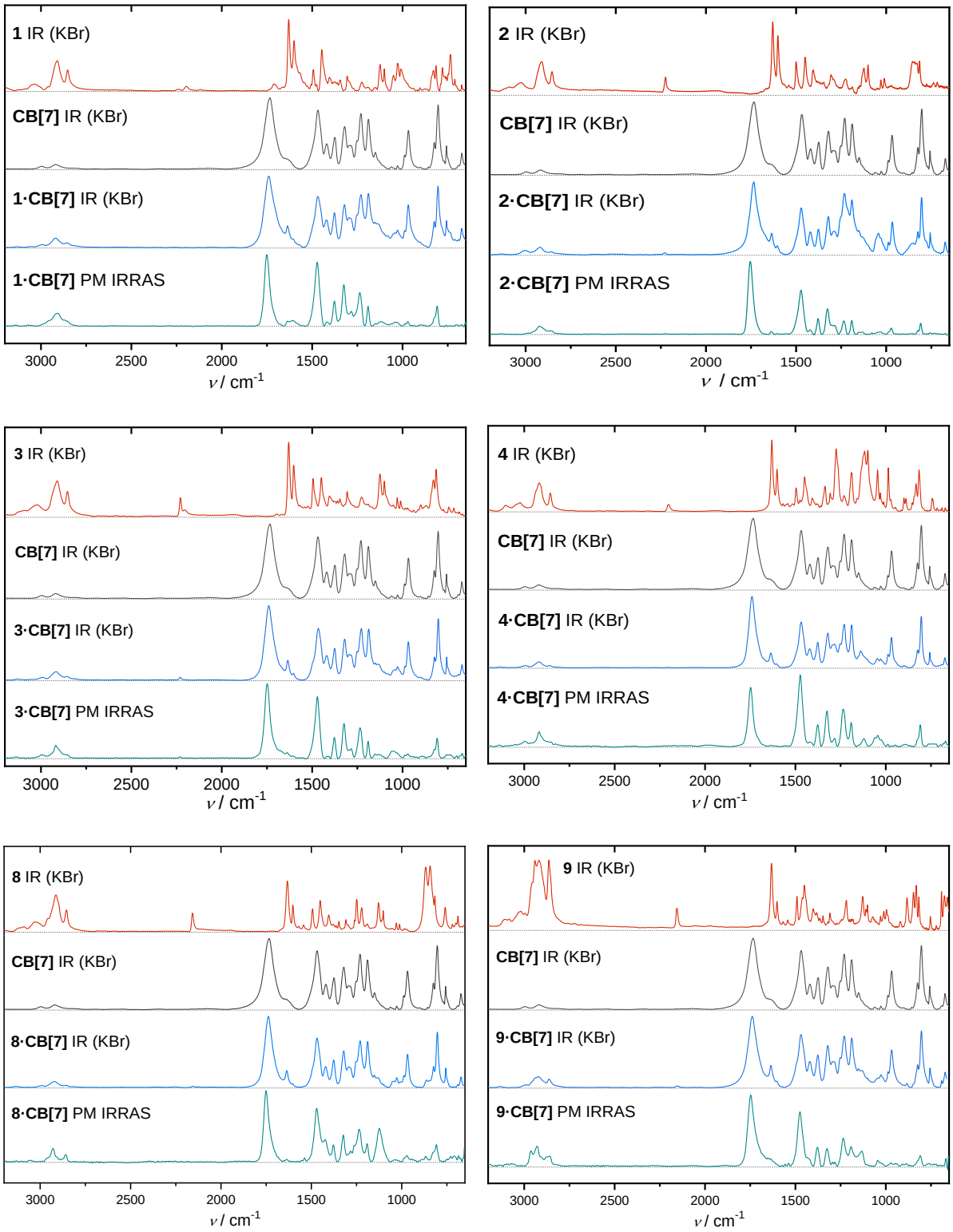

Figure S48. Isotropic spectra of the (a) free guests **1-4**, **8** and **9**, (b) **CB[7]** and (c) **CB[7]** complexes measured in KBr pellets and (d) PM-IRRAS spectra of the monolayers of the complexes on Au(111) surface.

8.7 Raman Spectroscopy and SERS

Raman spectroscopy of **1**, **CB[7]** and **1·CB[7]** was performed on Renishaw inVia™ Qontor® upright confocal Raman microscope equipped with 532 nm, 633 nm, 785 nm lasers and with 1800 l/mm and 1200 l/mm gratings. LWD 50× (NA 0.55, LWD 8.2 mm) and 100× (NA 0.85, WD 0.33 mm) objectives (Leica) were used. To obtain the best results, experimental set-up (laser wavelength, power, time of exposition and data accumulation) was optimized for each studied sample. To characterize the surface of prepared layers of **1·CB[7]** on gold substrates, several points on surface were analyzed firstly (**Figure S49**), followed by measurement of Raman map of surface 100×100 mm. Gold substrates prepared by Method 4 were used.

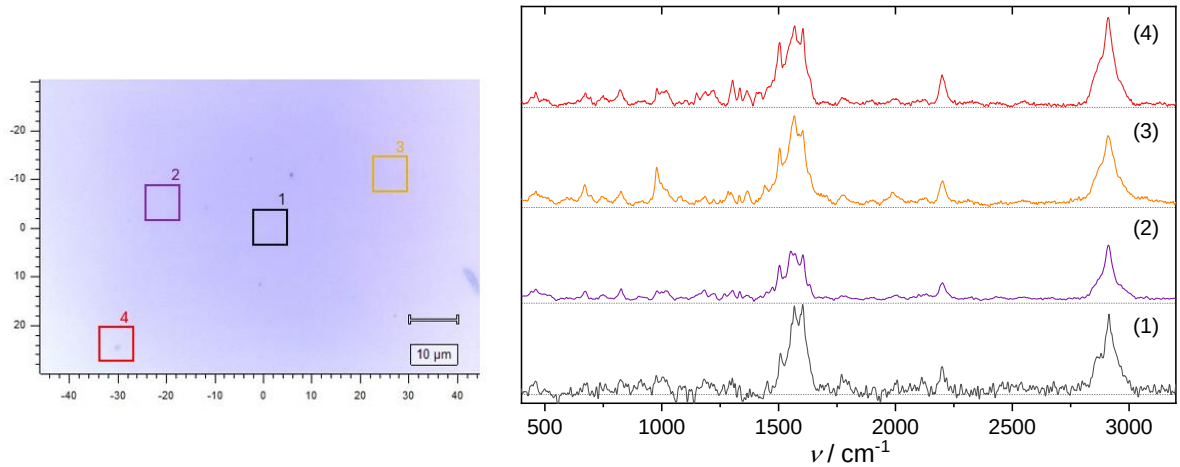

Figure S49. Raman spectra obtained from measuring various points on the surface of gold substrate with **1·CB[7]**.

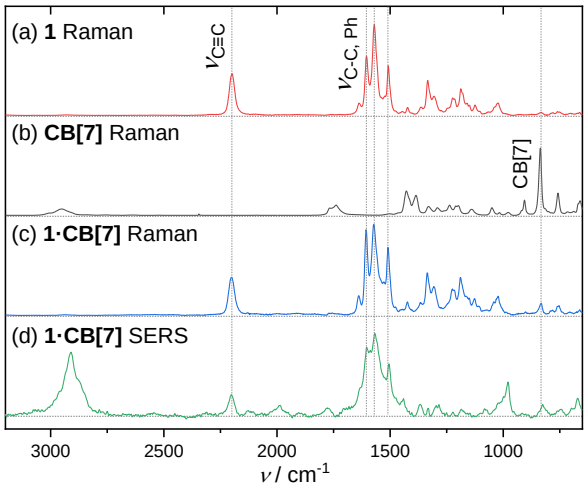

Figure S50. Raman spectra of (a) guest **1**, (b) **CB[7]** and (c) **1·CB[7]** and (d) SERS of monolayers of **1·CB[7]** on gold surface.

8.8 UV-Vis Spectroscopy of Semi-Transparent Gold Substrates

UV–vis spectra of the **1-4·CB[7]** monolayers on gold substrates (**Figures S51–S57**) were recorded using the same instrumentation described in **Section 4**. Gold substrates prepared according to Method 5 (**Section 8**) were used for all measurements. Thermal relaxation experiments were performed in a quartz cuvette (2 × 10 mm) with *n*-decane as an inert medium to ensure efficient heat transfer between the samples and the cooling unit. For the photostability

experiments, the samples were placed in the UV–vis spectrometer chamber, directly in the path of the UV beam. The chamber was continuously purged with nitrogen. Monolayer stability was evaluated by subjecting the samples to repeated photoirradiation cycles.

For UV–vis measurements on gold substrates, the acquisition time ("Ave Time") was set to 1 s, corresponding to a scan rate of 60 nm min^{-1}. The total duration of each kinetics experiment was set to approximately three half-lives at the respective temperatures. Each kinetic dataset was independently collected for three different samples, with at least one temperature point re-measured on the same sample to confirm reproducibility.

The differential UV–Vis spectra of the diarylethene monolayer (**4·CB[7]**) on the semitransparent 5 nm Au film display a characteristic bipolar response in the 570–650 nm region (**Figures S57**). Upon UV irradiation, a reversible, photoinduced decrease at the original plasmon maximum accompanied by a positive feature at longer wavelengths is observed. This behavior is consistent with modulation of the local refractive index in the vicinity of the gold nanostructures caused by photoisomerization of the diarylethene, which leads to perturbation of the LSPR position.[21,22,23,24] The resulting differential spectrum thus likely reflects the convolution of the intrinsic diarylethene absorption change with a concurrent bathochromic LSPR shift.

21. Spangenberg, P.; Métivier, R.; Yasukuni, R.; Shibata, K.; Brosseau, A.; Grand, J.; Aubard, J.; Yu, P.; Asahi, T.; Nakatani, K. Photoswitchable Interactions Between Photochromic Organic Diarylethene and Surface Plasmon Resonance of Gold Nanoparticles in Hybrid Thin films. *Phys. Chem. Chem. Phys.* **2013**, *15*, 9670-9678. https://doi.org/10.1039/C3CP50770J.

22. Photon-Working Switches (2018). In: Yokoyama Y., Nakatani K. (eds), Springer Japan, ISBN 978-4-431-56542-0.

23. Snegir, S.; Mukha, I.; Sysoiev, D.; Lacaze, E.; Huhn, T.; Pluchery, E. Optically Controlled Properties of Nanoparticles Stabilized by Photochromic Difurylethene-base Diarylethenes. *Mat.-wiss. u. Werkstofftech*. **2016**, 47, No. 2–3. https://doi.org/10.1002/mawe.201600472.

24. Nishi, H.; Asahib, T.; Kobatake, S. Plasmonic Enhancement of Gold Nanoparticles on Photocycloreversion Reaction of Diarylethene Derivatives Depending on Particle Size, Distance from the Particle Surface, and Irradiation Wavelength. *Phys. Chem. Chem. Phys.* **2012**, *14*, 4898-4905. https://doi.org/10.1039/C2CP23820A.

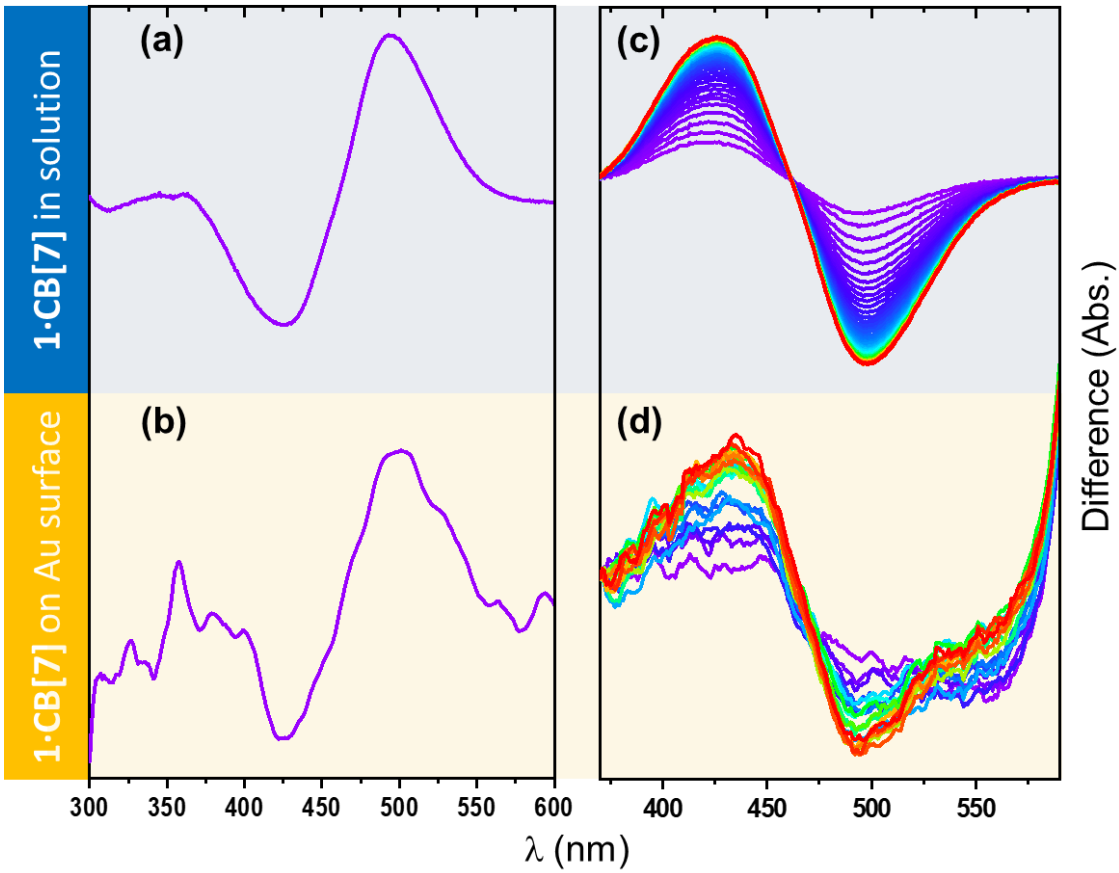

Figure S51. Differential UV–vis absorption spectra of **1·CB[7]** in DMSO solution (a) and on a gold substrate (b) before and after photoirradiation at 400 ± 5 nm, recorded at 25 °C in solution and at 15 °C on the gold surface. Thermal relaxation of **1·CB[7]** in DMSO solution (c) and on the gold substrate (d) was monitored through differential UV–vis absorption spectra measured at 25 °C and 10 °C, respectively.

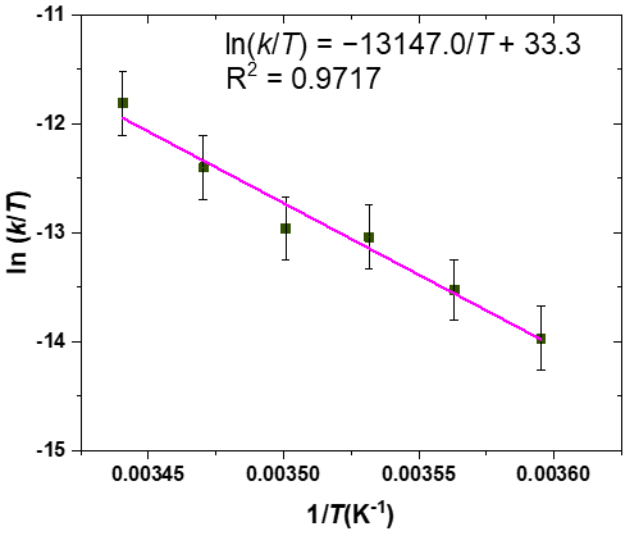

Figure S52. Eyring plot of **1·CB[7]** in SAM on a semitransparent gold surface including error bars (black).

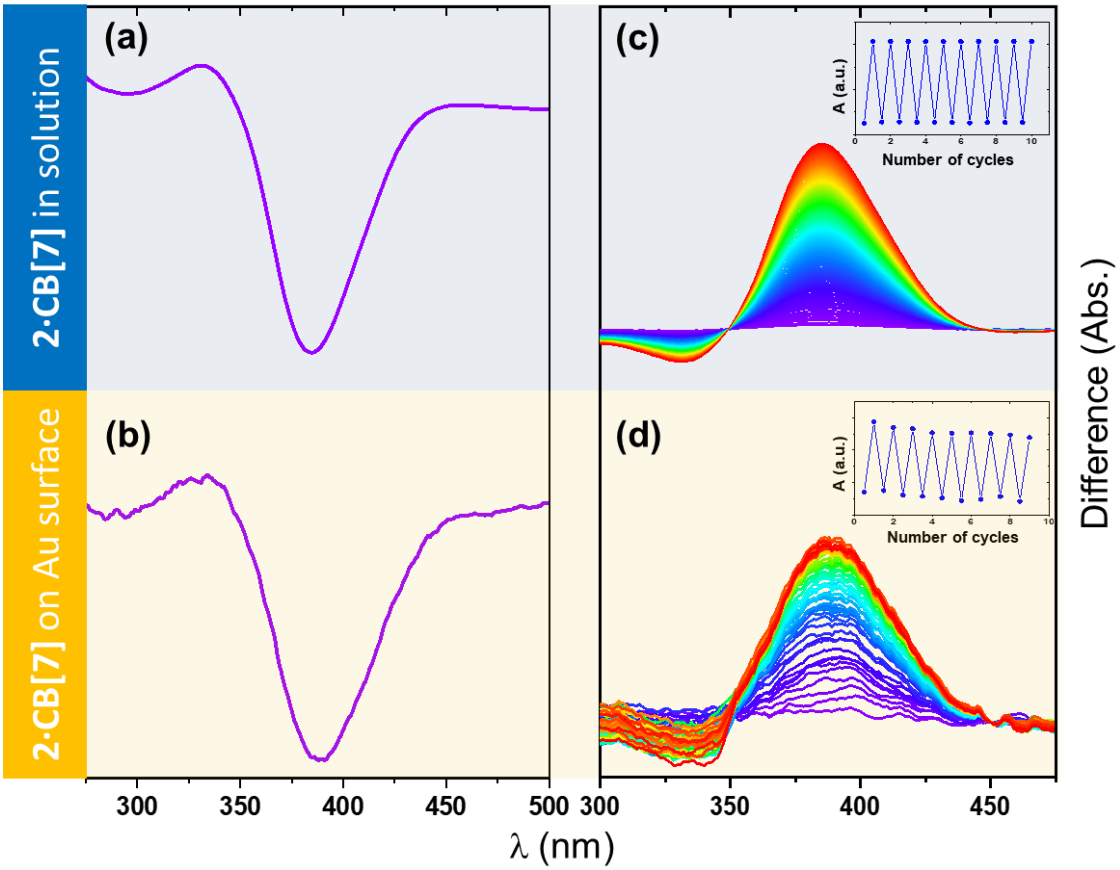

Figure S53. Differential UV–vis absorption spectra of **2·CB[7]** in DMSO solution (a) and within a SAM on a gold substrate (b) before and after photoirradiation at 400 ± 5 nm, recorded at 20 °C in solution and 15 °C in the SAM. Panels (c) and (d) show the corresponding thermal relaxation of **2·CB[7]** at 30 °C in solution and 40 °C in the SAM. *Insert:* Photostability of **2·CB[7]** monitored at 374 nm in solution and 390 nm in the SAM during alternating irradiation with 400 nm light (6 min in solution; 25 s in SAM, 70% intensity) and 450 nm light (1 min in solution; 15 s in SAM, 50% intensity).

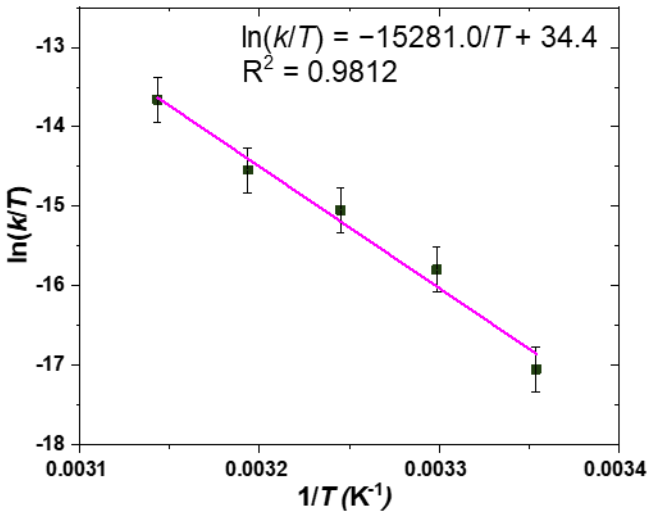

Figure S54. Eyring plot of thermal *cis*-to-*trans* interconversion of **2·CB[7]** in SAM on a semitransparent gold surface including error bars (black).

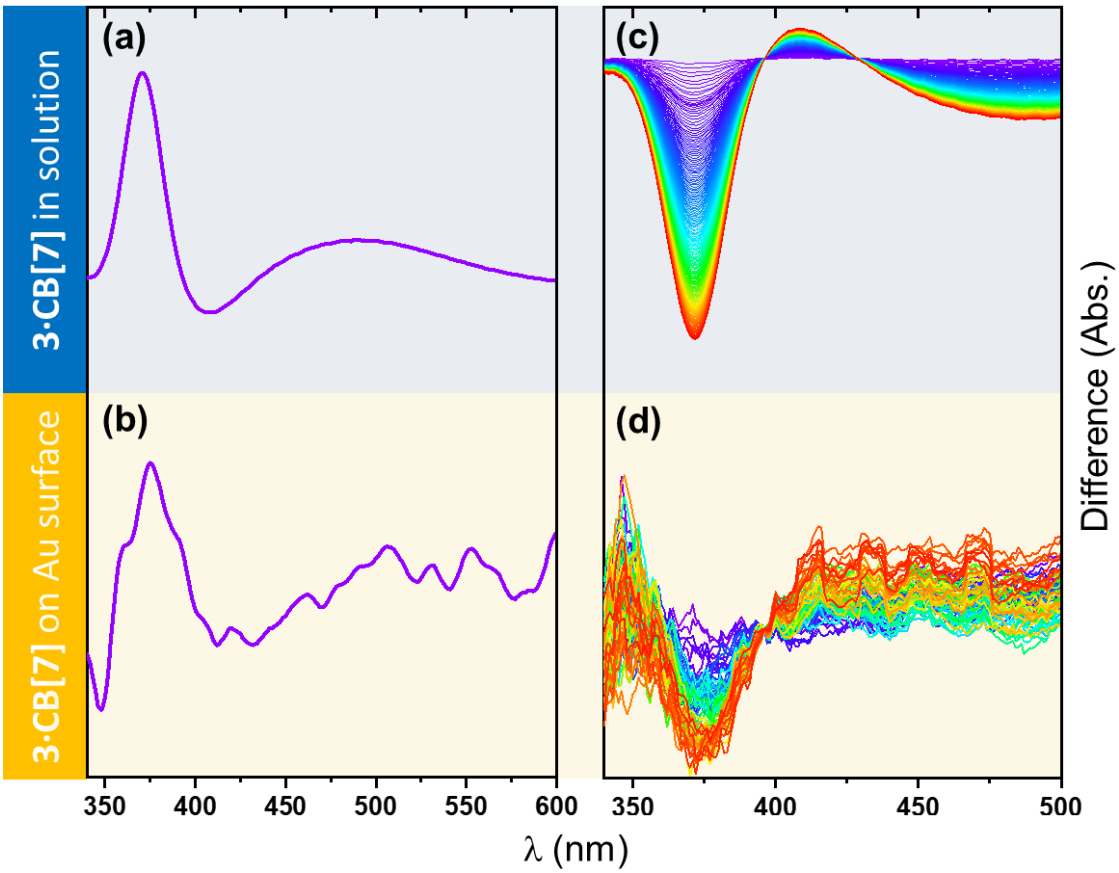

Figure S55. Differential UV–vis absorption spectra of **3·CB[7]** in DMSO solution (a) and within a SAM on a gold substrate (b) before and after photoirradiation at 400 ± 5 nm, recorded at 20 °C in solution and 15 °C in the SAM. Panels (c) and (d) display the corresponding thermal relaxation of **3·CB[7]** at 20 °C in solution and in SAM.

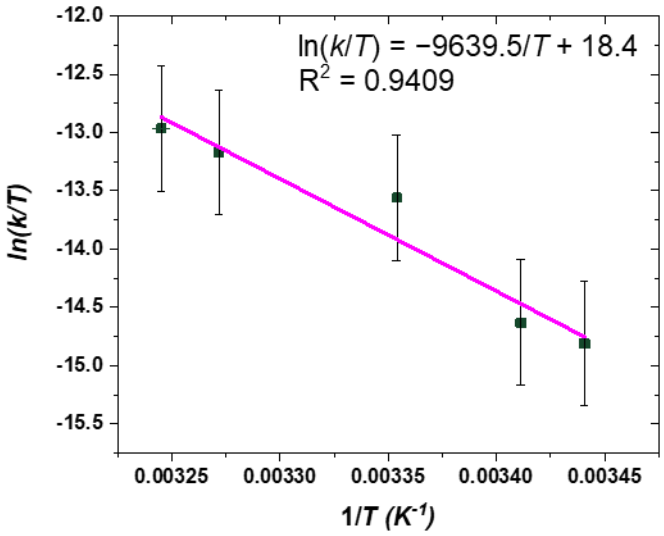

Figure S56. Eyring plot of thermal *trans*-to-*cis* interconversion of **3·CB[7]** in SAM on a semitransparent gold surface including error bars (black).

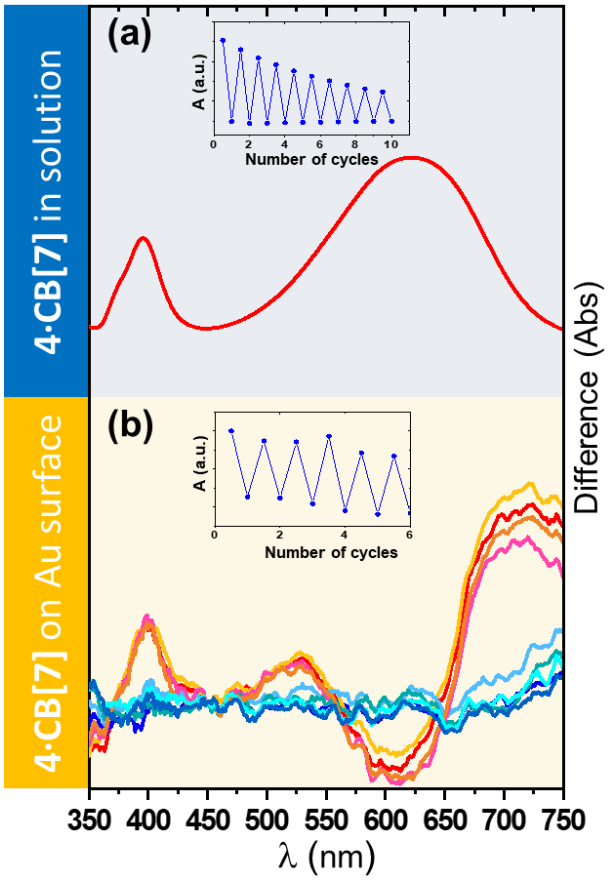

Figure S57. Differential UV–vis absorption spectra of **4·CB[7]** in DMSO solution (a) and as monolayers on a gold substrate (b), showing the spectral changes between the open and closed forms upon photoirradiation at 308 and 600 nm. Multiple photoswitching cycles are shown for the SAM to illustrate the reversibility of the process. *Insert:* Photostability of **4·CB[7]** in solution at 600 nm and within the SAM at 392 nm during repeated irradiation cycles at 308 nm (13 min in solution; 80 s in SAM, 70% light intensity) and 600 nm (6 min in solution; 150 s in SAM, 70% light intensity).

8.9 Determination of CB[7] Surface Coverage from AFM and UV-Vis Data

Determination of Surface Coverage from AFM

Surface coverage was calculated from AFM height images by counting depressions corresponding to individual **CB[7]** molecules. Sixteen regions from two separately prepared substrates were analyzed. Images were pre-processed in Gwyddion (plane leveling, row alignment) and contrast was adjusted to make the depressions clearer. Only well-defined depressions with sizes matching the expected **CB[7]** cavity (about 1.6 nm) were counted.

Assuming hexagonal closest packing,[25] the area assigned to one **CB[7]** molecule (geometric cross-section plus the associated packing voids) was taken as 2.217 nm². Based on this value, the surface coverage was determined to be **58 ± 10%**. This result is consistent with previous studies showing that **CB[7]** forms stable monolayers on gold via noncovalent interactions between its carbonyl rims and the metal surface. Reported surface coverages

25. Metze, F. K.; Filipucci, I.; Klok, H. A. Supramolecular Polymer Brushes Grown by Surface-Initiated Atom Transfer Radical Polymerization from Cucurbit[7]uril-based Non-Covalent Initiators, *Angew. Chem. Int. Ed.* **2023**, *62*, e202305930. https://doi.org/10.1002/anie.202305930.

typically range from 40 to 50%, based on electrochemical and AFM measurements, which agrees with partial monolayer formation.[26, 27]

Determination of Surface Coverage from UV–Vis Data

Surface coverage was also estimated from UV–Vis absorption measurements. Although gold substrates exhibit a strong background signal in the UV–Vis region, a distinct absorption band at approximately 350 nm was observed for the complexes **2·CB[7]**, **3·CB[7]**, and **4·CB[7]**. Subtracting the spectrum of a clean gold substrate from that of the **CB[7]**-modified substrate yielded the absorbance attributable to the monolayer. For **1·CB[7]**, the surface coverage could not be determined because its molar absorption coefficient in the relevant region is very low, and the corresponding band is effectively obscured by the gold substrate background.

Surface coverage was calculated from the absorbance difference using the molar absorption coefficient (ε) determined in solution, assuming that ε remains unchanged upon surface attachment. Applying the Beer–Lambert law ($A = \varepsilon \times c$) provided the surface concentration (c, in mol cm^{-2}). The calculated surface concentration was converted to the number of molecules per nm^2 and subsequently to surface area per molecule.

As outlined above, a single **CB[7]** molecule in a densely packed hexagonal arrangement occupies 2.217 nm^2 (222 $Å^2$). Using this value together with the UV–Vis–derived surface concentration, the surface coverage of the gold substrates was determined to be **60 ± 15%**.

26. An, Q.; Li, G.; Tao, C.; Li, Y.; Wu, Y.; Zhang, W. A General and Efficient Method to Form Self-Assembled Cucurbit[n]Uril Monolayers on Gold Surfaces. *Chem. Commun.* **2008**, No. 17, 1989. https://doi.org/10.1039/b719927a.

27. Gomez-Casado, A.; Jonkheijm, P.; Huskens, J. Recognition Properties of Cucurbit[7]Uril Self-Assembled Monolayers Studied with Force Spectroscopy. *Langmuir* **2011**, *27* (18), 11508–11513. https://doi.org/10.1021/la202346r.

9. NMR Spectra of Newly Synthesized Compounds

^{1}H NMR (500 MHz, DMSO-d_6): Compound **1**

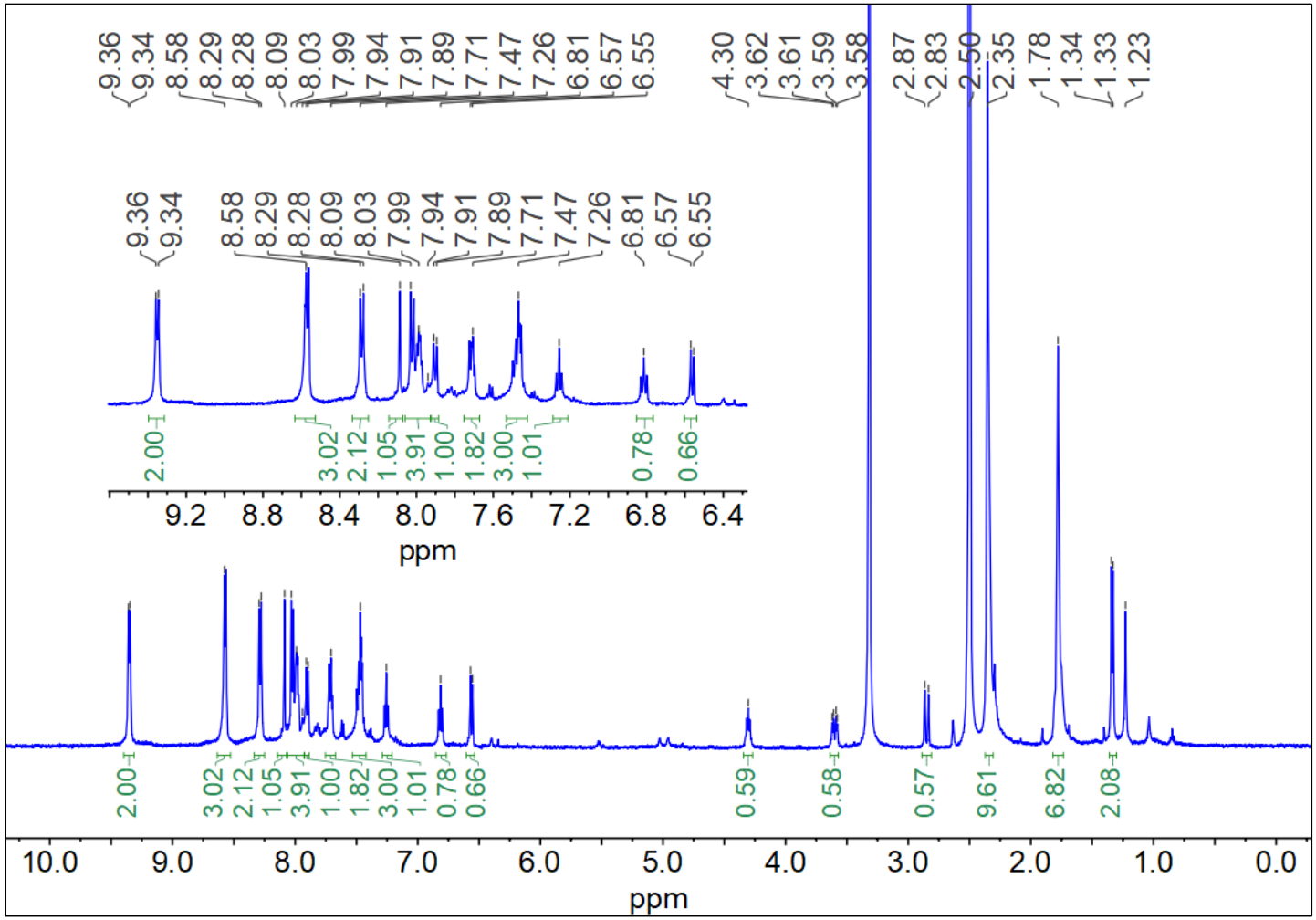

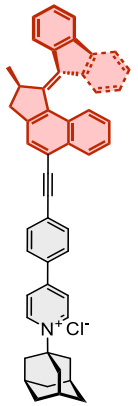

^{13}C {^{1}H} NMR (125 MHz, DMSO-d_6): Compound **1**

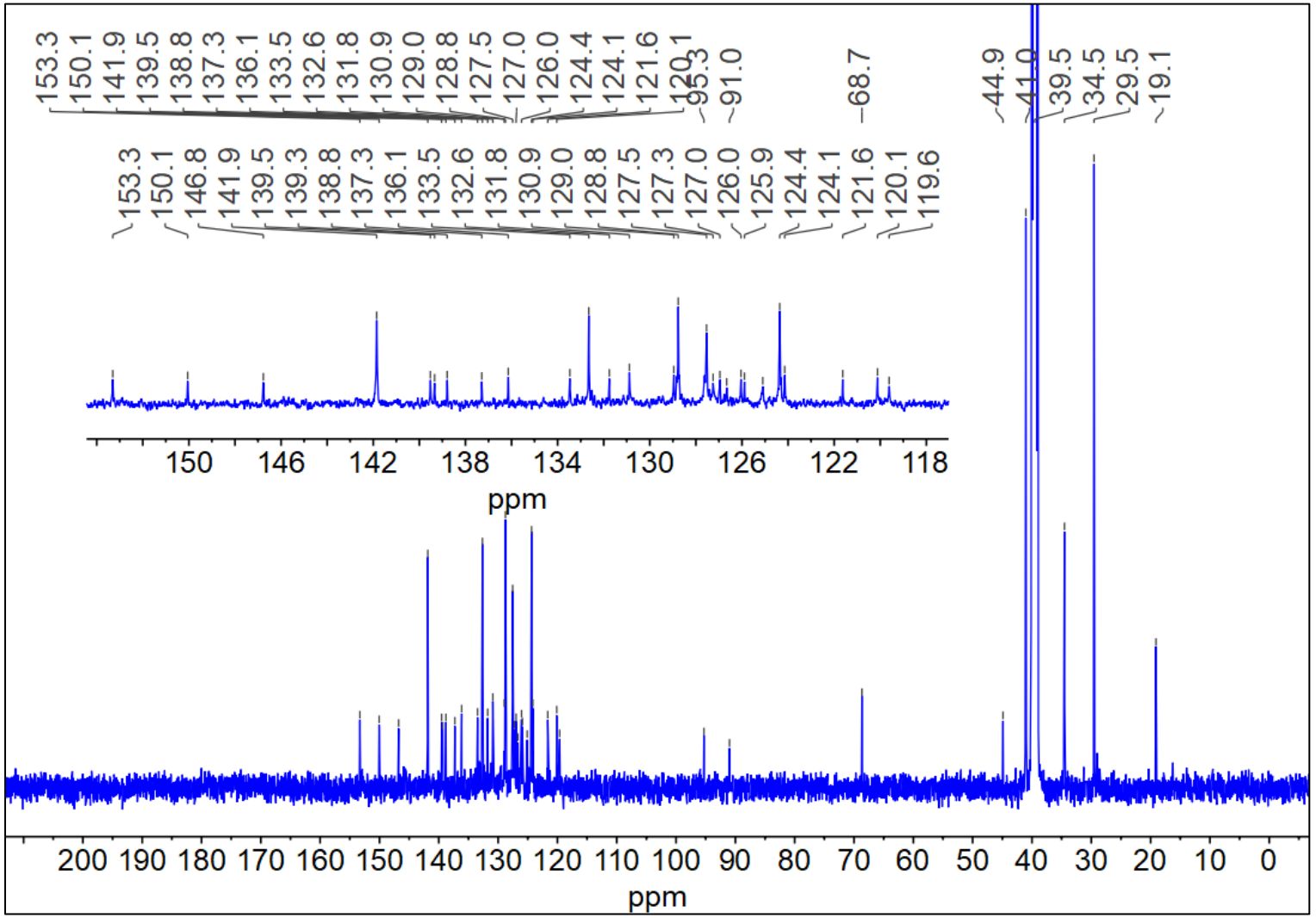

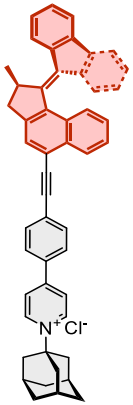

^{13}C {^{1}H} APT NMR (125 MHz, DMSO-d_6): Compound **1**

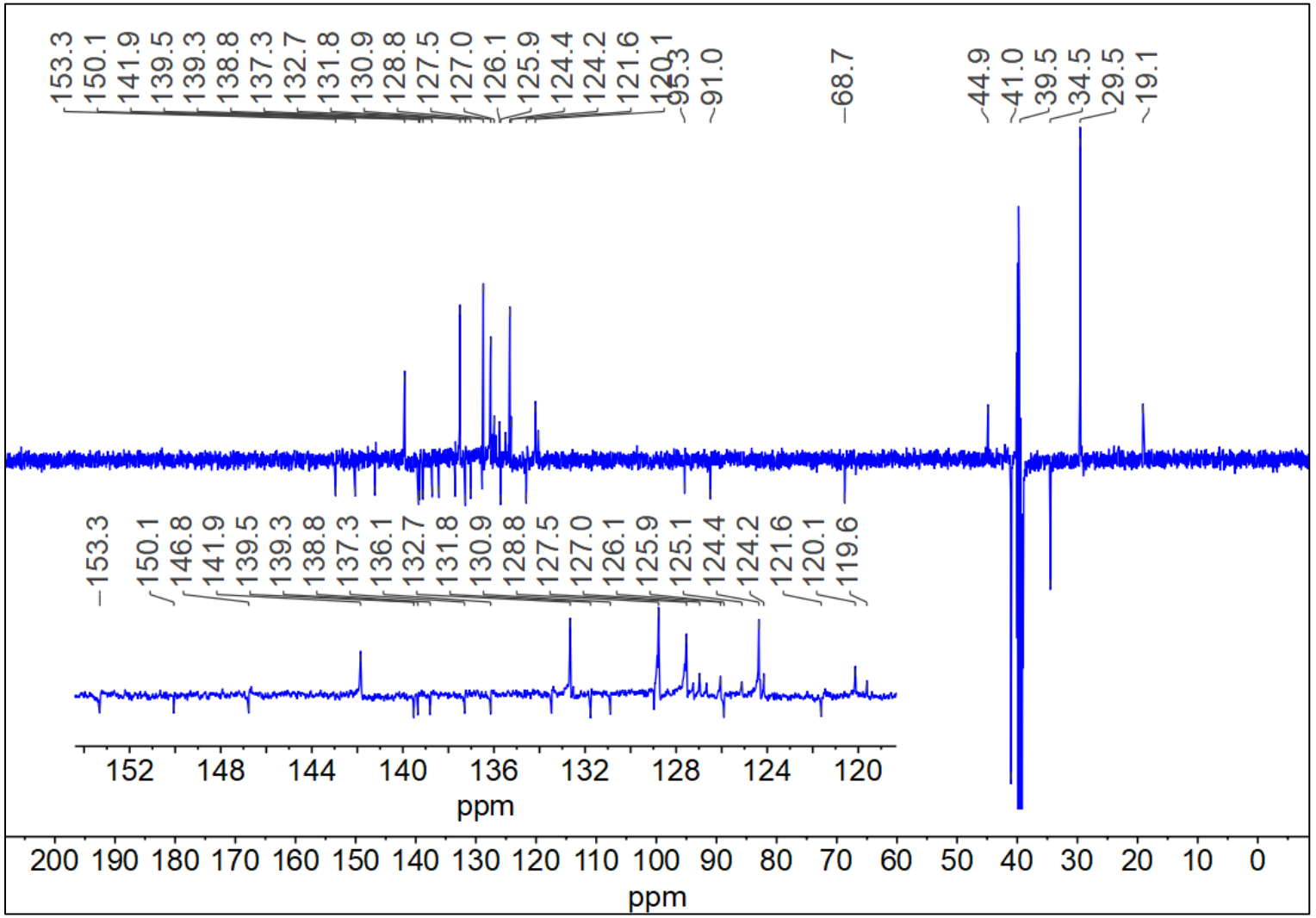

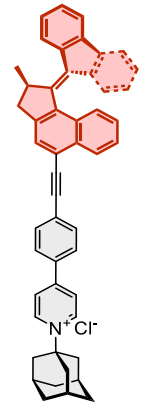

^{1}H-^{1}H COSY (DMSO-d_6): Compound **1**

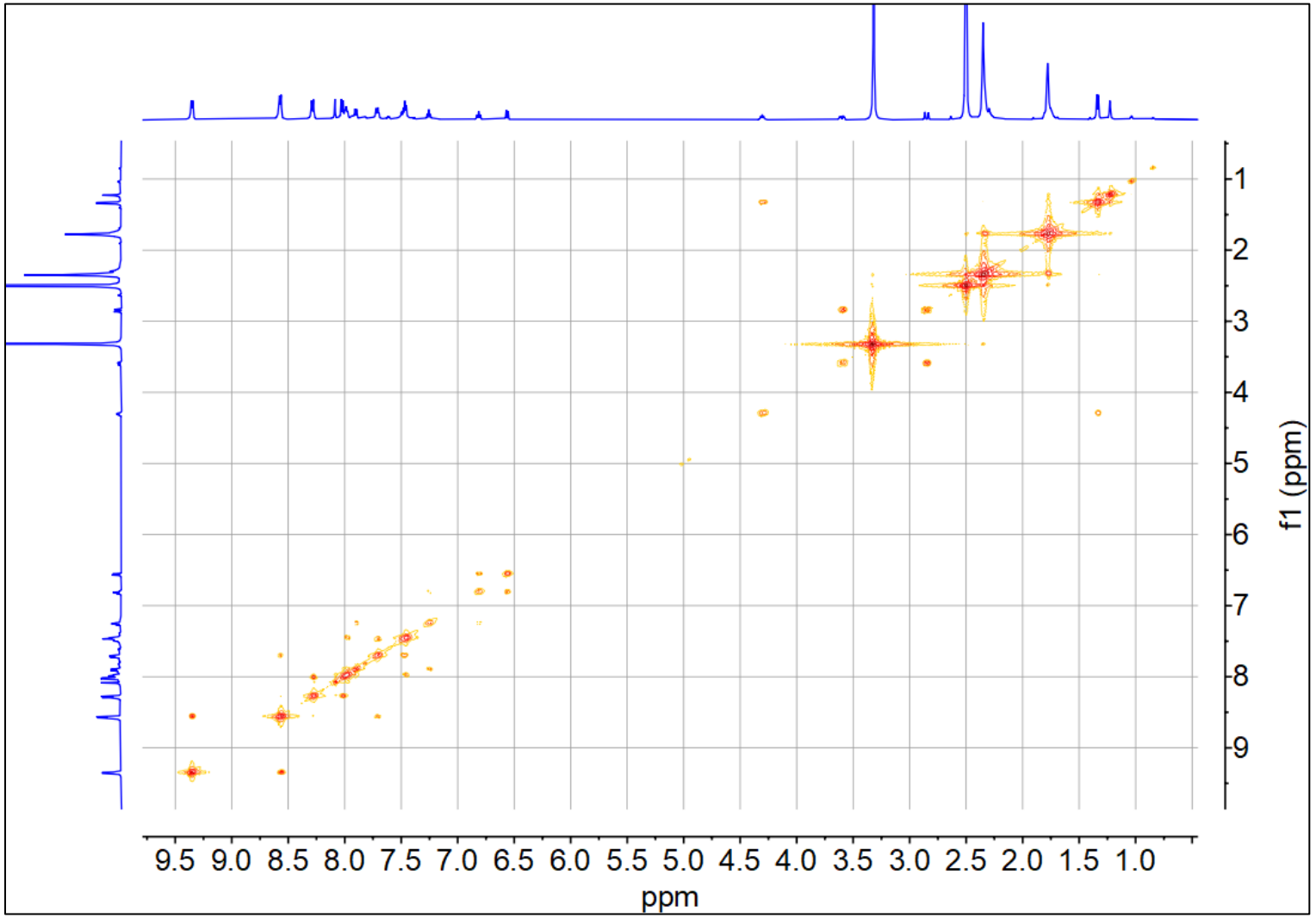

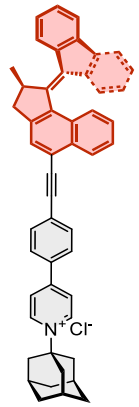

^{1}H-^{13}C HSQC (DMSO-d_6): Compound **1**

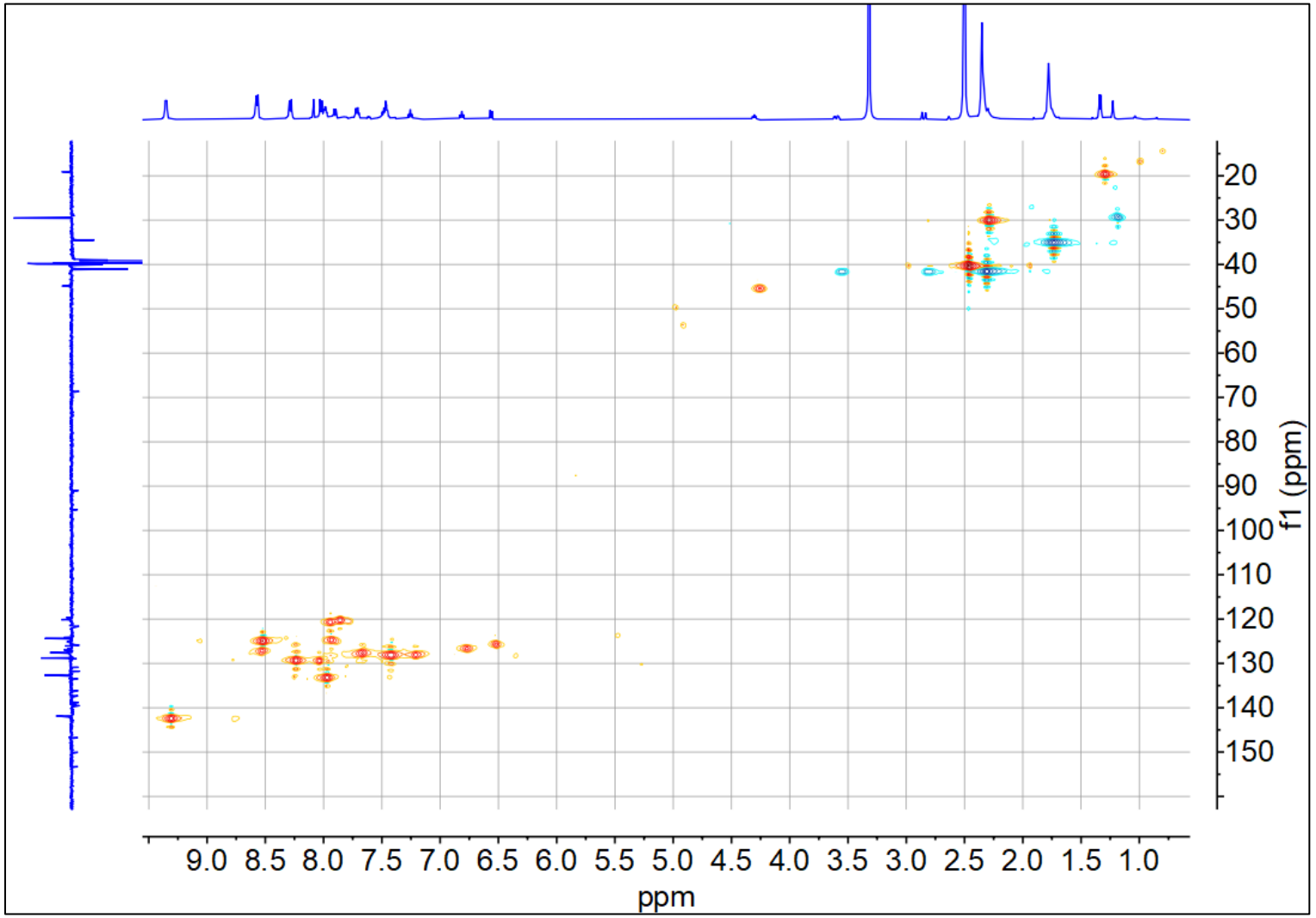

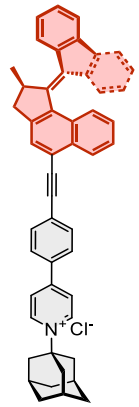

^{1}H-^{13}C HMBC (DMSO-d_6): Compound **1**

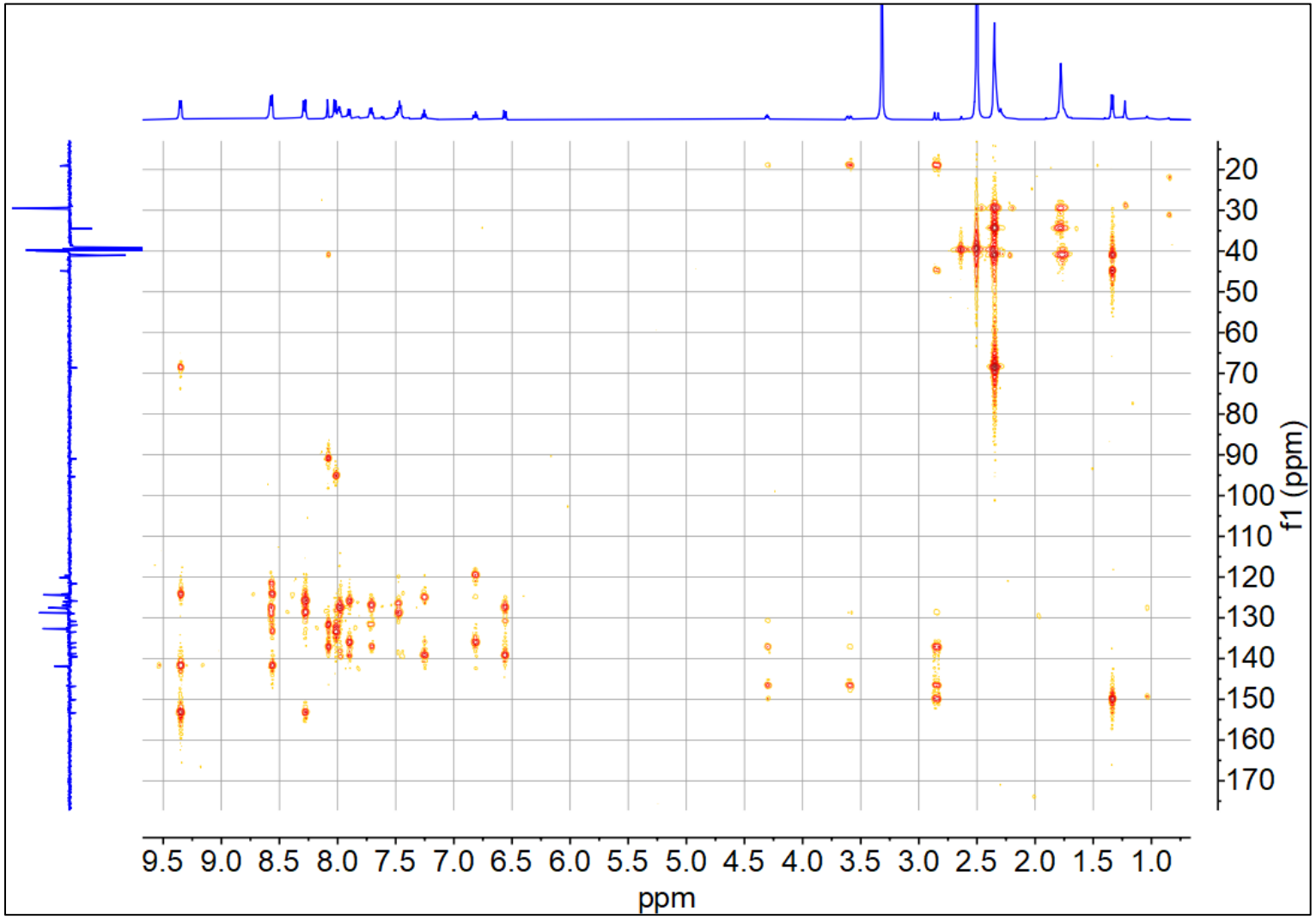

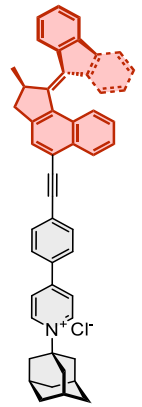

^{1}H NMR (400 MHz, DMSO-d_6): Compound **2**

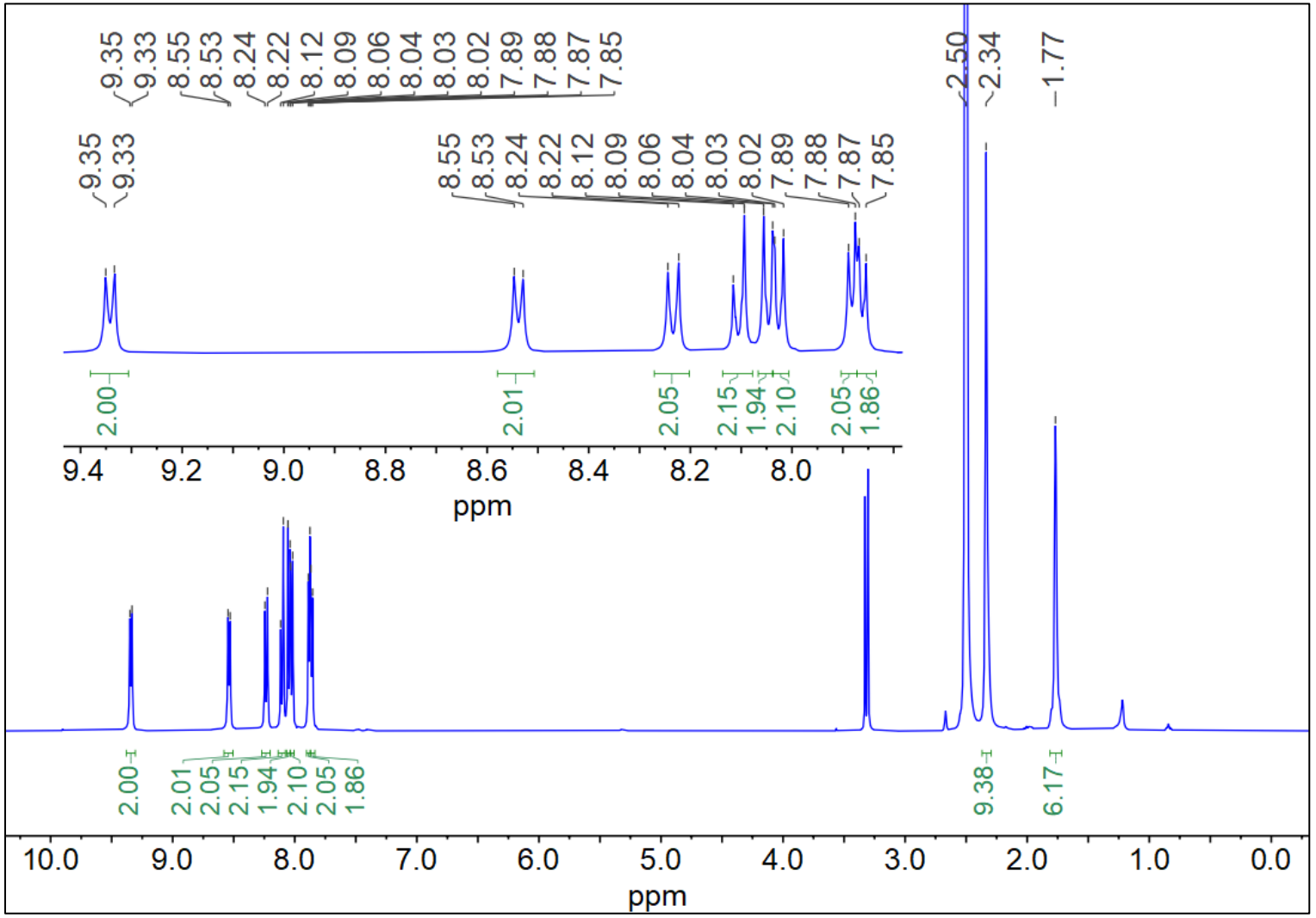

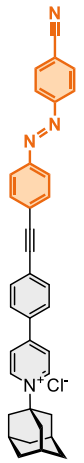

^{13}C {^{1}H} NMR (100 MHz, DMSO-d_6): Compound **2**

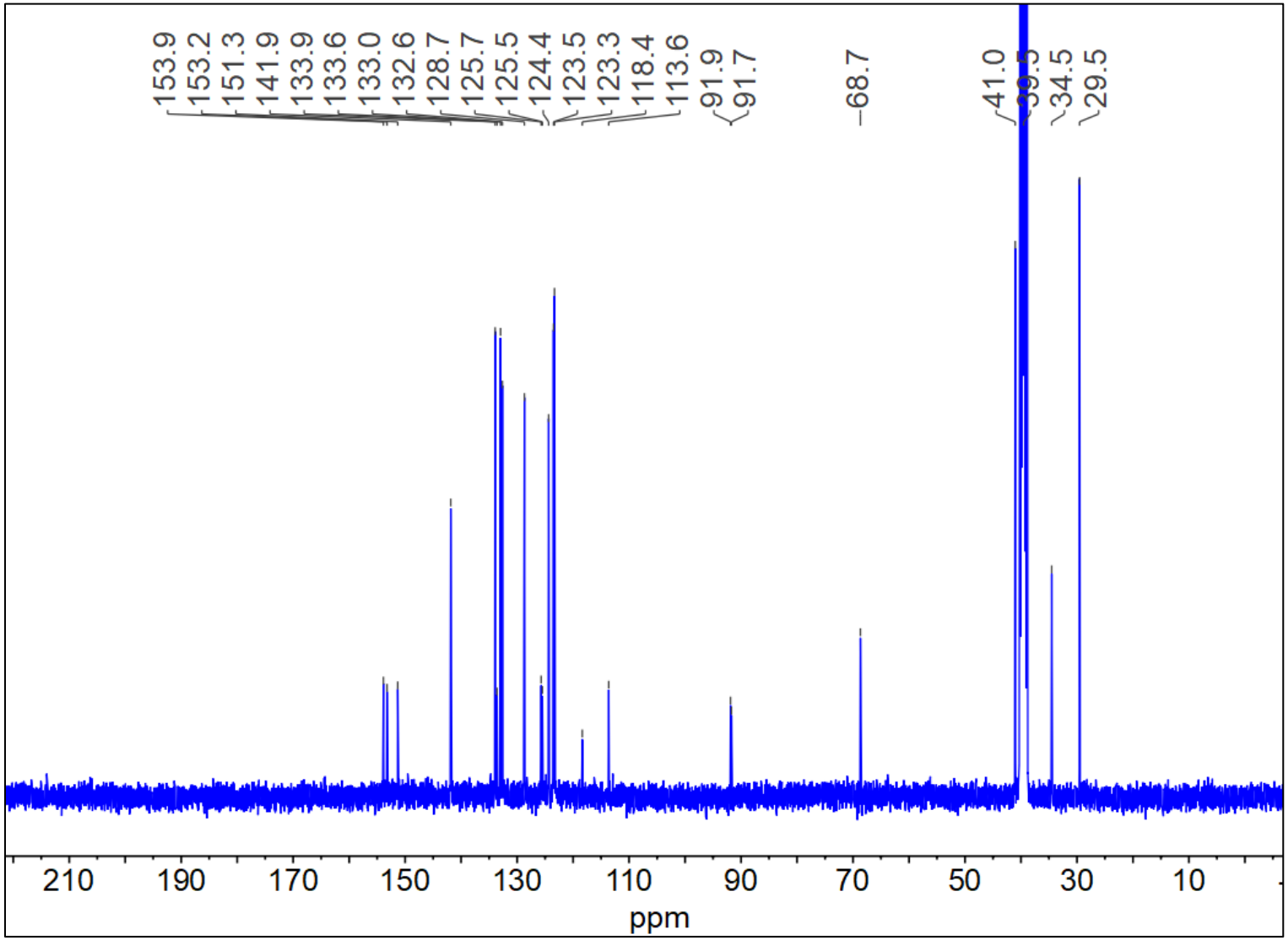

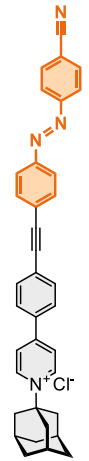

^{13}C {^{1}H} APT NMR (100 MHz, DMSO-d_6): Compound **2**

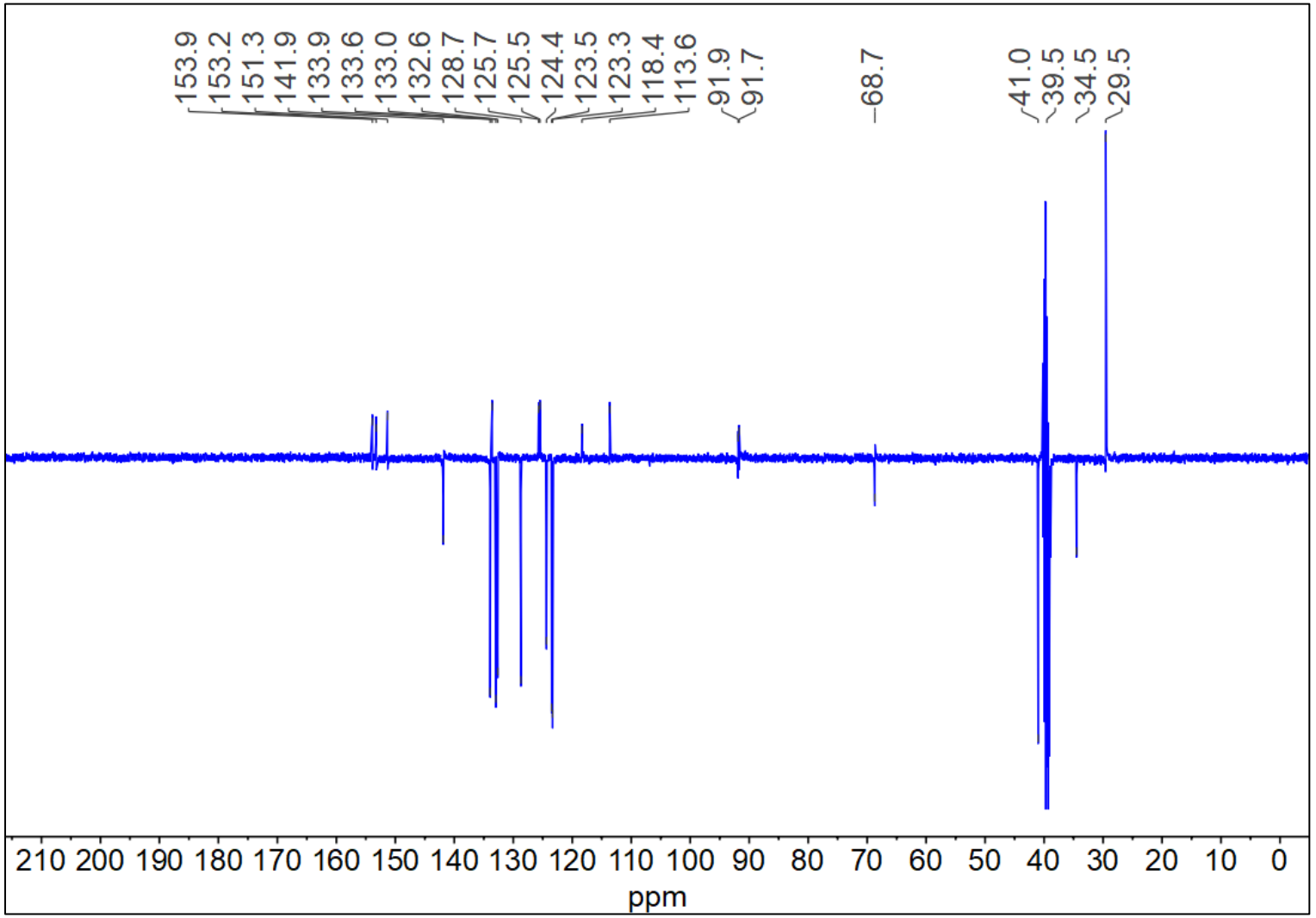

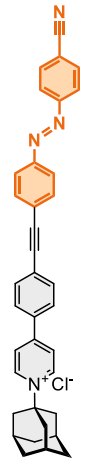

^{1}H-^{1}H COSY (DMSO-d_6): Compound **2**

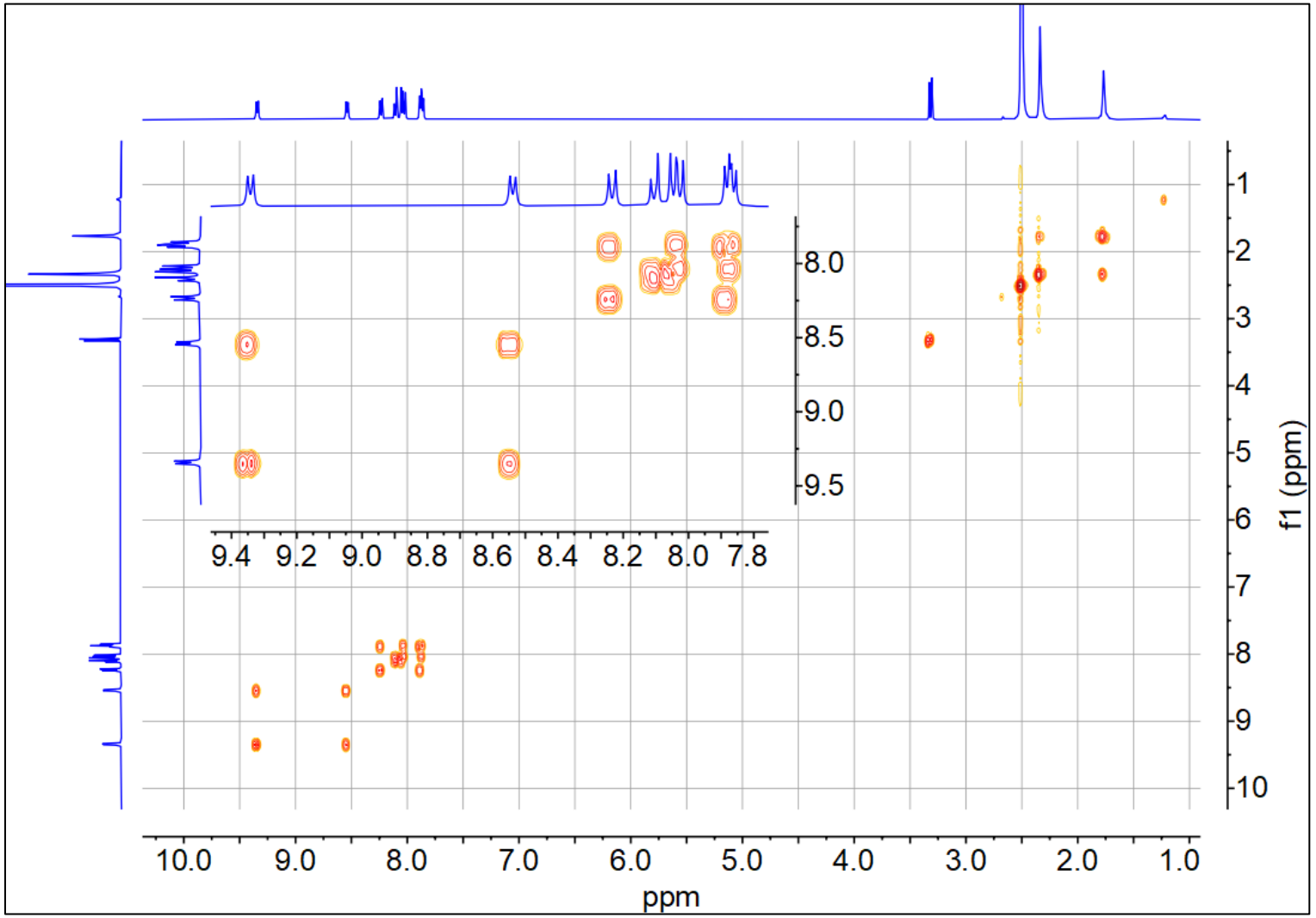

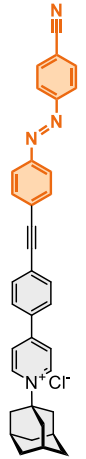

^{1}H – ^{13}C HSQC (DMSO-d_6): Compound **2**

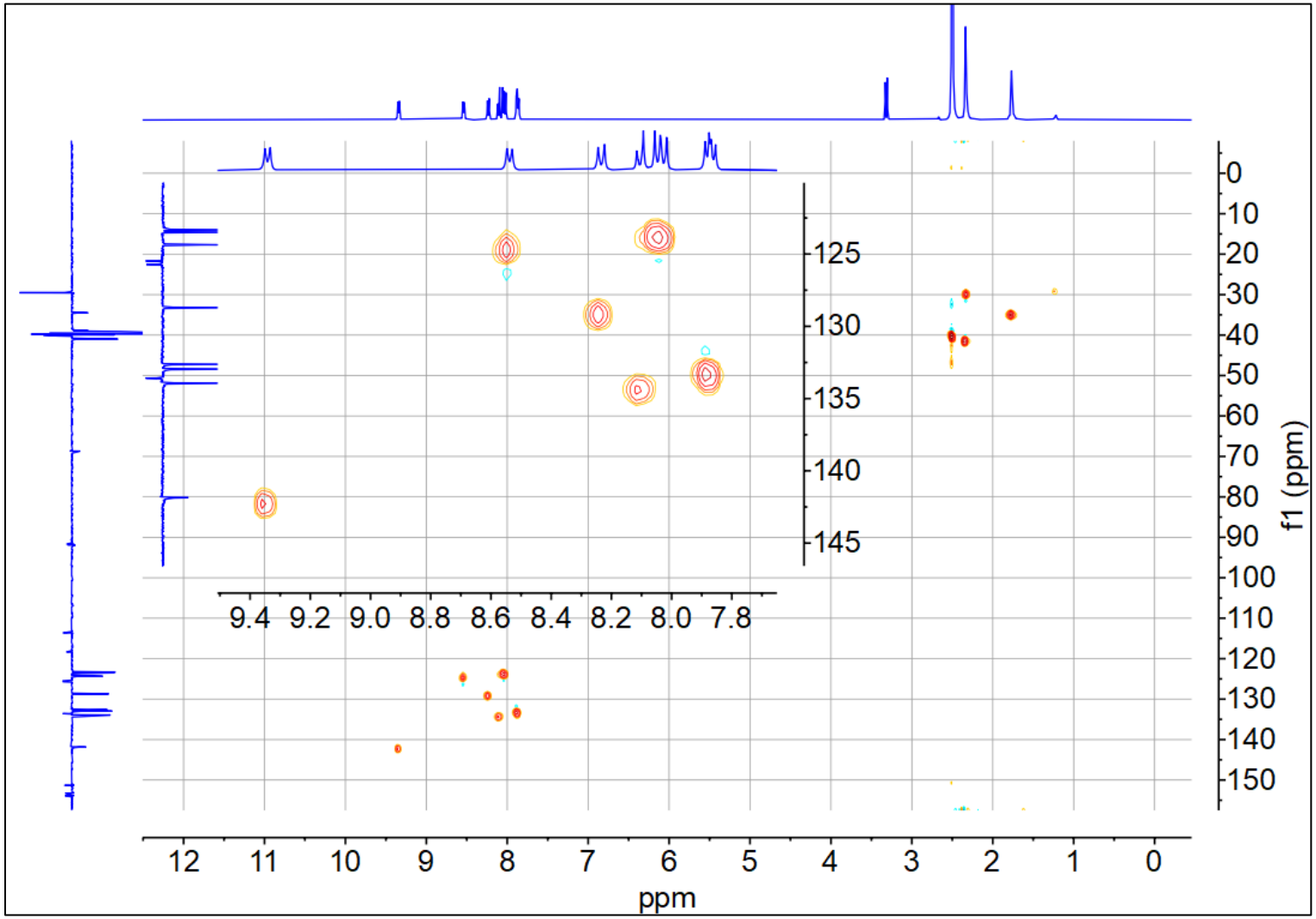

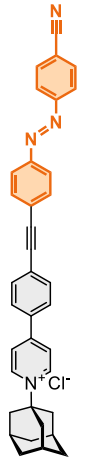

^{1}H -^{13}C HMBC (DMSO-d_6): Compound **2**

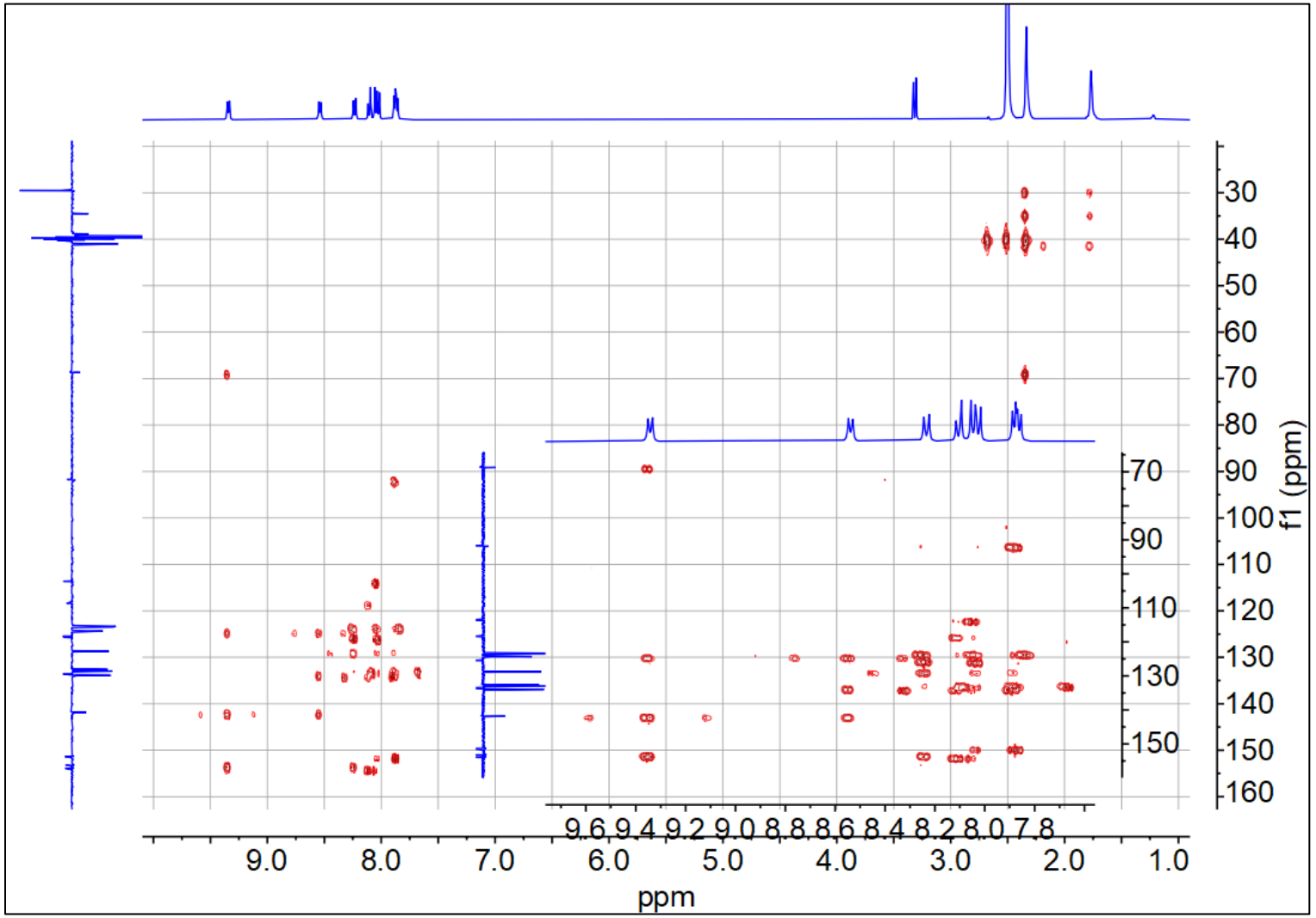

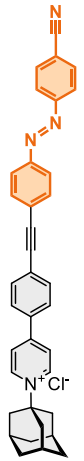

^{1}H NMR (500 MHz, DMSO-d_6): Compound **3**

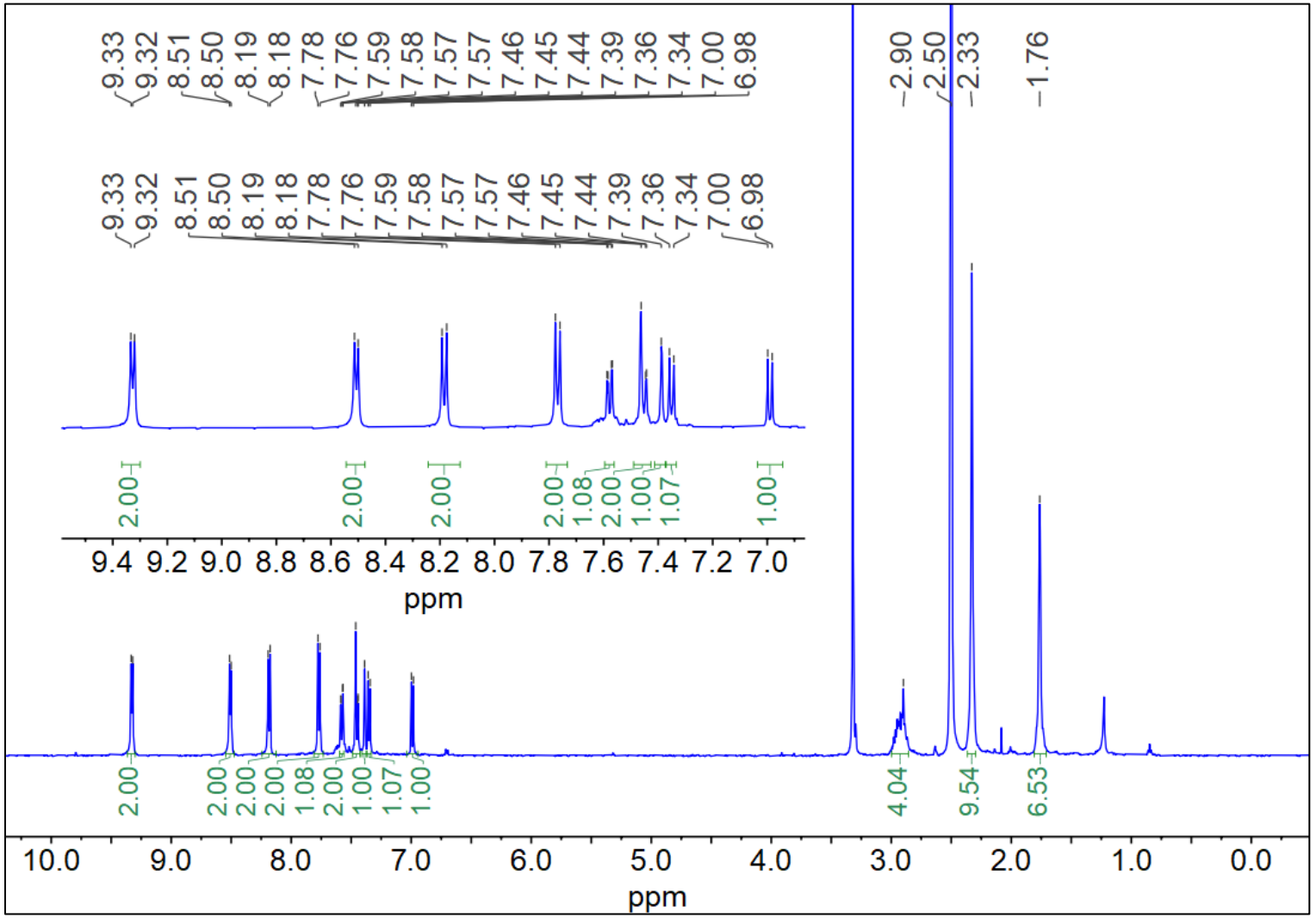

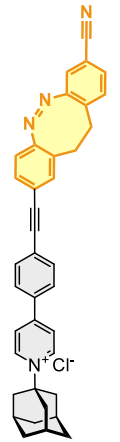

^{13}C {^{1}H} APT NMR (125 MHz, DMSO-d_6): Compound **3**

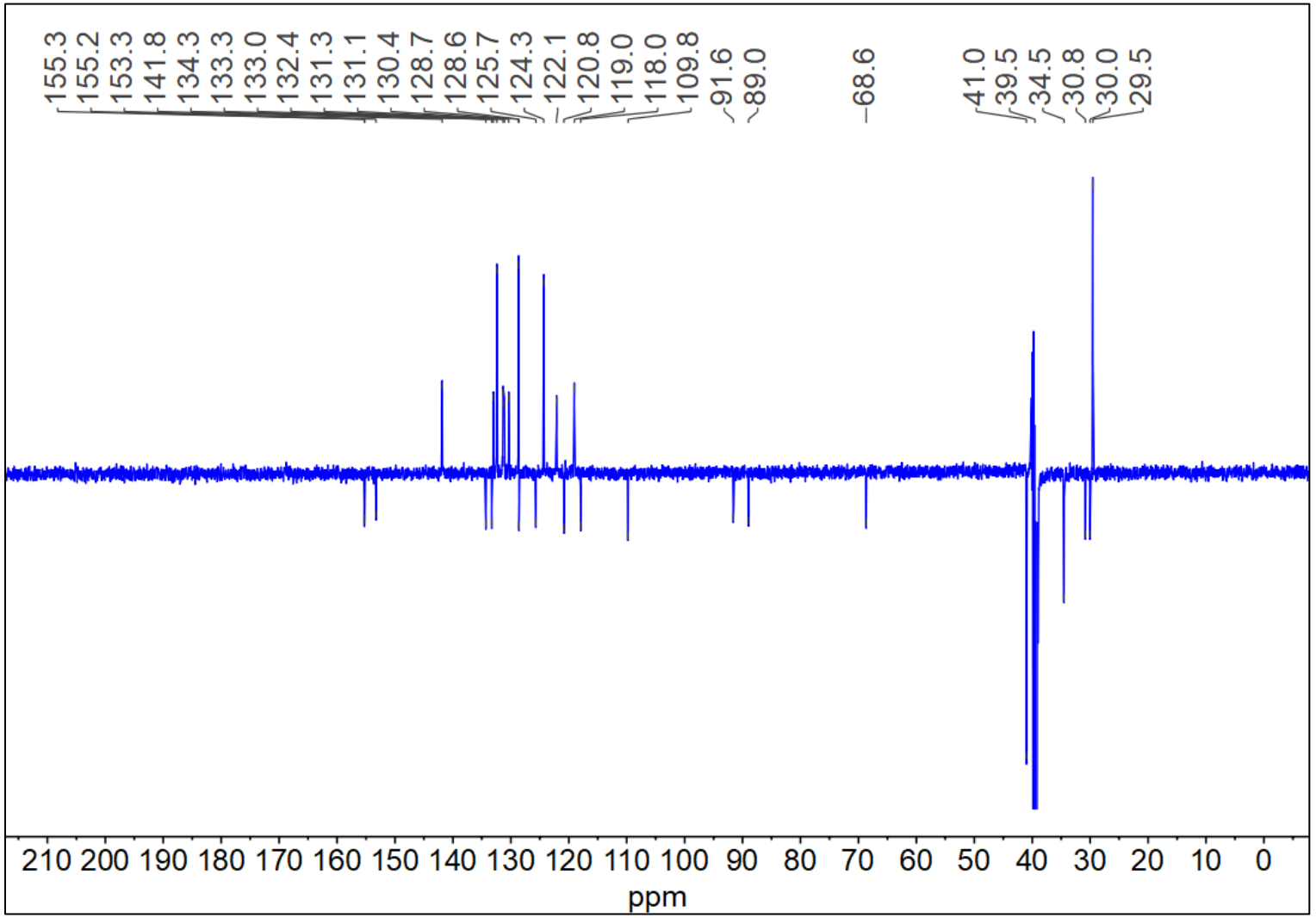

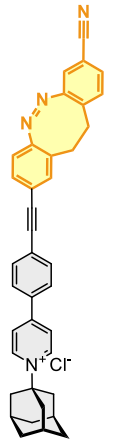

^{1}H-^{1}H COSY (DMSO-d_6): Compound **3**

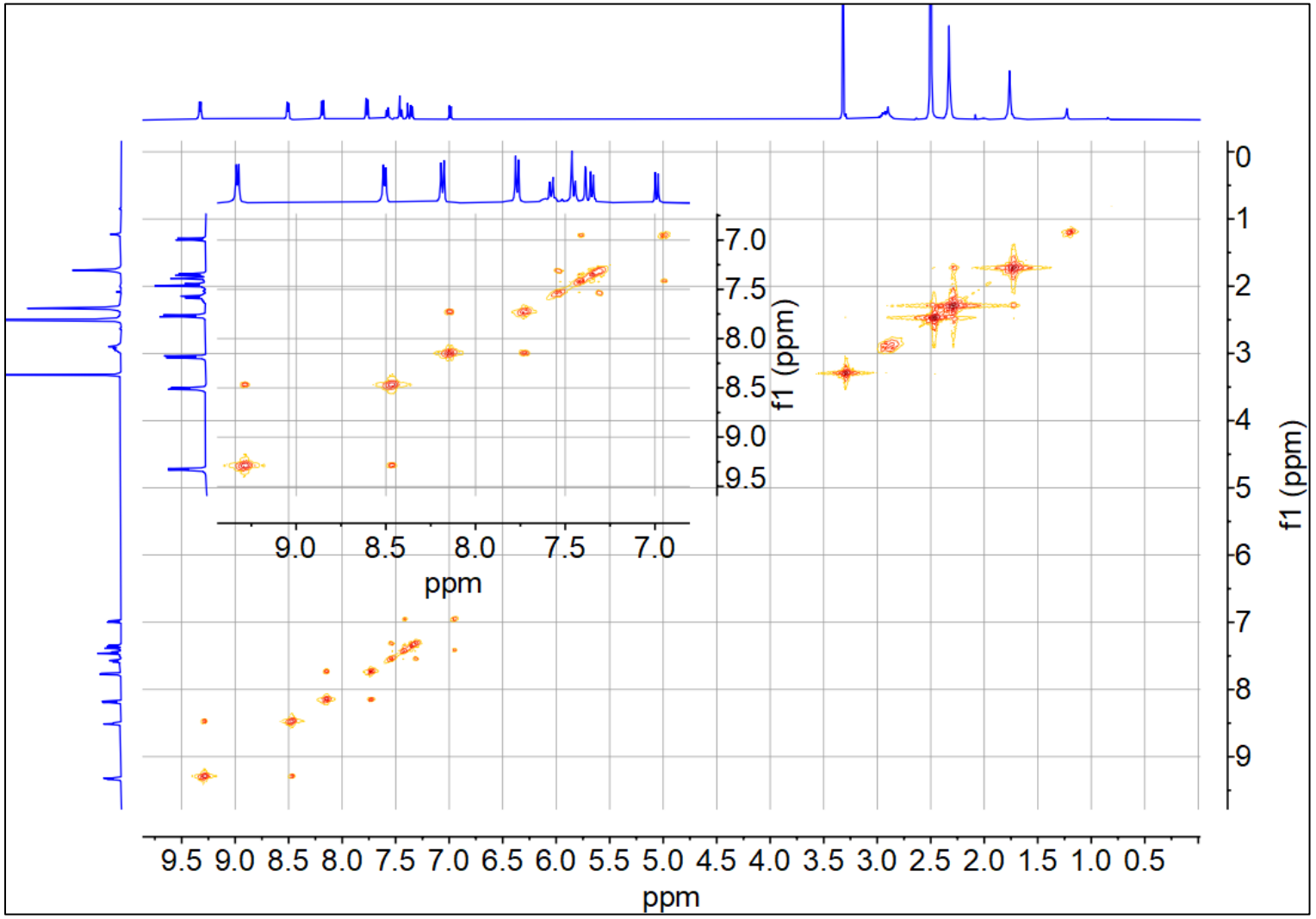

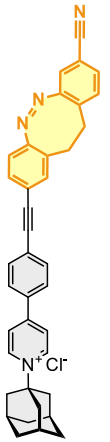

^{1}H -^{13}C HSQC (DMSO-d_6): Compound **3**

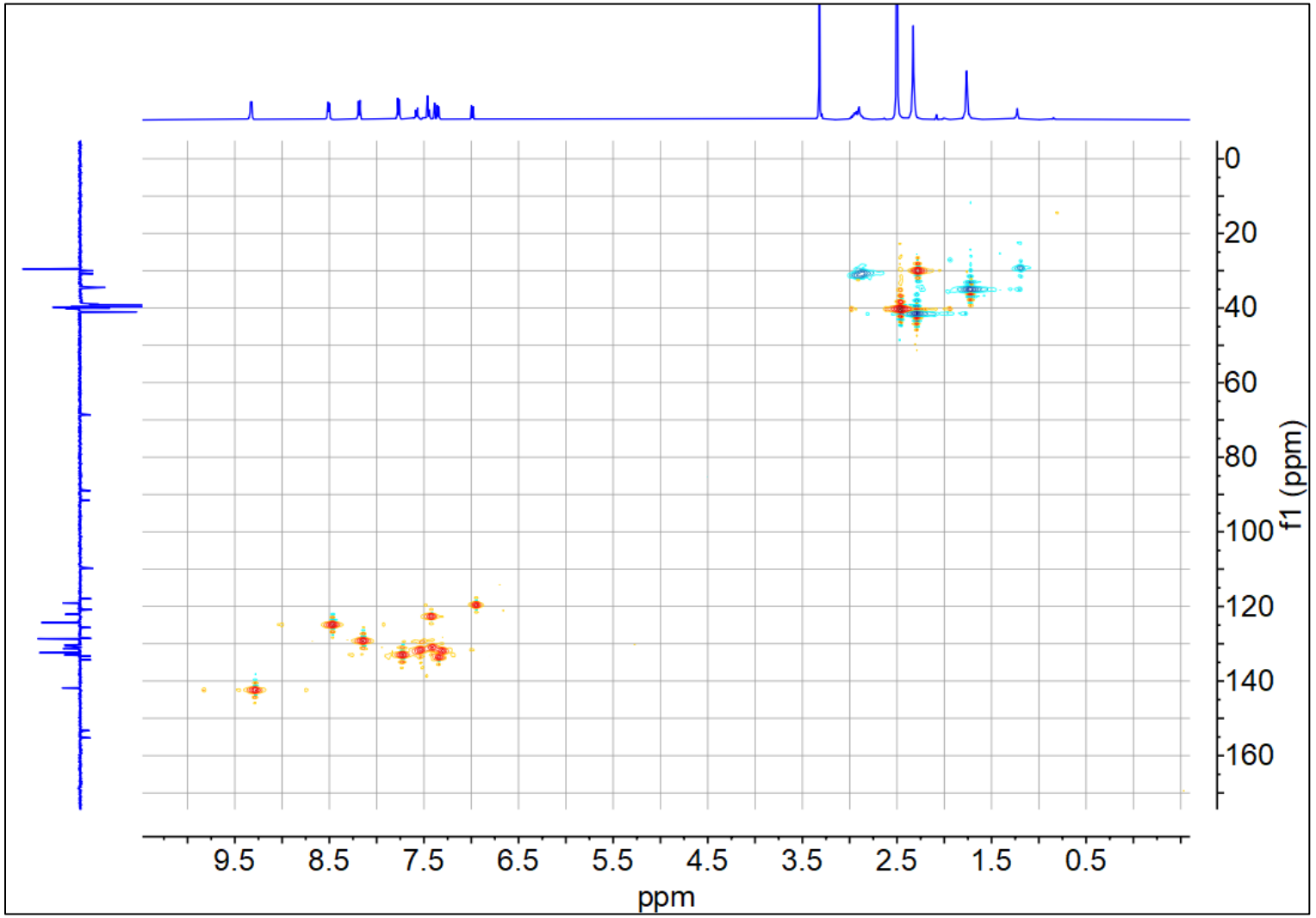

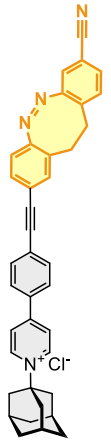

^{1}H-^{13}C HMBC (DMSO-d_6): Compound **3**

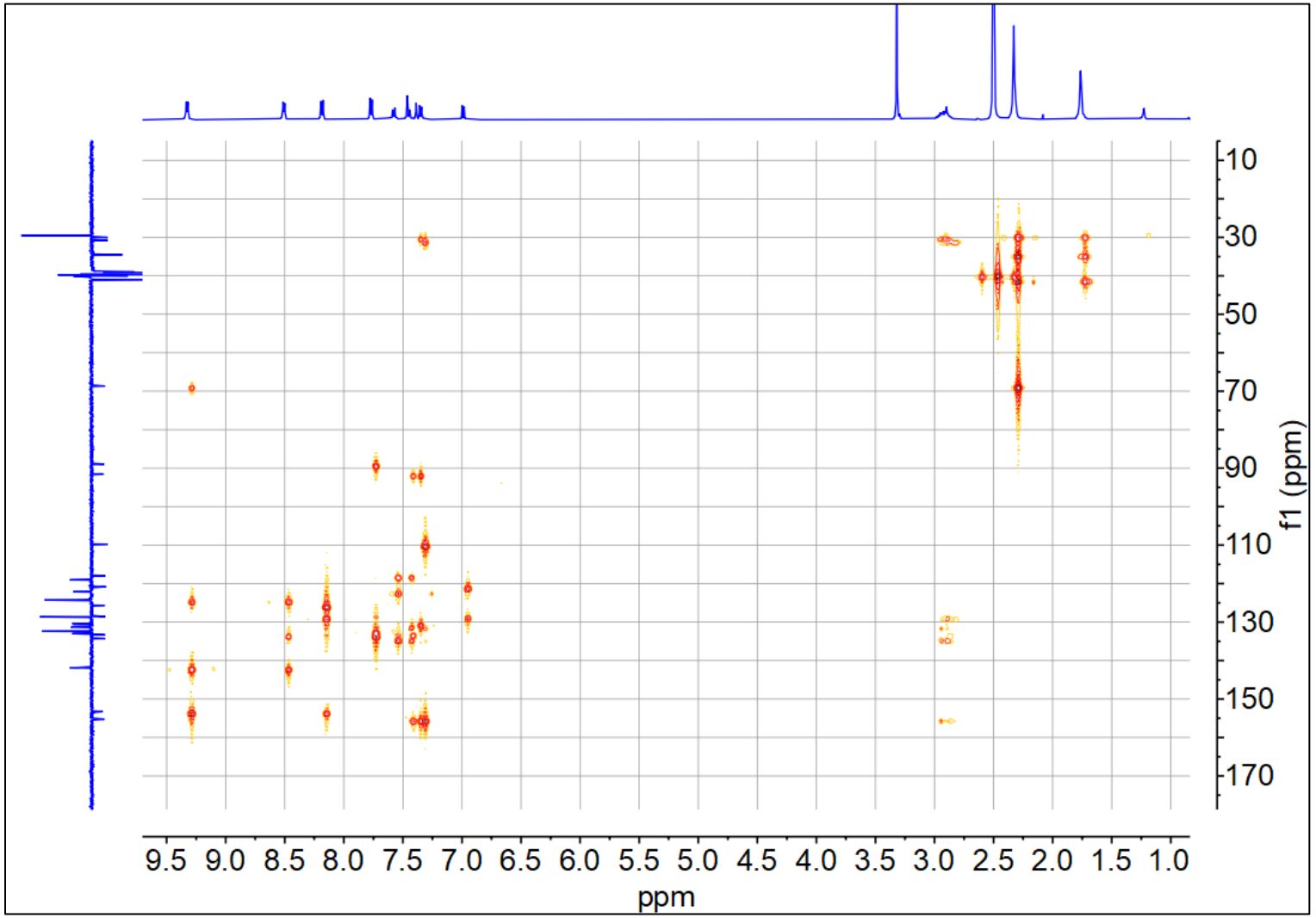

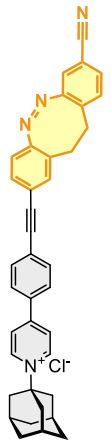

^{1}H NMR (400 MHz, DMSO-d_6): Compound **4**

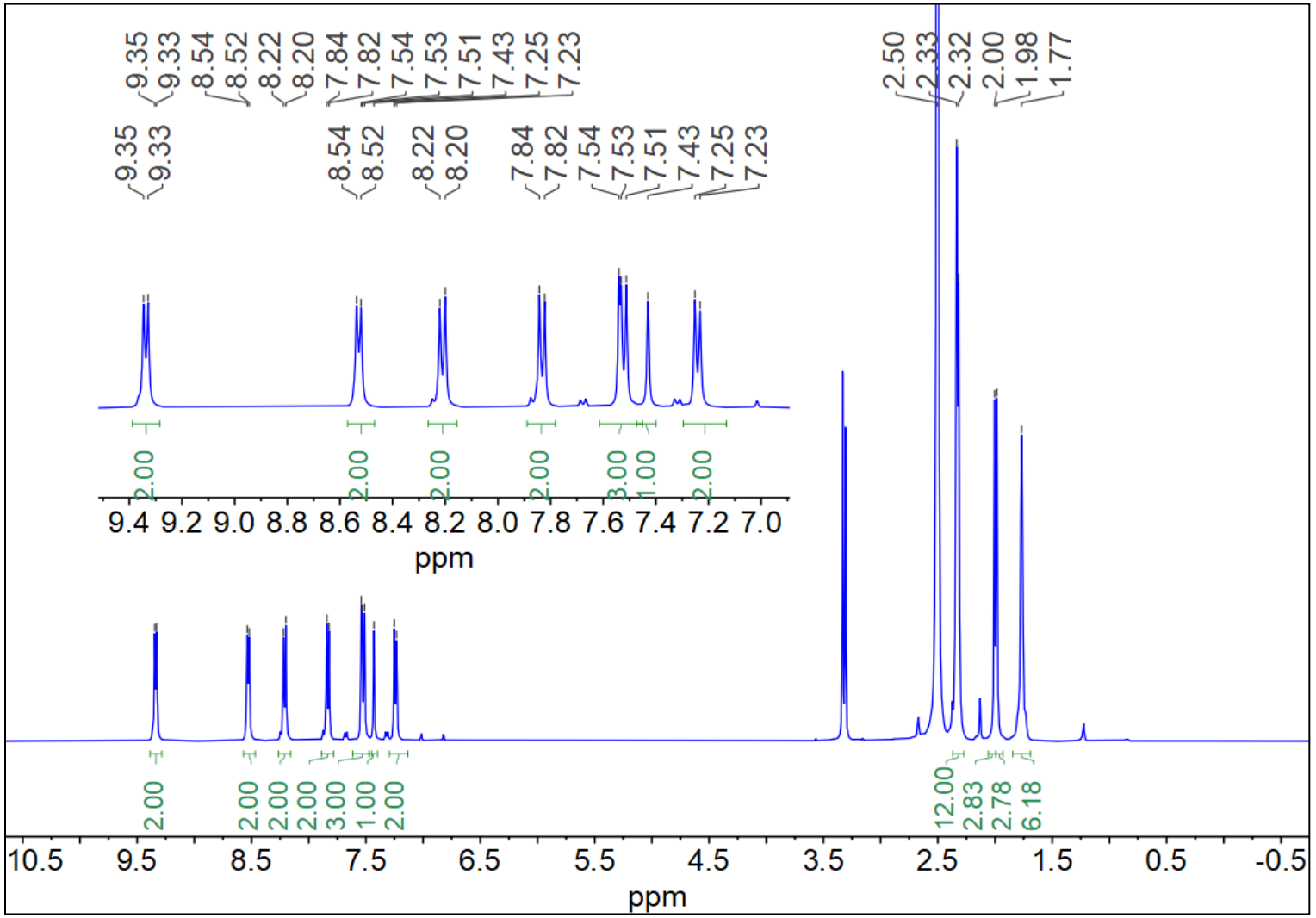

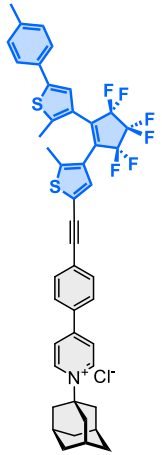

^{13}C {^{1}H} NMR (100 MHz, DMSO-d_6): Compound **4**

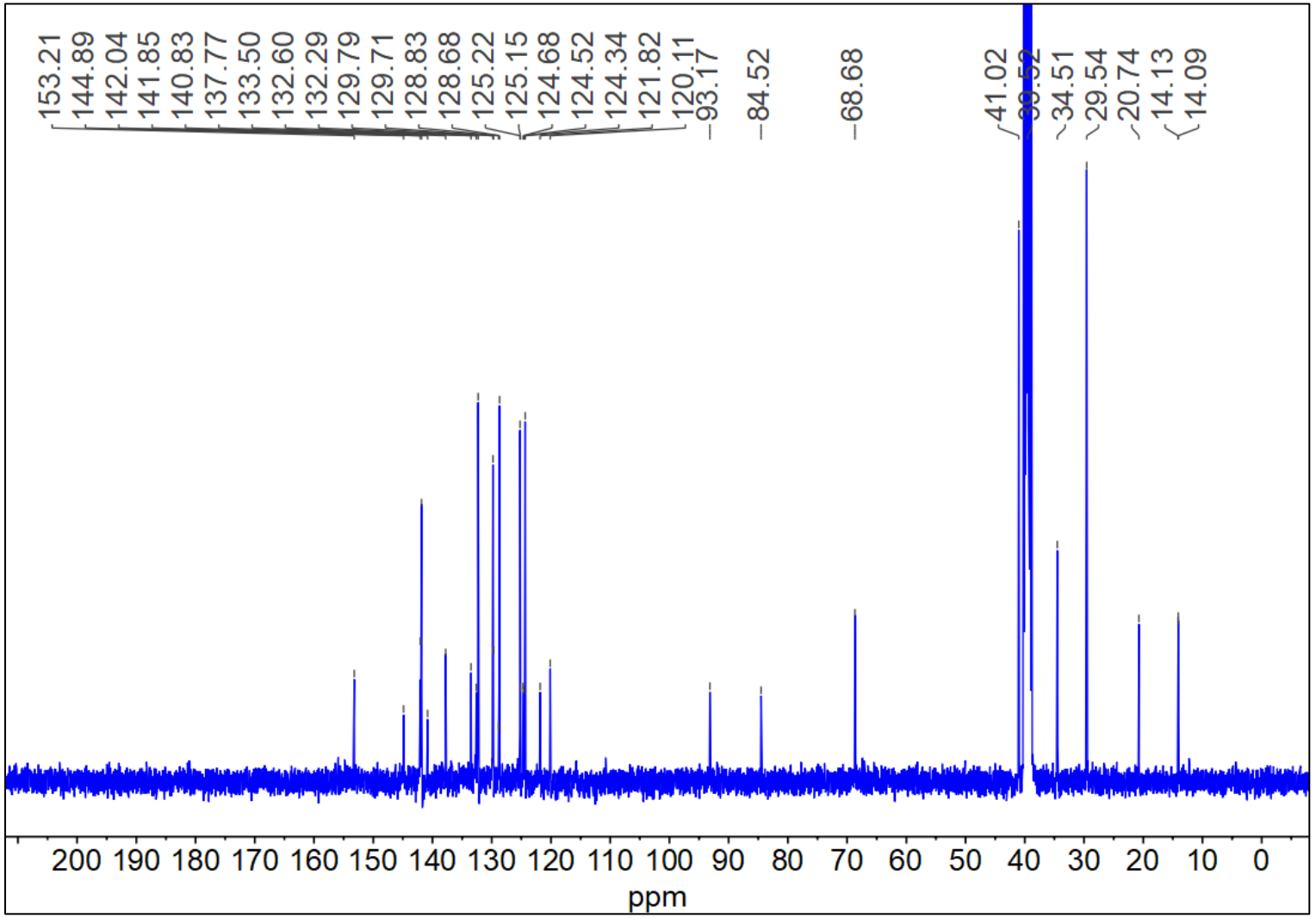

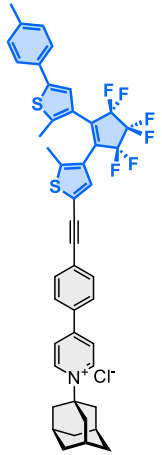

^{13}C {^{1}H} APT NMR (100 MHz, DMSO-d_6): Compound **4**

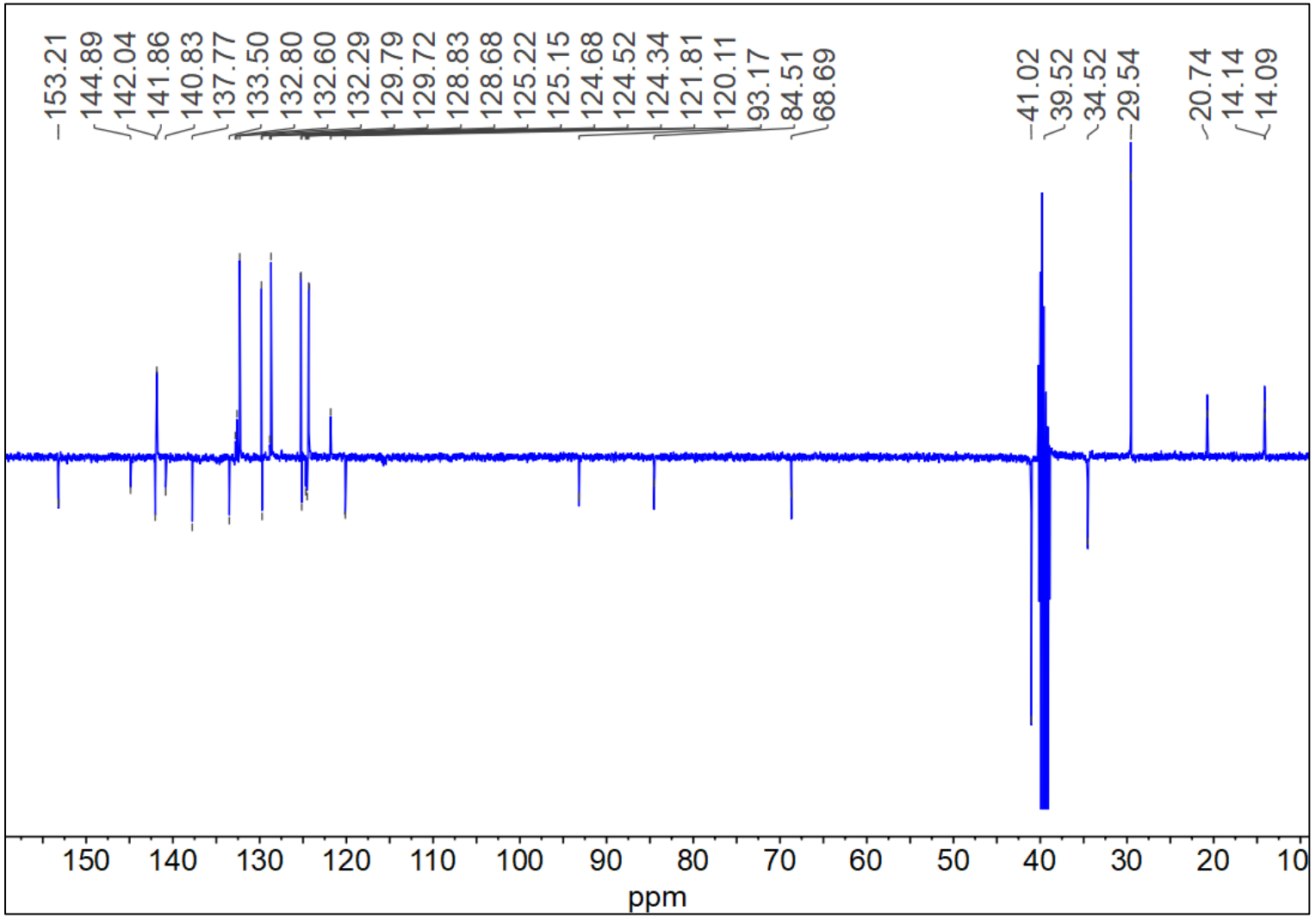

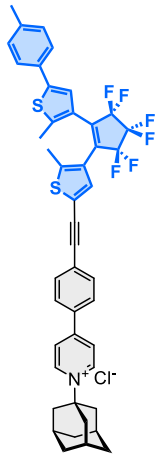

^{1}H-^{1}H COSY (DMSO-d_6): Compound **4**

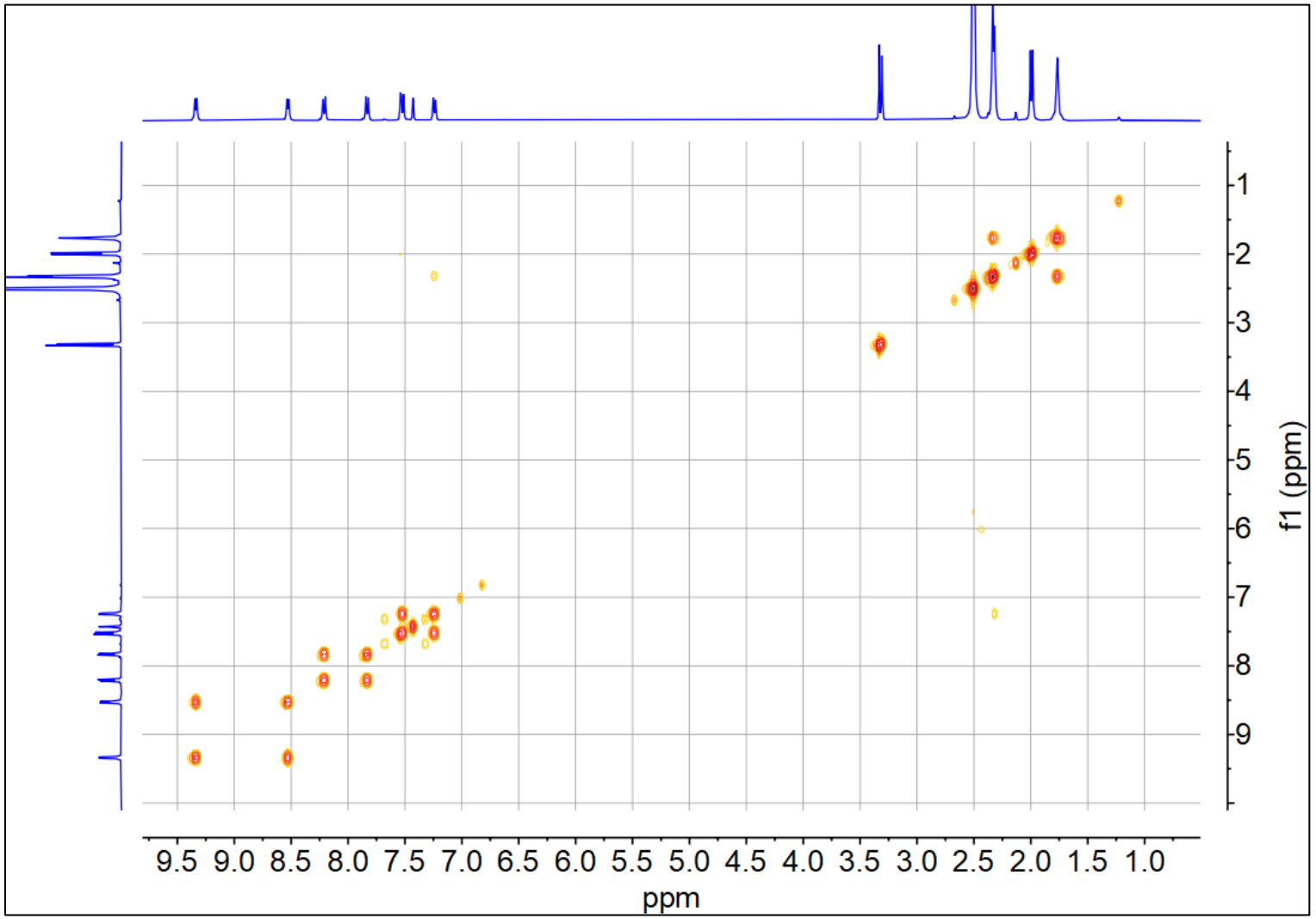

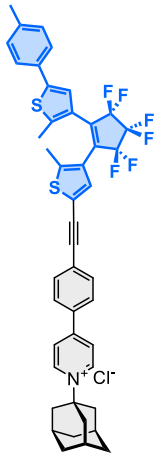

^{1}H-^{13}C HSQC (DMSO-d_6): Compound **4**

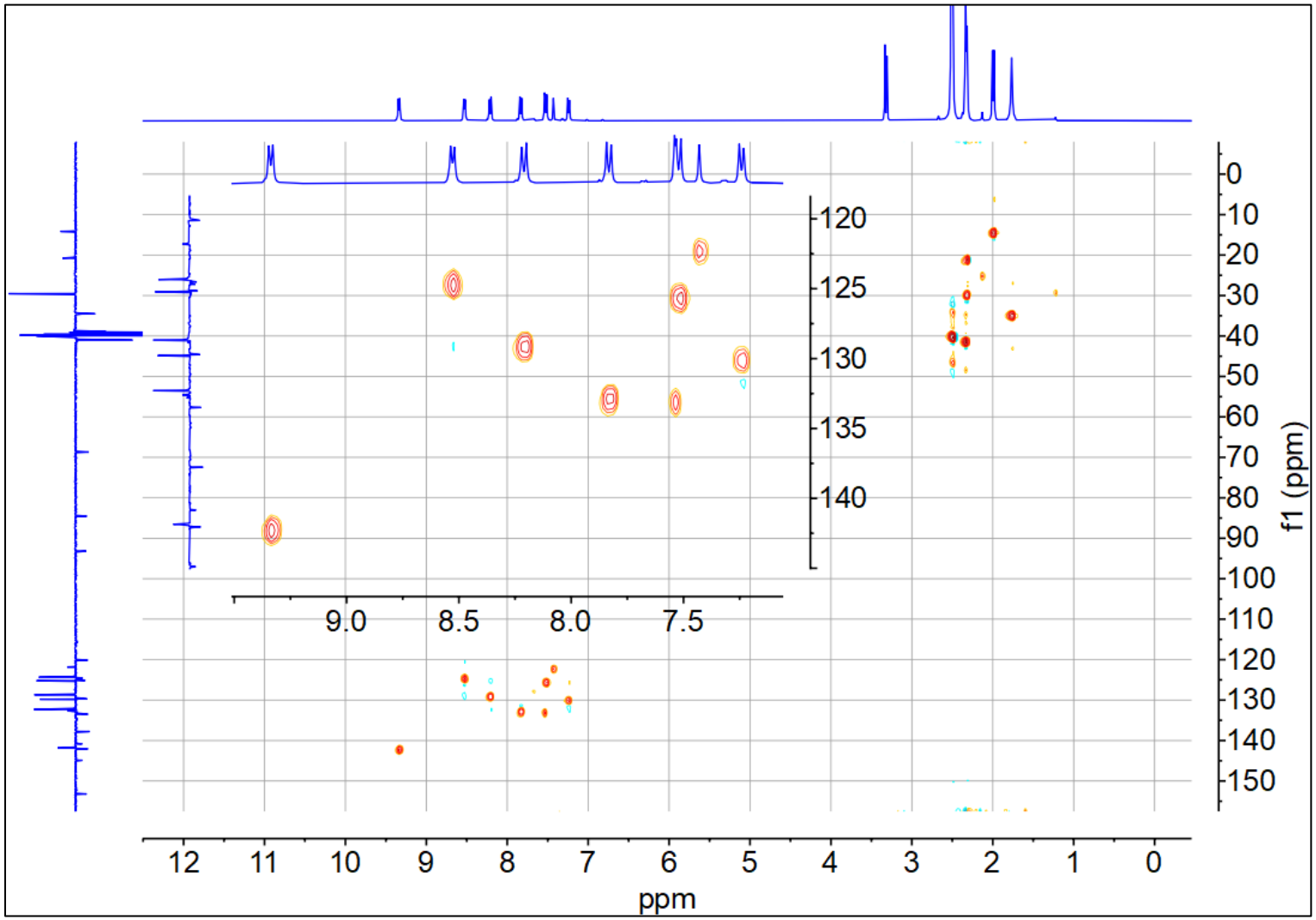

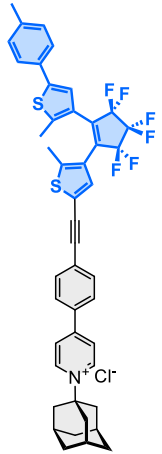

^{1}H-^{13}C HMBC (DMSO-d_6): Compound **4**

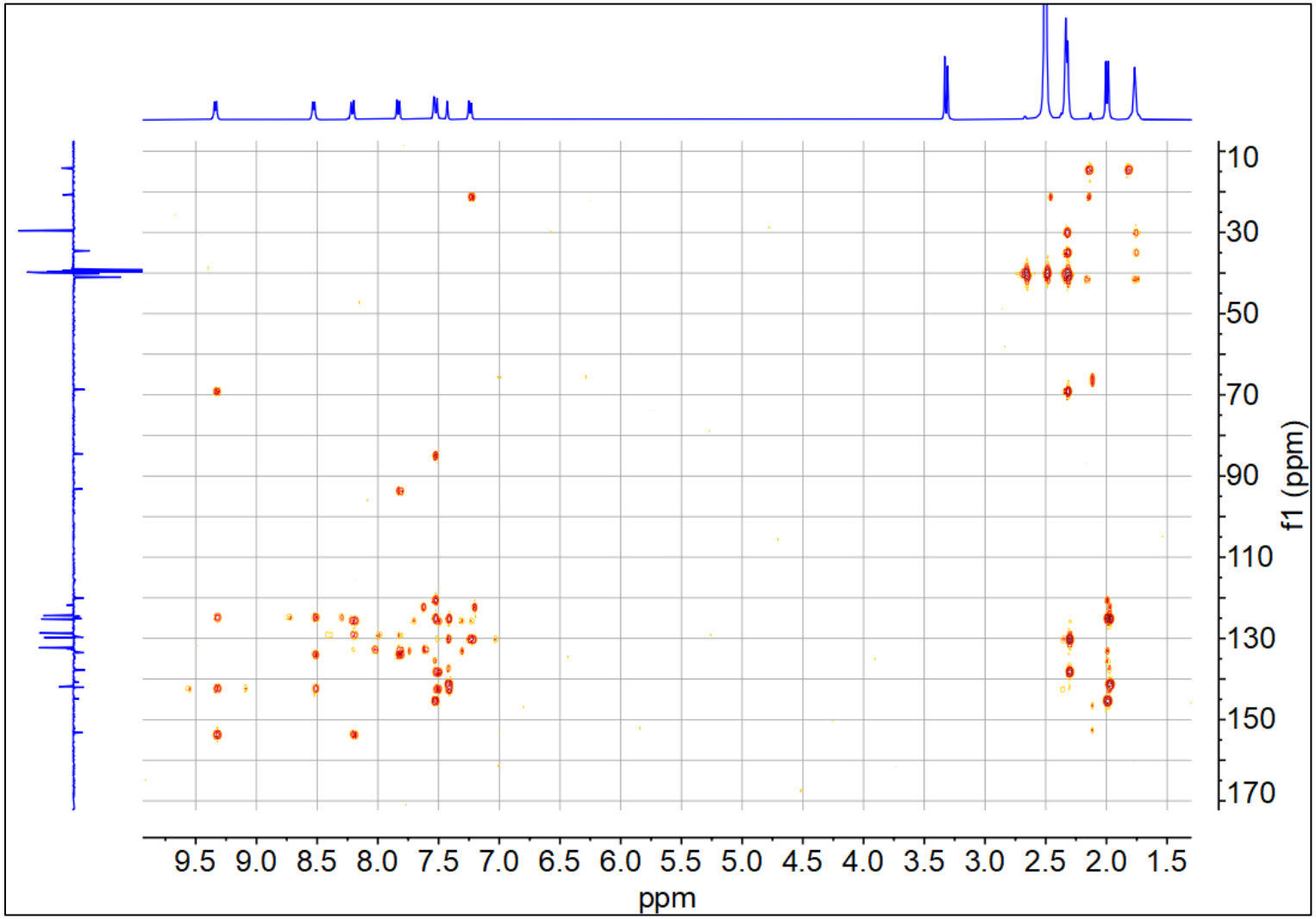

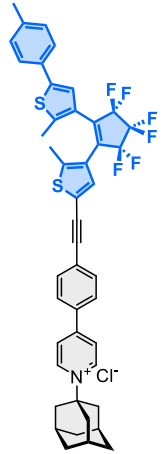

^{1}H NMR (400 MHz, DMSO-d_6): 1-(Adamantan-1-yl)-4-((trimethylsilyl)ethynyl)phenyl)pyridin-1-ium chloride (**8**)

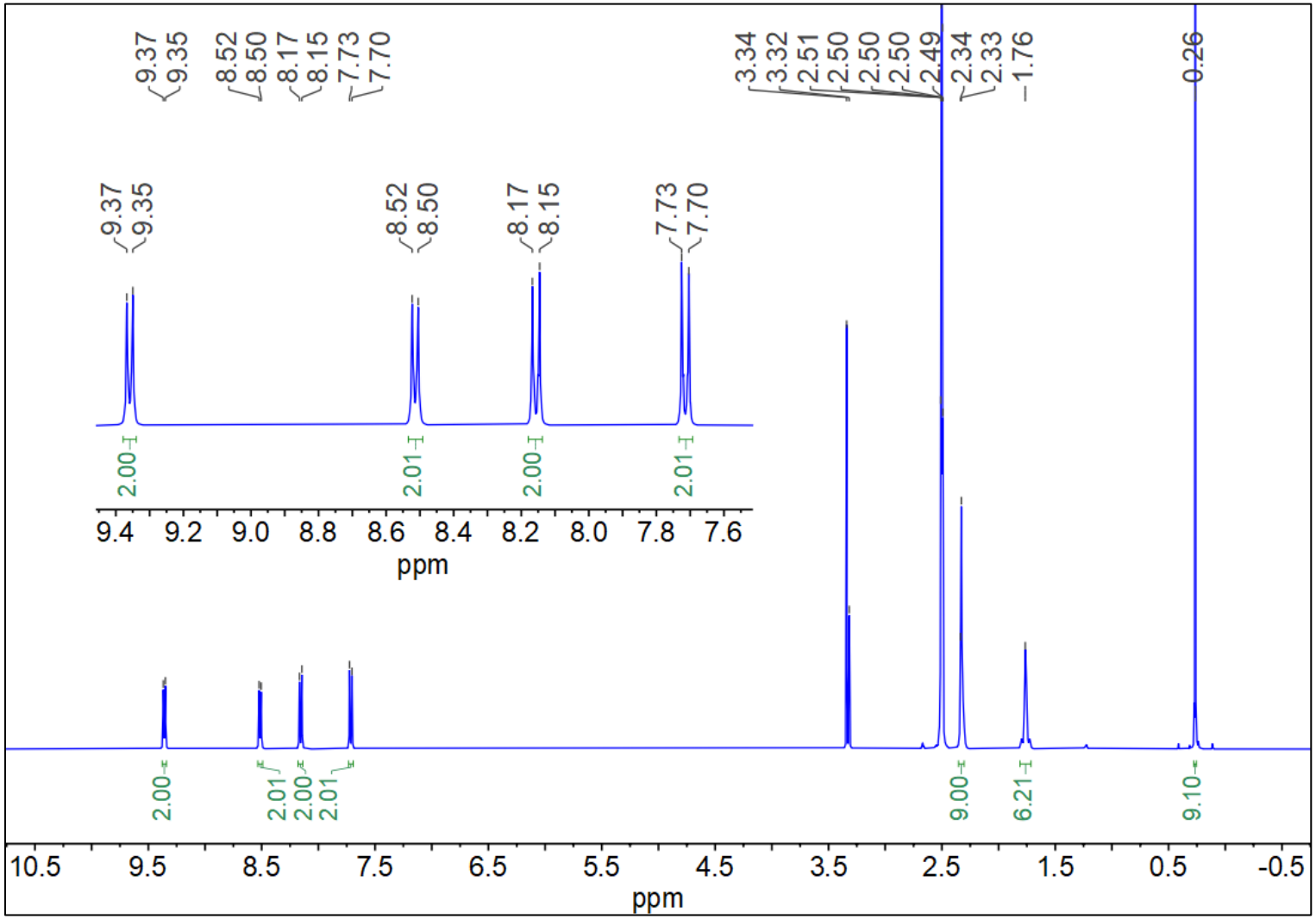

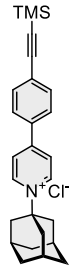

^{13}C {^{1}H} NMR (100 MHz, DMSO-d_6): 1-(Adamantan-1-yl)-4-((trimethylsilyl)ethynyl)phenyl)pyridin-1-ium chloride (**8**)

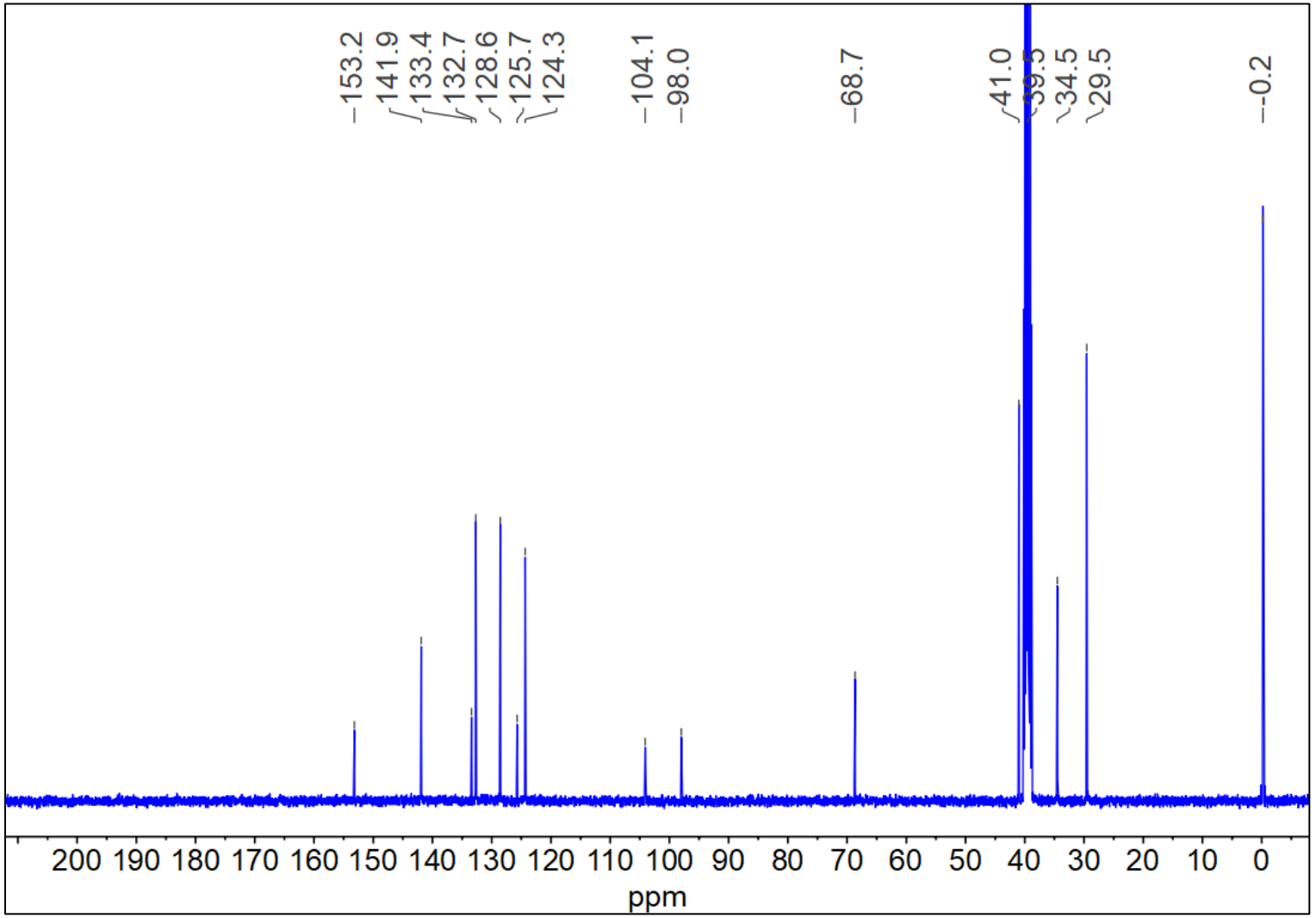

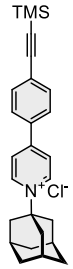

^{13}C APT NMR (400 MHz, DMSO-d_6): 1-(Adamantan-1-yl)-4-((trimethylsilyl)ethynyl)phenyl)pyridin-1-ium chloride (**8**)

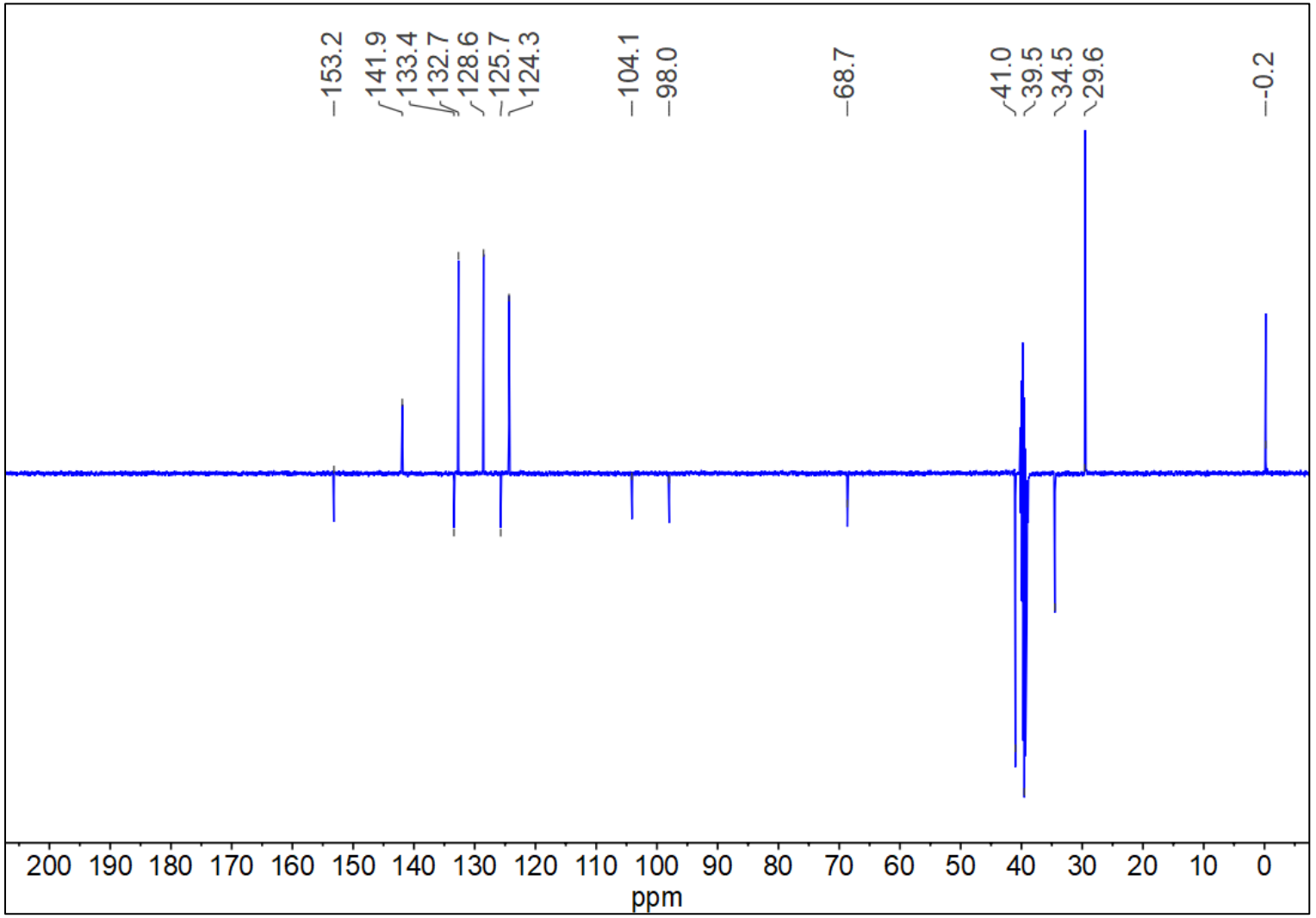

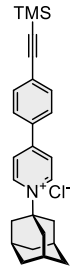

^{1}H-^{1}H COSY NMR (400 MHz, DMSO-d_6): 1-(Adamantan-1-yl)-4-((trimethylsilyl)ethynyl)phenyl)pyridin-1-ium chloride (**8**)

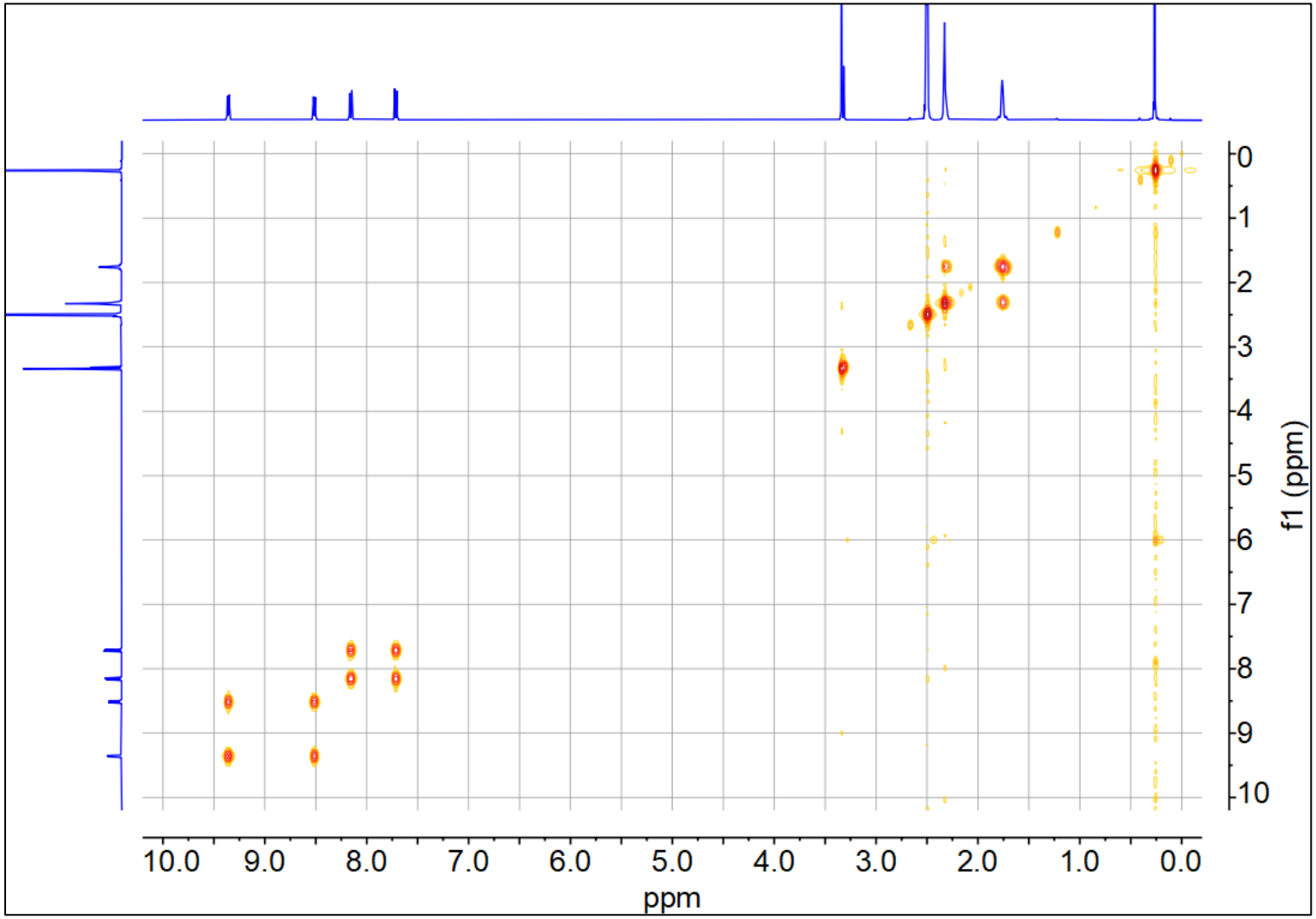

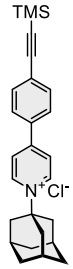

^{1}H – ^{13}C HSQC NMR (400 MHz, DMSO-d_6): 1-(Adamantan-1-yl)-4-((trimethylsilyl)ethynyl)phenyl)pyridin-1-ium chloride (**8**)

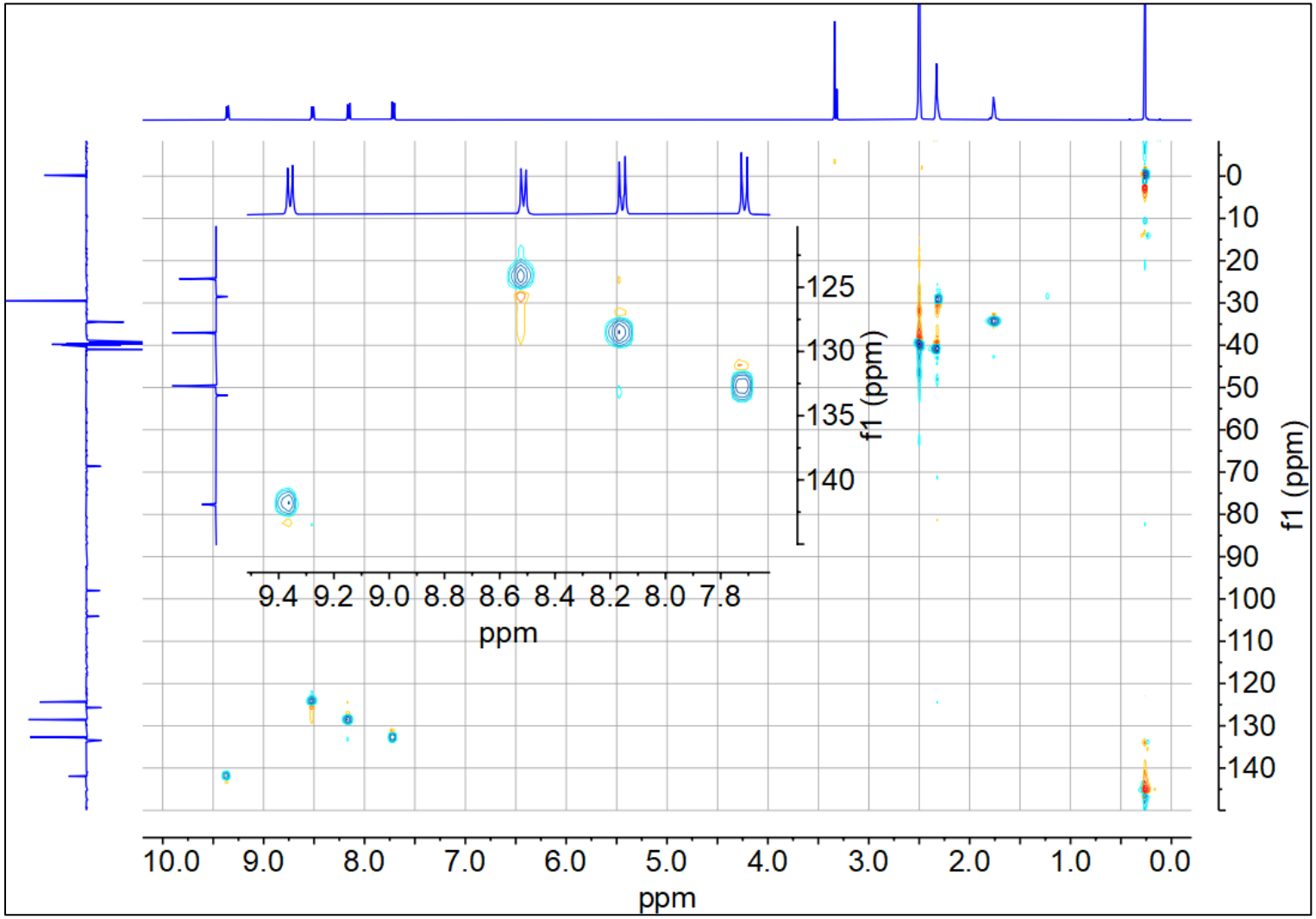

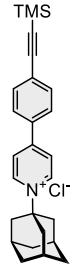

$^{1}H - {}^{13}C$ HMBC (400 MHz, DMSO-d_6): 1-(Adamantan-1-yl)-4-((trimethylsilyl)ethynyl)phenyl)pyridin-1-ium chloride (**8**)

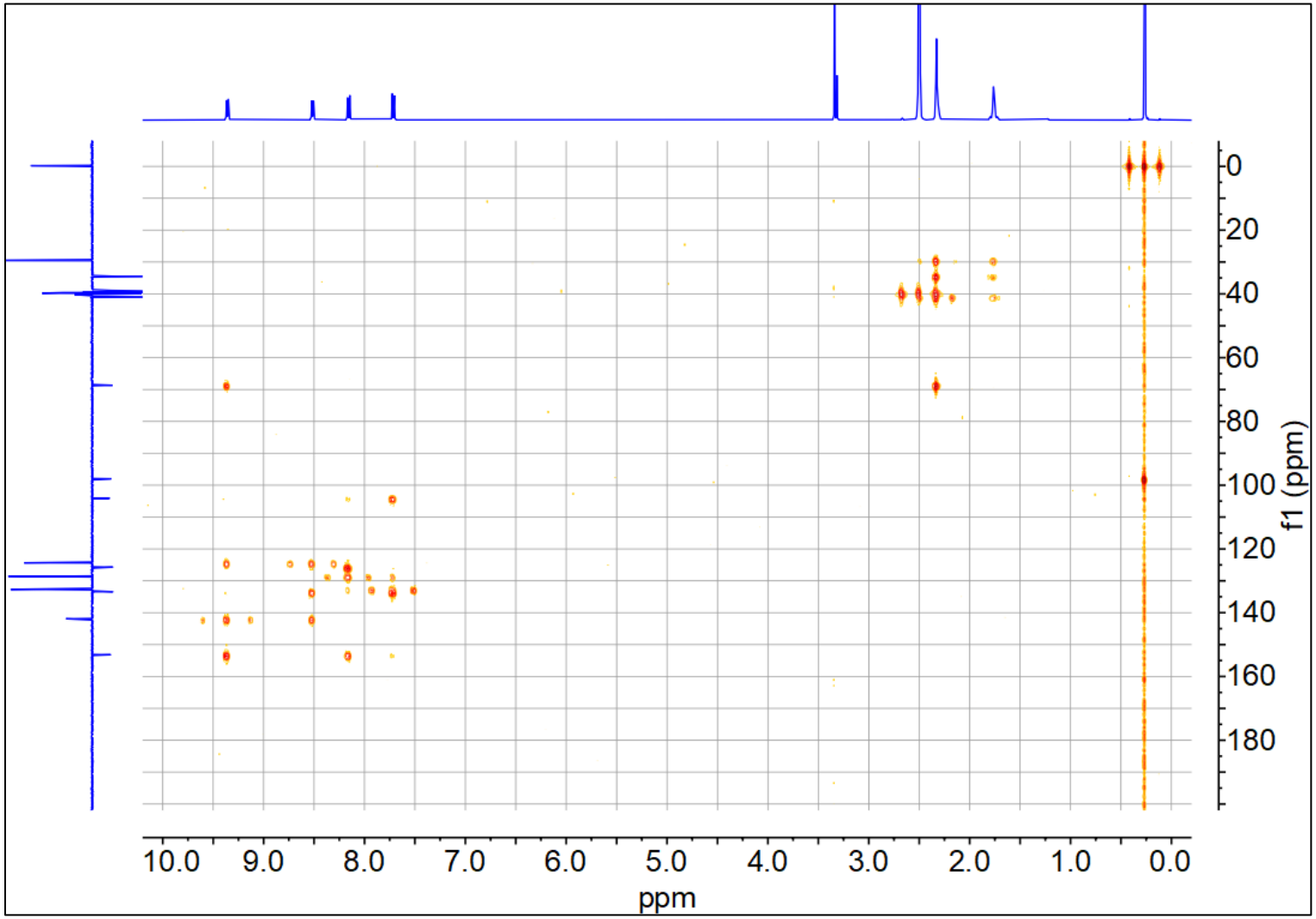

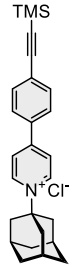

^{1}H NMR (400 MHz, DMSO-d_6):1-(Adamantan-1-yl)-4-((triisopropylsilyl)ethynyl)phenyl)pyridin-1-ium chloride (**9**)

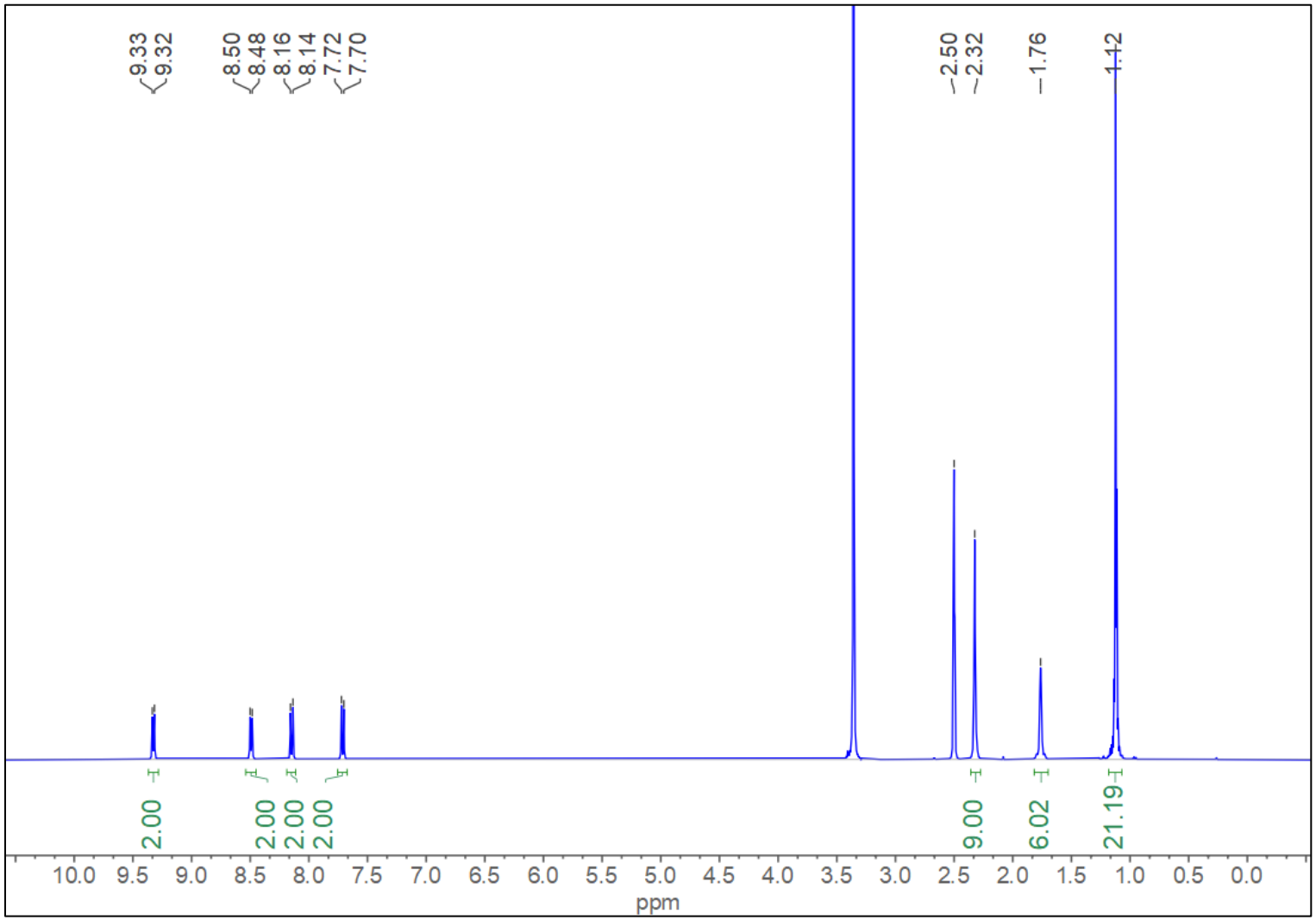

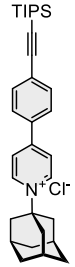

^{13}C APT {^{1}H} NMR (100 MHz, DMSO-d_6):1-(Adamantan-1-yl)-4-((triisopropylsilyl)ethynyl)phenyl)pyridin-1-ium chloride (**9**)

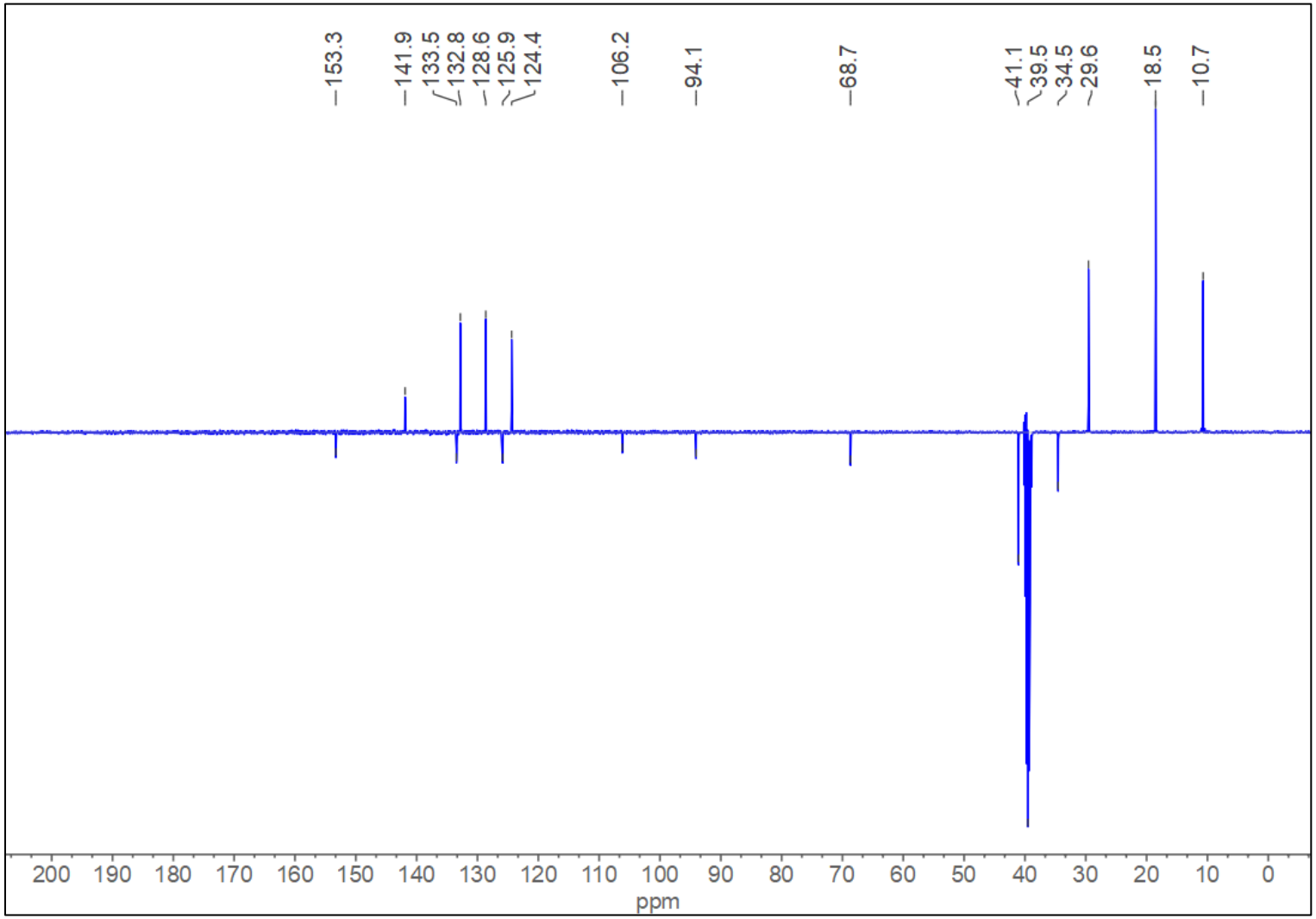

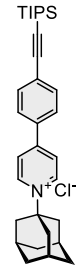

^{1}H-^{1}H COSY (DMSO-d_6): 1-(Adamantan-1-yl)-4-((triisopropylsilyl)ethynyl)phenyl)pyridin-1-ium chloride (**9**)

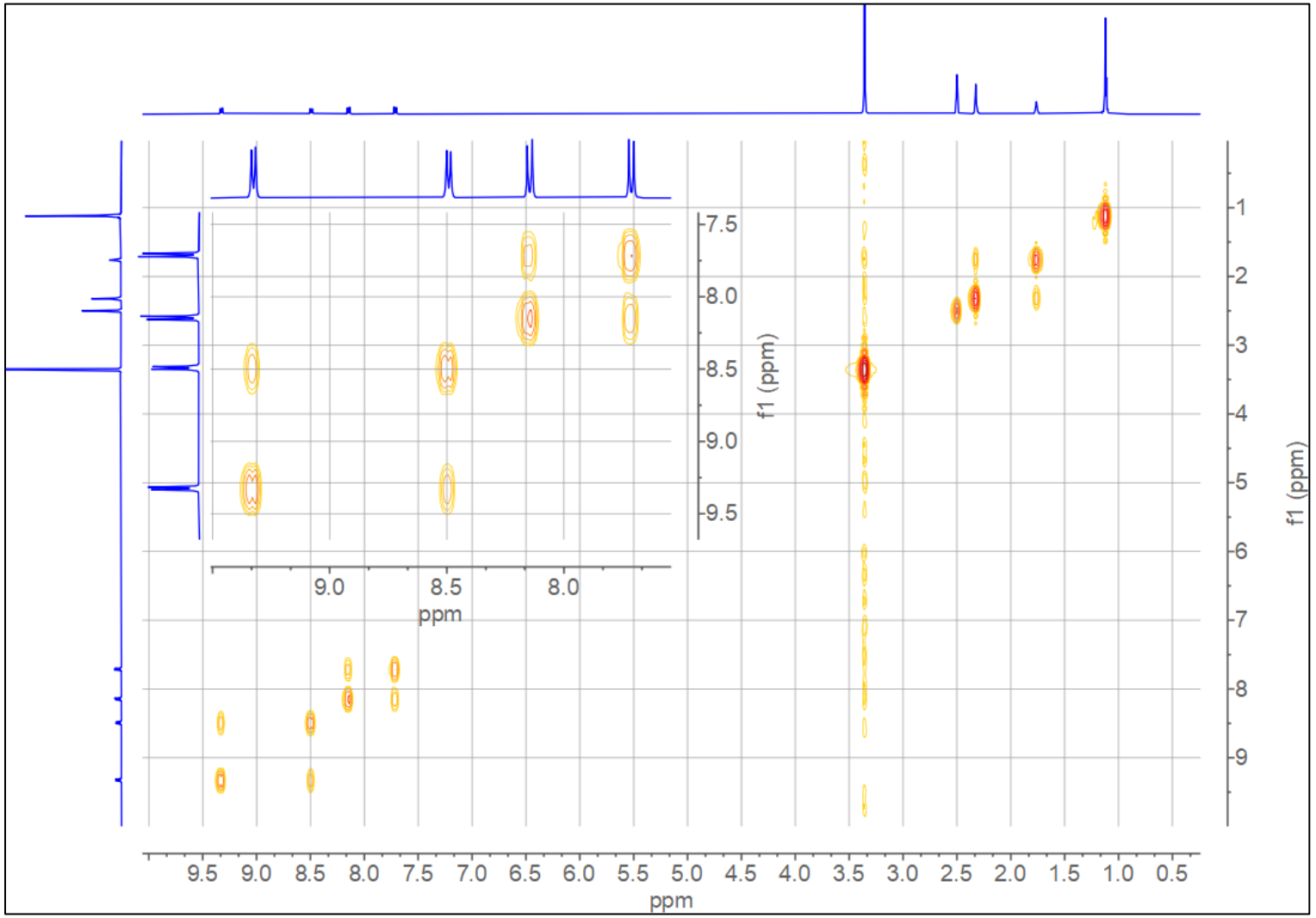

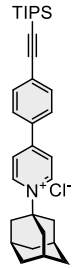

^{1}H-^{13}C HSQC (DMSO-d_6): 1-(Adamantan-1-yl)-4-((triisopropylsilyl)ethynyl)phenyl)pyridin-1-ium chloride (**9**)

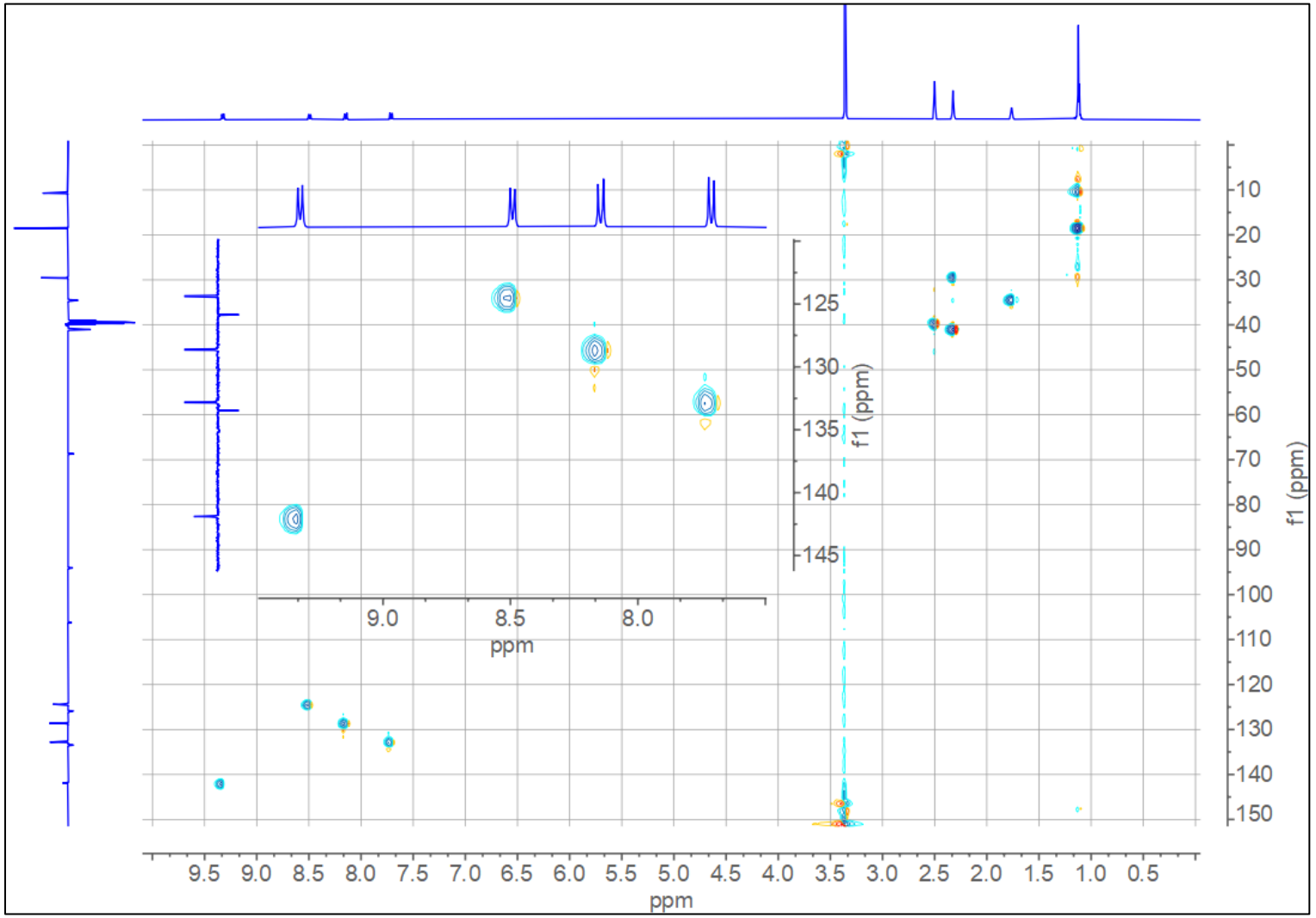

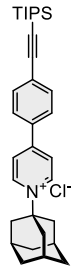

^{1}H-^{13}C HMBC (DMSO-d_6): 1-(Adamantan-1-yl)-4-((triisopropylsilyl)ethynyl)phenyl)pyridin-1-ium chloride (**9**)

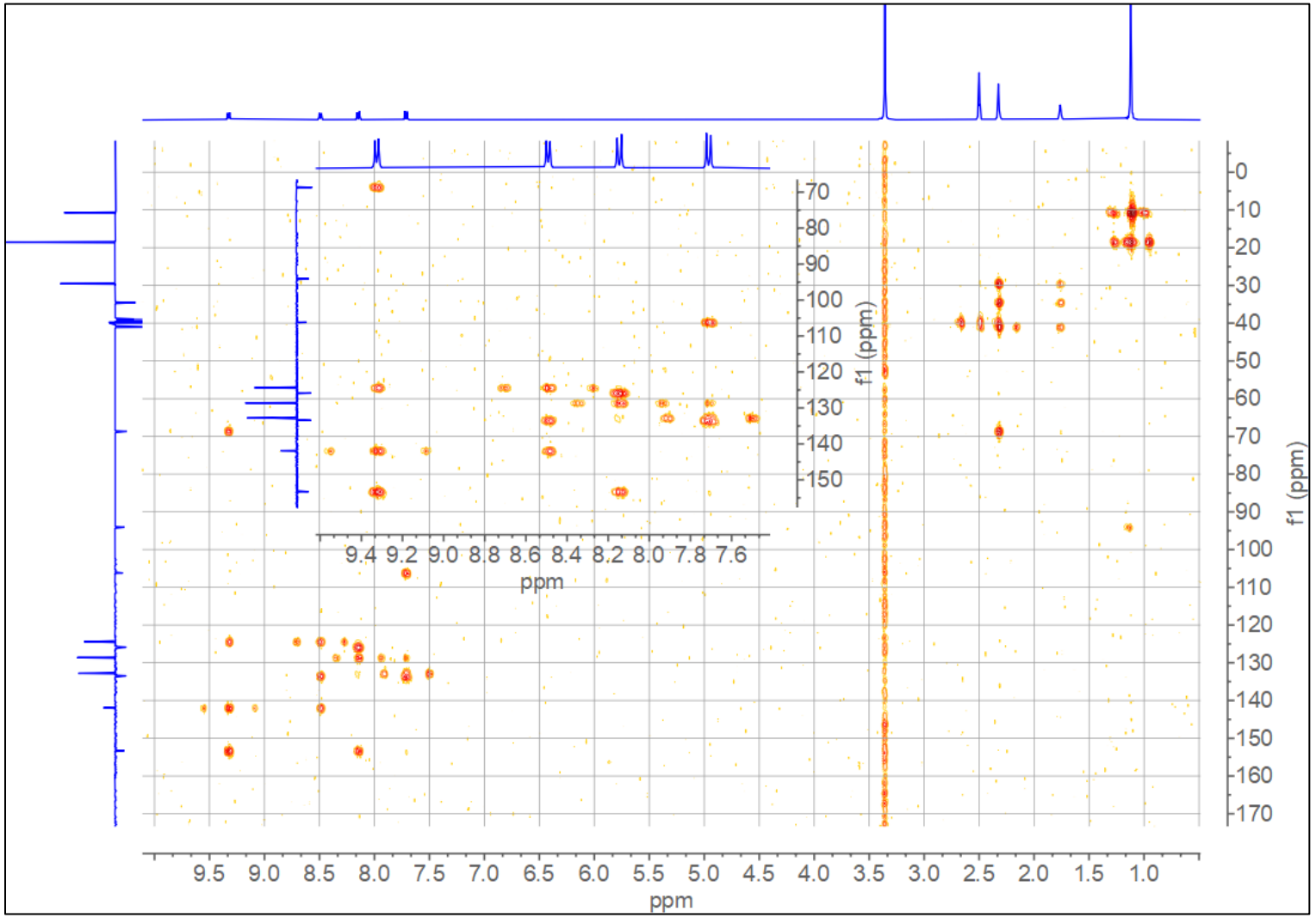

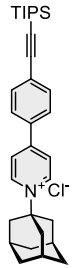

10. X-Ray Crystallographic Data

Table S4. Parameters of Single Crystals of **2** and **8**.

Compound	2	8
CCDC	2457322	2457321
Formula	$C_{36}H_{31}N_4Cl{\cdot}CH_2Cl_2{\cdot}H_2O$	$2(C_{26}H_{32}NSi){\cdot}C_2H_3N{\cdot}2(Cl)$
M.w.	658.04	885.18
Crystal system	Triclinic	Monoclinic
Space group	*P*-1 (No. 2)	$P2_1/n$ (No.14)
a [Å]	12.2842 (4)	10.5011 (4)
b [Å]	16.8227 (5)	36.2781 (14)
c [Å]	34.6745 (10)	13.3571 (4)
α [°]	77.137 (2)	
β [°]	82.673 (2)	91.845 (1)
γ [°]	74.771 (2)	
Z	8	4
V[Å^3]	6722.3 (4)	5085.9 (3)
Temperature	120	120
D_x [g cm^{-3}]	1.300	1.156
Wavelength, Å	1.54178	0.71073
Crystal size [mm]	0.33 × 0.31 × 0.02	0.21 × 0.18 × 0.09
Crystal color, shape	Plate, orange	Prism, colourless
μ [mm^{-1}]	1.300	0.21
T_{min}, T_{max}	0.461, 0.947	0.956, 0.982
Measured reflections	102635	112258
Independent diffractions (R_{int}[a])	24579, (0.041)	11693, (0.028)
Observed diffract. [I>2σ(I)]	21046	10426
No. of parameters	1649	557
R[b]	0.071	0.039
wR(F^2) for all data	0.204	0.105
GOF[c]	1.03	1.03
Residual electron density [e/Å^3]	1.10-1.04	1.04-0.76

[a] $R_{int} = \Sigma \left| F_o^2 - F_{o,mean}^2 \right| / \Sigma F_o^2$; [b] $R(F) = \Sigma \left| \left| F_o \right| - \left| F_c \right| \right| / \Sigma \left| F_o \right|$; $wR(F^2) = [\Sigma(w(F_o^2 - F_c^2)^2)/(\Sigma w(F_o^2)^2)]^{½}$; [c] GOF = $[\Sigma(w(F_o^2 - F_c^2)^2)/(N_{diffrs} - N_{params})]^{½}$

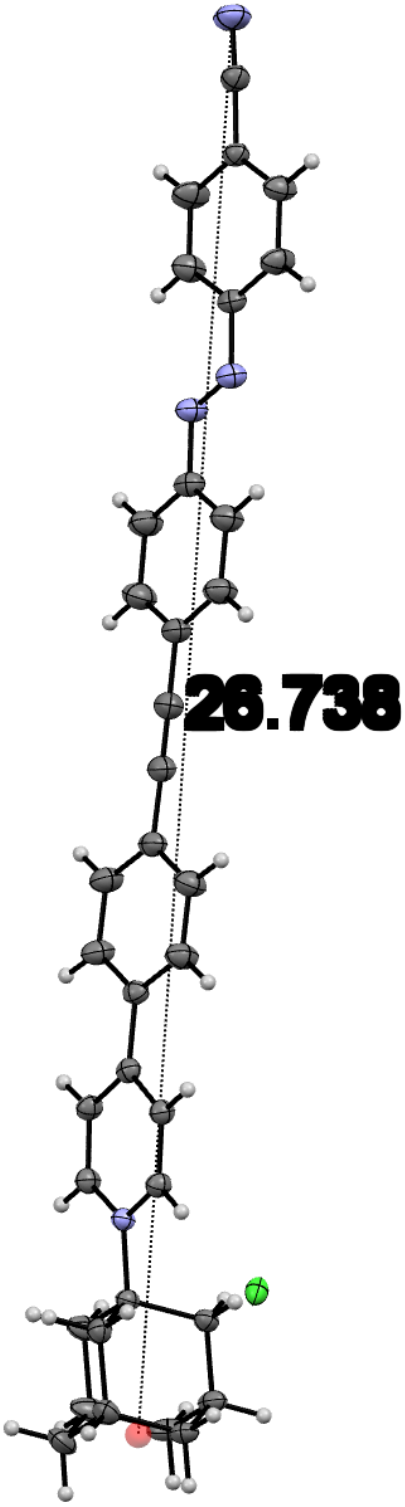

Figure S58. ORTEP visualization of **2**, with marked measure of the length. The displacement ellipsoids are shown at the 50% probability level.

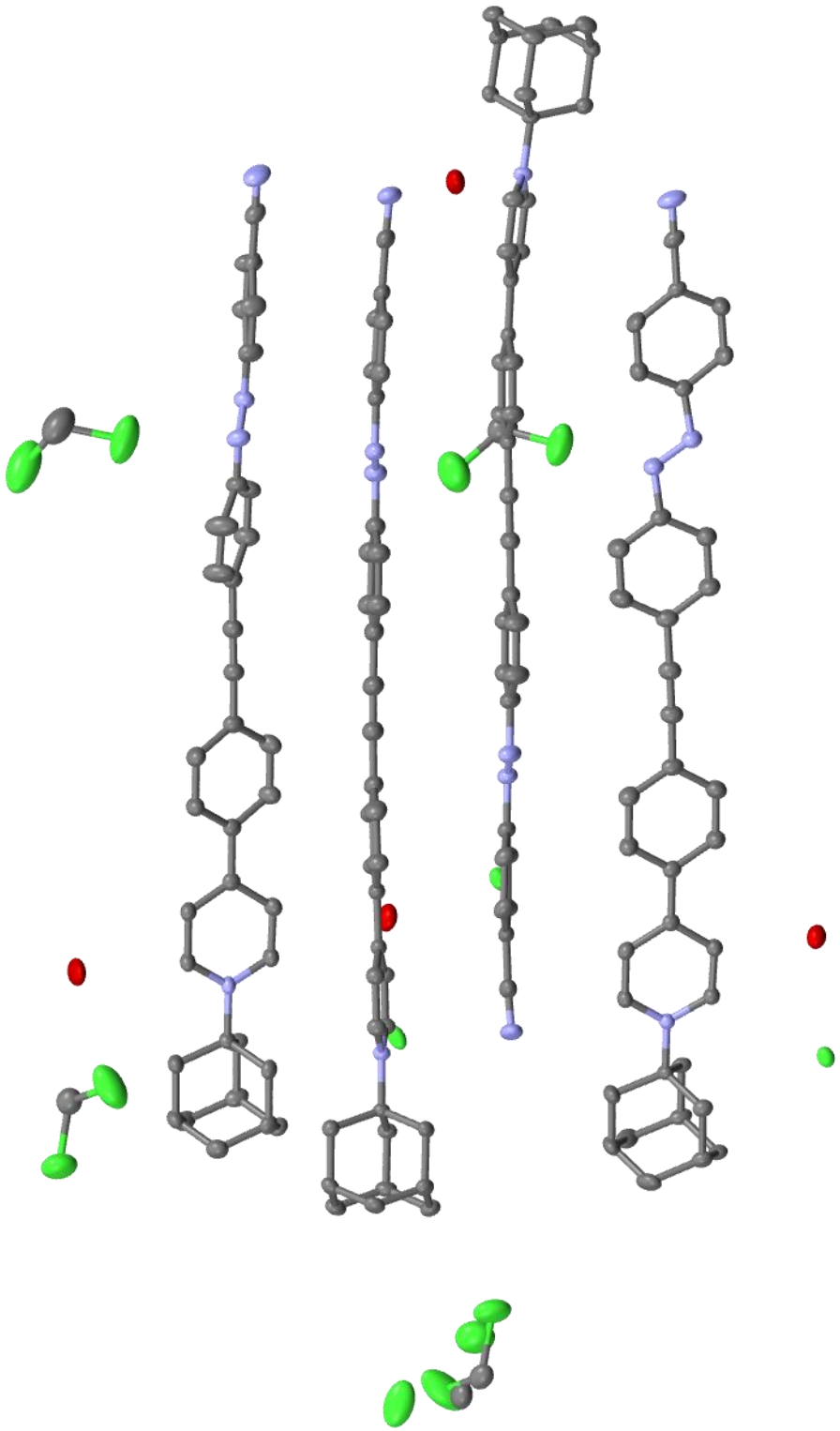

Figure S59. Crystal packing of compound **2**. Hydrogen atoms are omitted for clarity.

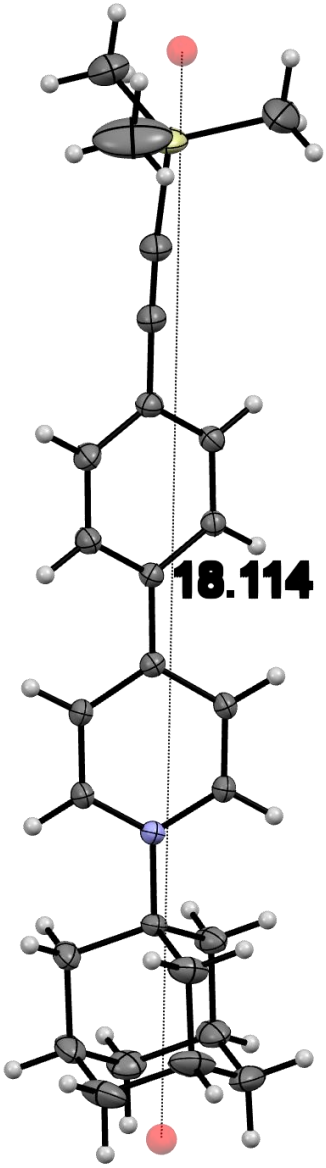

Figure S60. ORTEP visualization of **8**, with marked measure of the length. The displacement ellipsoids are shown at the 50% probability level.

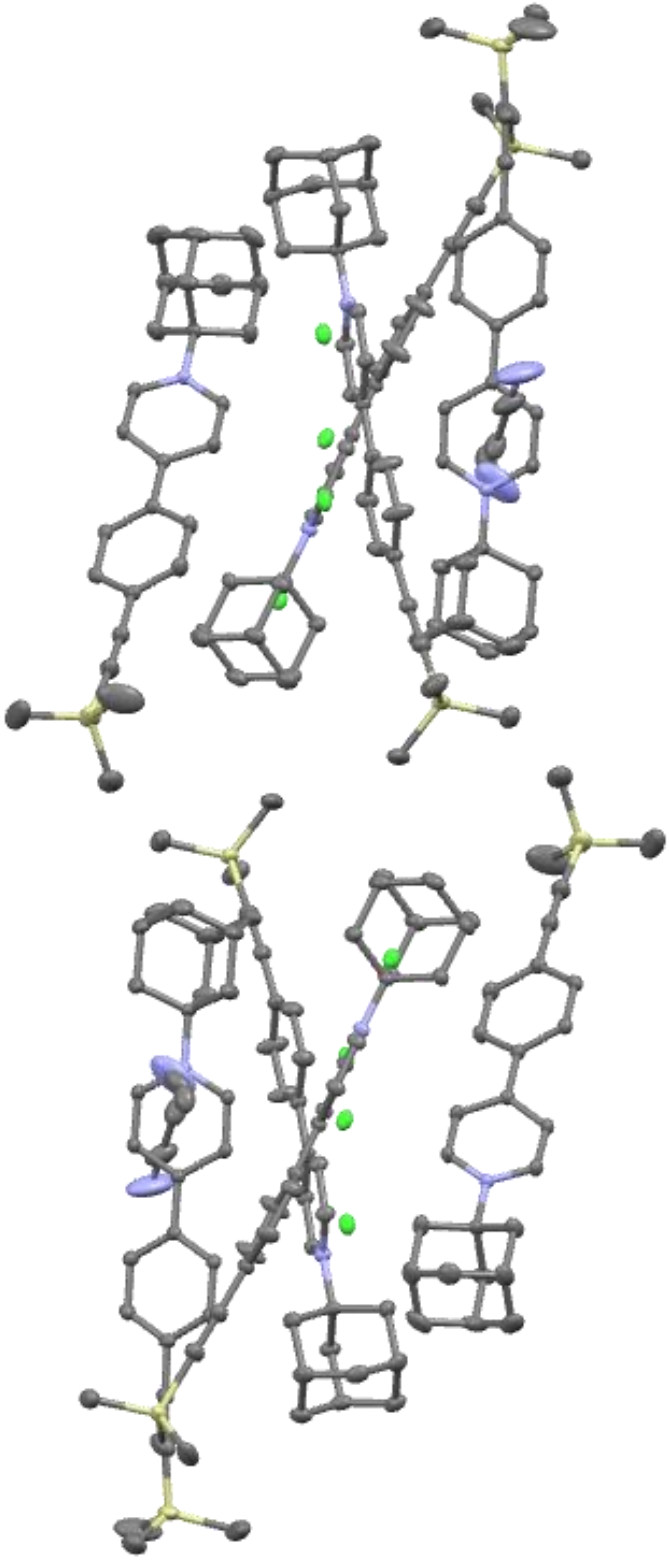

Figure S61. Crystal packing of compound **8**. Hydrogen atoms are omitted for clarity.